Coordinated Control of a Mobile Manipulator

MS-CIS-94-12
GRASP LAB 371

Yoshio Yamamoto

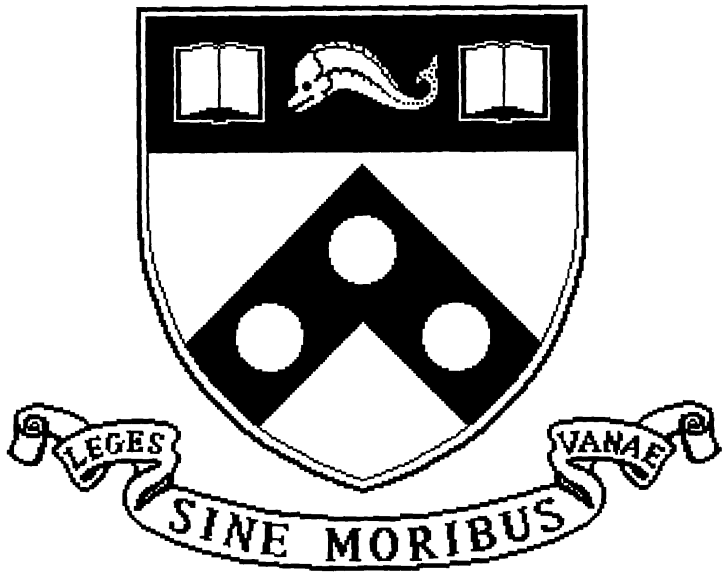

University of Pennsylvania
School of Engineering and Applied Science
Computer and Information Science Department
Philadelphia, PA 19104-6389

March 1994

Coordinated Control of a Mobile Manipulator

Yoshio Yamamoto

GRASP Laboratory
Department of Mechanical Engineering
and Applied Mechanics
School of Engineering and Applied Science
University of Pennsylvania

March 3, 1994

Abstract

In this technical report, we investigate modeling, control, and coordination of mobile manipulators. A mobile manipulator in this study consists of a robotic manipulator and a mobile platform, with the manipulator being mounted atop the mobile platform. A mobile manipulator combines the dextrous manipulation capability offered by fixed-base manipulators and the mobility offered by mobile platforms. While mobile manipulators offer a tremendous potential for flexible material handling and other tasks, at the same time they bring about a number of challenging issues rather than simply increasing the structural complexity. First, combining a manipulator and a platform creates redundancy. Second, a wheeled mobile platform is subject to nonholonomic constraints. Third, there exists dynamic interaction between the manipulator and the mobile platform. Fourth, manipulators and mobile platforms have different bandwidths. Mobile platforms typically have slower dynamic response than manipulators. The objective of the thesis is to develop control algorithms that effectively coordinate manipulation and mobility of mobile manipulators.

We begin with deriving the motion equations of mobile manipulators. The derivation presented here makes use of the existing motion equations of manipulators and mobile platforms, and simply introduces the velocity and acceleration dependent terms that account for the dynamic interaction between manipulators and mobile platforms. Since nonholonomic constraints play a critical role in control of mobile manipulators, we then study the control properties of nonholonomic dynamic systems, including feedback linearization and internal dynamics. Based on the newly proposed concept of preferred operating region, we develop a set of coordination algorithms for mobile manipulators. While the manipulator performs manipulation tasks, the mobile platform is controlled to always bring the configuration of the manipulator into a preferred operating region. The control algorithms for two types of tasks — dragging motion and following motion — are discussed in detail. The effects of dynamic interaction are also investigated.

To verify the efficacy of the coordination algorithms, we conduct numerical simulations with representative task trajectories. Additionally, the control algorithms for the dragging motion and following motion have been implemented on an experimental mobile manipulator. The results from the simulation and experiment are presented to support the proposed control algorithms.

Contents

1 Introduction **1**
- 1.1 Problem Statement . . . 1
- 1.2 Previous Works . . . 2
- 1.3 Scope and Outline of Thesis . . . 6

2 Modeling of Mobile Manipulators **9**
- 2.1 Equations of Motion of Manipulators . . . 9
- 2.2 Equations of Motion of Wheeled Mobile Platforms . . . 12
  - 2.2.1 Constraint Equations . . . 12
  - 2.2.2 Dynamic Equations . . . 15
  - 2.2.3 State Space Realization . . . 16
- 2.3 Equations of Motion of Mobile Manipulators . . . 17

3 Feedback Control of Wheeled Mobile Platforms **21**
- 3.1 Input-State Linearization . . . 21
- 3.2 Input-Output Linearization and Decoupling . . . 22
  - 3.2.1 Controlling the Center Point P_o . . . 23
  - 3.2.2 Dynamic Feedback Control . . . 23
  - 3.2.3 Look-Ahead Control . . . 26
- 3.3 Internal Dynamics . . . 27
  - 3.3.1 Derivation of Internal Dynamics . . . 27
  - 3.3.2 Simulation . . . 30
  - 3.3.3 Experiments . . . 31

4 Coordinated Control of Mobile Manipulators: Dragging Task **36**
- 4.1 Motivation . . . 36
- 4.2 Preferred Operating Regions . . . 37
- 4.3 Control Scheme . . . 38
- 4.4 Coordination Strategy . . . 39
- 4.5 Simulation Results . . . 40

5 Coordinated Control of Mobile Manipulators: Following Task **49**
- 5.1 Motivation . . . 49
- 5.2 Force Control Algorithm of Manipulator . . . 50
- 5.3 Coordination Strategy . . . 52

6 Dynamic Interaction **54**
6.1 Introduction 54
6.2 Feedback Control 54
6.2.1 Output Equations 55
6.2.2 Input-Output Linearization 56
6.3 Simulation Results 57

7 Experiments **66**
7.1 Experimental Setup 66
7.2 Control Scheme of LABMATE Mobile Platform 69
7.3 Experimental Results of Dragging Task 70
7.4 Experimental Results of Following Task 70

8 Summary **76**
8.1 Contributions 76
8.2 Works to be done 77

A Functional Dependence of Inertial Matrix, $M_r^{(ij)}$ **79**

B Functional Dependence of Velocity Term, $C_{r2}^{(i)}$ **82**

Bibliography **83**

List of Figures

1.1 Multiple agents working in a coordinated environment. 2

2.1 Serial manipulator with N degrees-of-freedom. 10
2.2 Link parameters and coordinate frames. 11
2.3 Schematic of the wheeled mobile platform. 12
2.4 Schematic of the mobile manipulator. 17

3.1 Dynamic feedback controller of a mobile robot. 25
3.2 The trajectories of the reference point (simulation). 31
3.3 The trajectories of the point P_o on the wheel axis (simulation). 32
3.4 The trajectory of the mobile platform in Case 3. 32
3.5 The trajectories of the reference point (experiment). 33
3.6 The trajectories of P_o on the wheel axis (experiment). 34
3.7 The heading angles of the mobile platform (experiment). 34
3.8 The trajectory of the mobile platform with an offset (experiment). 35

4.1 Example of preferred configuration of mobile manipulator. 38
4.2 Schematic of the mobile platform with 2-DOF manipulator. 39
4.3 Two paths used in the simulation. 41
4.4 Trajectory of the point P_o for Case (i). 42
4.5 Desired and actual trajectories of the reference point for Case (i). 43
4.6 Manipulability measure for Case (i). 43
4.7 Joint angles for Case (i). 44
4.8 Heading angle for Case (i). 44
4.9 Velocity of the point P_o for Case (i). 45
4.10 Trajectory of the point P_o for Case (ii). 45
4.11 Desired and actual trajectories of the reference point for Case (ii). 46
4.12 Manipulability measure for Case (ii). 46
4.13 Joint angles for Case (ii). 47
4.14 Heading angle for Case (ii). 47
4.15 Velocity of the point P_o for Case (ii). 48

5.1 A mobile manipulator pushing against a moving surface. 49
5.2 Controller architecture of the mobile manipulator. 50
5.3 Schematic of a PUMA250 mounted on a LABMATE mobile platform. . . . 51
5.4 Diagram of the explicit force control scheme. 52

6.1 2-DOF arm mounted on the mobile platform. 55
6.2 Example of the Case (i). 58
6.3 Tracking errors for the Case (i). 59
6.4 Example of the Case (ii). 60
6.5 Tracking errors for the Case (ii). 60
6.6 Example of the Case (iii). 61
6.7 Tracking errors for the Case (iii). 61
6.8 Effect of the motion of the platform on the manipulator. 63
6.9 Effect of the motion of the manipulator on the platform (${}^{v}X$-direction). . . 64
6.10 Effect of the motion of the manipulator on the platform (${}^{v}Y$-direction). . . 65

7.1 Mobile manipulator used in the experiments. 67
7.2 Hardware architecture for the experimental setup. 68
7.3 Trajectory of the P_o and the motion of platform. 70
7.4 Trajectories of the reference point. 71
7.5 Velocity of the point P_o of LABMATE. 71
7.6 Joint angles of PUMA 250. 72
7.7 Manipulability measure. 72
7.8 Trajectory of the reference point. 73
7.9 Experimental trajectory of the mobile platform. 73
7.10 Heading angle. 74
7.11 Manipulability measure. 75
7.12 Measured forces. 75

Chapter 1

Introduction

1.1 Problem Statement

Traditionally, robotic manipulators are bolted onto floor. The workspace of such a *fixed-base manipulator* is a limited volume of the space that can be reached by the end-effector of the manipulator. Tasks must be carefully structured so that the manipulator can reach parts to be assembled. This is typically achieved by means of conveyor belts or other transporting devices.

In the recent years, there has been a great deal of interest in *mobile robots* [1, 2, 3]. A mobile robot is typically a mobile platform or vehicle, equipped with a computer(s) and various sensors. The study of mobile robots is mostly concentrated on a central question: how to move from here to there in a structured/unstructured environment. It involves many issues such as motion planning, navigation, sensor fusion, and localization.

The subject of this thesis is *mobile manipulators*. A mobile manipulator consists of a manipulator and a mobile platform (or a mobile robot). The manipulator is mounted on the top of the mobile platform. A mobile manipulator combines the dextrous manipulation capability offered by fixed-base manipulators and the mobility offered by mobile platforms. A mobile manipulator has a considerably larger workspace than a fixed-based one.

Mobile manipulators have many potential applications in manufacturing, nuclear reactor maintenance, construction, planetary exploration [4, 5, 6]. A conceptual example of such applications utilizing mobile manipulators is depicted in Figure 1.1. In the figure, multiple mobile manipulators cooperatively perform material handling tasks.

The objective of this thesis is to investigate modeling, control, and coordination of mobile manipulators. The emphasis will be placed on coordinating manipulation and mobility of a single mobile manipulator. While performing manual tasks, humans always coordinate the body movement and arm movement in a natural and elegant manner. For instance, when writing on a blackboard, one positions his/her arm in a comfortable posture by laterally moving his/her body rather than reaching out his/her arm. In a sense, humans execute an optimal coordination algorithm to take full advantage of (fine) hand motions and (gross) body motions. Therefore, this study is motivated to develop coordination algorithms that enable mobile manipulators to perform tasks efficiently and effectively.

Mobile manipulators offer a tremendous potential for performing material handling and

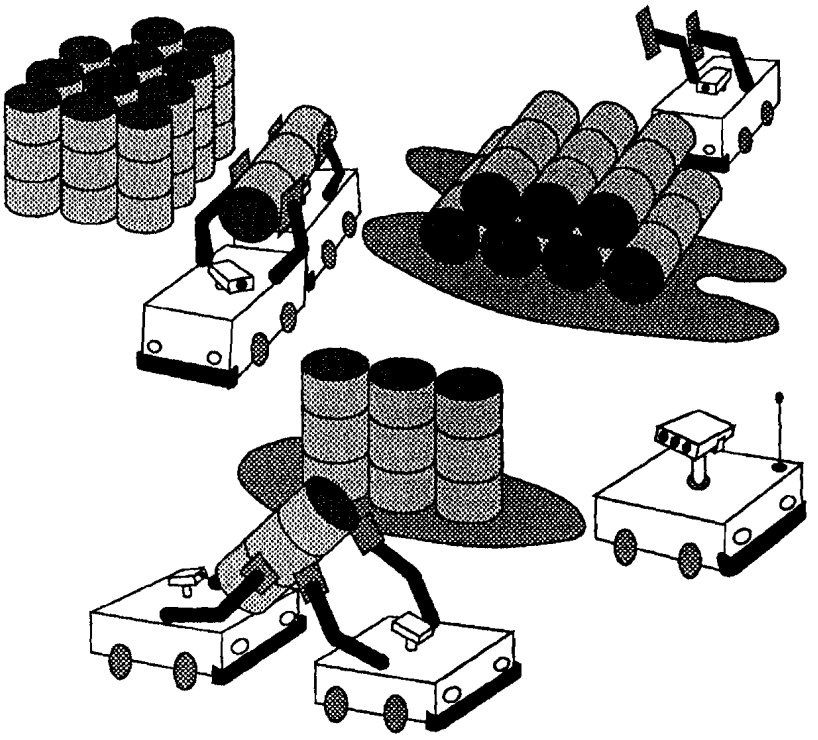

Figure 1.1: Multiple agents working in a coordinated environment.

other tasks. At the same time, they bring about a number of challenging problems rather than simply increasing the structural complexity. The following issues will be addressed in this thesis:

- Combining a manipulator and a platform creates redundancy.
- A wheeled mobile platform is subject to nonholonomic constraints.
- There exists dynamic interaction between the mobile platform and the manipulator.
- Manipulators and mobile platforms have different bandwidths. Mobile platforms typically have slower dynamic response than manipulators.

1.2 Previous Works

Study of the coordination and control of mobile manipulators spans several different research domains. Some of them have been extensively studied while others are fairly new and relatively little research has been done. Major issues related to the topic include the kinematic and dynamic modeling and the control of a wheeled mobile platform, the path planning of the mobile robot, the coordination strategy of locomotion and manipulation of the mobile manipulator, the dynamic interaction of the manipulator and the

mobile platform, and force control issues if the manipulator is required to interact with an environment.

In this section, the previous works related to the above issues are reviewed. The control and path planning problems of wheeled mobile robots have recently drawn a lot of attentions in nonlinear control community because of its unique properties due to the presense of nonholonomic constraints. Therefore, the review on the nonholonomic systems with emphasis on the control characteristics of wheeled mobile platforms is given in details which are pertinent to Chapter 2 and 3. However, there is only a limited literature available on the issues of coordination and dynamic interaction of a mobile manipulator although the advantage of a mobile manipulator over a conventional fixed-base manipulator has been widely acknowledged. We provide a careful review on these issues which are closely related to Chapter 4 and 6, followed by a brief review on force control which is relevant to Chapter 5.

Nonholonomic Systems

A classical example of nonholonomic systems is a rigid disk rolling on a horizontal plane without slippage in [7], which is equivalent from the control perspective to a wheeled cart driven by two wheels. As a matter of fact, a car-like system in general is a nonholonomic system except a few examples of omnidirectional vehicles [8, 9, 10, 11, 12]. Other examples of nonholonomic systems can be seen in

- Underwater vehicle [13, 14]
- Robotic fingers [15, 16]
- Space Manipulators [17, 18, 19]
- Falling cat and astronaut maneuvering [20, 21, 22]

For more extensive treatment of nonholonomic systems in general, the reader is referred to Neĭmark and Fufaev [23]. Also a good survey of the recent development in terms of nonholonomic motion planning is given by Li and Canny [24].

Path Planning of a Mobile Robot as a Nonholonomic System

As mentioned earlier, significant efforts in terms of the study of mobile robots from nonholonomic system's perspective have been focused on the path planning problem and nonlinear control. Laumond [25] provided a proof by construction for controllability of four-wheeled mobile robots. Later he proved controllability of a two-wheeled mobile robot with n trailers based on the analysis of Lie brackets. Jacobs and Canny [26] developed a path planning algorithm for a mobile robot with a minimum turning radius which enables to generate a robust collision-free path that is a suboptimal solution in length. Barraquand and Latombe [27] presented a path planning algorithm for a four-wheeled model under an unstructured environment and extended the result for the mobile robot with a trailer.

Latombe [28] discretized the configuration space and apply A^* algorithm to search an obstacle-free path for a four-wheeled model.

Motion Control of a Wheeled Mobile Robot

Motion control of the mobile robots are largely divided into two approaches, *i.e.,* open-loop control and closed-loop control, the latter of which is our case. For the open-loop control approach, Lafferriere and Sussmann [29] proved that a nilpotent or feedback-nilpotentizable system can be steered between two arbitrary points with control efforts along a set of P. Hall bases which consists of distributions and systematically chosen Lie brackets of a system. They also showed that two-wheeled cart, four-wheeled cart, and four-wheeled cart with a trailer are nilpotentizable by appropriate feedback transformation. Murray and Sastry [30, 31] introduced a chained form for two-input nonholonomic control systems and developed the algorithm which steers the system to the desired destination by using sinusoidal inputs. Sordalen [32] showed that a two wheeled cart model dragging n trailers can be transformed into the chained form by choosing a different set of generalized coordinates.

Brockett [33] proved that, for a control system without drift which is subjected to one or more nonholonomic constraints[1], there exists no smooth static state feedback law which asymptotically stabilizes the system to a point. This work clearly showed the direction of studies not to be pursued by presenting no existence of certain type of solutions. Based on Brockett's result, there have been several alternative approaches proposed to avoid violating his claim. Campion et al. [34] and Samson and Ait-Abderrahim[35] independently showed that although their cart models are both locally controllable and reachable, there is no pure smooth state feedback law that can locally stabilize this class of system. Kanayama et al. [36] used a two-wheeled model for tracking control and proved the asymptotic convergence of the linearized system to the desired trajectory by using a Lyapunov function. Samson and Ait-Abderrahim [37] derived the sufficient conditions in terms of desired velocities (linear velocity and steering velocity) to ensure the global convergence of a two-wheeled vehicle, and showed that the desired trajectory has to keep moving to assure asymptotic convergence. Samson [38, 39] and Pomet [40] used a time-varying state feedback control to stabilize a mobile robot to a point. Also Pomet et al. [41] proposed a hybrid strategy to improve the convergent speed, in which a time-invariant feedback is used when the system is far from the desired point and a time-varying feedback is used in the neighborhood of the desired point. Relating to [38, 39, 40, 41], Gurvits and Li [42] proved that a general affine control system without drift cannot be exponentially stabilized by any smooth time-periodic feedback law. Bloch et al. [43, 44] presented a discontinuous controller for a knife-edge example which consists of an open-loop strategy, followed by a set of discontinuous feedbacks to make the origin stable for any initial condition. Canudas de Wit and Sordalen [45] proposed a piecewise smooth controller to render the origin exponentially stable for any initial condition. Using a two-wheeled model, they showed that the convergent speed is much faster than those using time-varying feedback. Although the feedback law was not differentiable at some points, it was proved that the motion of the

[1]This is exactly the case for a wheeled mobile robot in general.

vehicle is smooth even when it passes the non-differentiable points. In our approach, the result from [37] is utilized to assure the stable motion of the mobile platform.

There is another large group of studies on mobile robots which deals with building environmental maps from visual or acoustic sensory information to enable mobile robots to enter, navigate, and explore in a well-structured environment like a hallway or a laboratory [46, 47, 48, 49, 50, 51, 52, 53, 54, 55, 56]. However, these studies consider neither vehicles with manipulators nor a system's dynamics.

Mobile Manipulators

For the coordination and control of mobile manipulators, Seraji [57] treated the base degrees-of-mobility equally with the arm degrees-of-manipulation, and solved the redundancy by introducing a user-defined additional task variable. Pin and Culioli [58] defined a weighted multi-criteria cost function which is then optimized using Newton's algorithm. Carriker et al. [58] formulated the coordination of mobility and manipulation as a non-linear optimization problem. A general cost function for point-to-point motion in Cartesian space is defined and is minimized using a simulated annealing method. Miksch and Schroeder [59] proposed a controller design for a mobile manipulator. The controller consists of a feedforward part which executes off-line optimization along the desired trajectory and a feedback part which realizes decoupling and compensation of the tracking errors. As a performance criteria to be minimized for the static optimization, they used manipulability measure, joint ranges, kinetic energy of the system, and actuator torques. This approach is computationally expensive and is suitable to global motion planning in which the desired trajectory to be followed is precisely known *a priori* while we are interested in local coordination. Liu and Lewis [60, 61] described a decentralized robust controller for a mobile robot by considering the platform and the manipulator as two separate systems with which two interconnected subsystems are stable if the unknown interconnections are bounded. Their model used for simulation consists of a two-link manipulator attached on a planar base in which the angular motion of the base is excluded, at least in their simulation, although it is included in the equation of motion. Wien [62] studied a one link manipulator on a planar vehicle, and observed the dynamic coupling between manipulator and vehicle in simulation. Joshi and Desrochers [63] considered a two link manipulator on a moving platform subject to random disturbances in its orientation. However, no linear motion or control issue of the vehicle was considered. Hootsmans [64] derived the Mobile Manipulator Jacobian Transpose Algorithm with which a manipulator achieves a desired trajectory in the presense of dynamic disturbance from a softly-suspended platform. It was shown that even with a limited sensing capability, the system is able to perform reasonably well with the proposed algorithm. But no nonholonomic constraint is taken into account. Among those previous works on mobile manipulators, only three of them [60, 62, 63, 64] mentioned or treated dynamic interaction in an explicit form. Motivation for many of these previous works stems from identifying the stability criteria so that the vehicle does not tip over. In this study, however, we are rather interested in identifying how significantly the dynamic interaction affects the performance of a mobile manipulator under an ordinary circumstance such as transporting an object.

Force Control of a Manipulator

There is an extensive literature regarding force control issues. Whitney [65] traces the development of force control algorithms and applications, also providing numerous references. For more recent review and comparison, the reader is referred to [66]. Since the early works by Inoue [67] and Paul and Shimano [68], much attention has been given to the development of active compliant motion control algorithms. Here we overview five representative force control schemes which are widely used[2]:

1. Explicit force control [71, 72, 73, 74] – This is essentially an endpoint force servo with actuator velocity feedback for damping. The active damping can be replaced by passive compliance. Force feedforward term may or may not be used.

2. Hybrid position/force control [75] – This combines conventional position control and explicit force control both of which can be implemented simultaneously in orthogonal directions along the tool coordinate axes. Some instability problems, however, were reported later by An and Hollerbach [76].

3. Stiffness control [77] – This implements a six-axis active spring in tool coordinates. The sensed forces are converted to offsets from the commanded position trajectory.

4. Damping control [78] – This implements a six-axis active damper in tool coordinates. The sensed forces are converted to offsets from the commanded velocity trajectory.

5. Impedance control [79] – A common implementation of this scheme achieves compliant motion by combining stiffness control and damping control. Errors in position, velocity, and force are used to determine the joint torque commands.

The force control scheme used in this study belongs to the first category, *i.e.,* explicit force control. More specifically, we use the Proportional-Integral control with active damping in the task coordinates plus force feedforward terms.

1.3 Scope and Outline of Thesis

The goal of this thesis is to investigate new control and coordination algorithms for a mobile manipulator. Under a coordinated environment where multiple agents need to work cooperatively for a common task as shown in Figure 1.1, there usually exists a leader-follower or master-slave relationship among the agents such that one agent takes a leadership and the follower agents support the leader for the smooth and safe execution of the common task goal, although each agent may be completely homogeneous and the relationship can be switched by necessity. However, unlike the conventional master-slave scenario in which a master agent provides a slave agent with very precise directions in

[2]For this part of review, the author owes to [69, 70]

terms of what to do (instead of *what not to do*), it is assumed that each agent possesses certain autonomy. In other words, a follower agent has a certain freedom at hand as long as it does not interfere with the accomplishment of a common goal. For instance, when two agents are to transport a large object, the leader agent follows a given trajectory which is assumed to be provided from a higher authority. The follower agent then trails the leader agent while supporting the object, but how to change the posture and how to coordinate itself is left to the follower's decision.

This thesis specifically considers the mobile manipulator in the follower's mode in addition to various problems which are innate to a mobile manipulator in general. One of the major issues is the local coordination of locomotion and manipulation which retain different kinematic and dynamic characteristics. Before this problem is addressed, the whole system has to be modeled carefully so that no misleading conclusion is reached.

Chapter 2 describes the equations of motion for a manipulator and a mobile platform separately. The reason of treating two subsystems separately is twofold. First, since a mobile platform has very unique control properties due to its nonholonomic nature, the modeling of the mobile platform should be addressed independently of the manipulator which is holonomic for the sake of clarity. Second, Chapter 3 discusses the design of the controller for the mobile platform based on the motion equations introduced in Section 2.2. Chapter 2 further derives the motion equations for the mobile manipulator in order to investigate the dynamic interaction between the manipulator and the platform. Instead of deriving the entire equations from scratch by Lagrange method which obscures the physical meaning of each term, a set of equations are derived based on the above motion equations obtained separately so that dynamic interaction forces/torques appear in an explicit form.

Chapter 3 describes the control properties and the design of nonlinear controller of wheeled mobile robots. The internal dynamics of the mobile platform including zero dynamics is also investigated by using the proposed controller. The results are verified by simulation and experiments.

Based on the controller designed in Chapter 3, the two different scenarios are tested; *dragging* and *following*. In the *dragging*, a manipulator is kept passive, *i.e.,* compensated for gravity and friction, and a human operator drags the end effector such that the whole system of mobile manipulator will largely follow the trajectory of the end effector. In the *following*, the manipulator is equipped with a force control scheme so that the mobile manipulator is able to push against an object while following the motion of the object simultaneously. Chapter 4 presents the coordination strategy of a mobile manipulator with the introduction of the concept of preferred operating regions which is used throughout the thesis. The simulation results of the dragging scenario in Chapter 4 demonstrate the efficacy of the control and coordination strategy by means of a couple of sample trajectories.

Chapter 5 describes the force control scheme and the coordination strategy which are used in the *following* scenario. Since the control algorithm for the experimental mobile platform is commonly used in both the dragging and following experiments, it will be

presented in Chapter 7.

In the above examples, the manipulator and the mobile platform are treated as separate subsystems and no consideration is made in terms of dynamic interaction between the two subsystems. This negligence does not cause a significant problem in practice if the inertia of the platform is relatively massive comparing to that of the manipulator or if the motion of the platform is very slow. If these assumptions do not hold, then the dynamic interaction should be taken into account for better performance. Based on the equations of motion derived in Section 2.3, Chapter 6 investigates the significance of the dynamic interaction by simulations. Unlike for the two previous cases, *i.e.,* dragging and following, the manipulator is position-controlled in an active manner so that the end effector traces a desired trajectory. The same coordination technique is then used to generate the motion of the mobile platform. Through some sample trajectories, Chapter 6 shows the dynamic effect of the motion of the manipulator on the mobile platform and vice versa.

Chapter 7 reports the experimental results corresponding to Chapter 4 and 5 by using a mobile manipulator which consists of a PUMA 250 robotic arm and a LABMATE platform. The description of the experimental setup is given first, followed by the control scheme. In the experiments of the dragging motion, a similar trajectory to one of those chosen for the simulation in Chapter 4 is tested for comparison purpose. For the following motion, the human operator guides the end effector along a semi-circular trajectory while resisting against the pushing manipulator. Then the motion of the manipulator which is controlled to maintain the contact force effects the platform so that the whole system results in following the motion of the human operator.

Finally, the contributions and future work are summarized in Chapter 8.

Chapter 2

Modeling of Mobile Manipulators

In this chapter, we first describe the equations of motion of a robot manipulator and of a wheeled mobile platform. Based on these equations, we then describe a method for establishing the equations of motion of a mobile manipulator which incorporates the dynamic interactions between the mobile platform and the manipulator.

2.1 Equations of Motion of Manipulators

Equations of motion for a manipulator can be obtained by forming Euler-Lagrange's equation on the basis of Lagrange's energy function. The resulting differential equations describe the motion in terms of the joint variables and the structural parameters of the manipulator. An alternative approach to the modeling of the manipulator dynamics is to consider each link as a free body and obtain the equations of motion for each link on the basis of Newton's and Euler's laws. The two methods lead to exactly the same answers, *i.e.,* the relationship between a set of generalized coordinates and corresponding generalized forces, while there exist certain merits and demerits for each method. More details of the methods can be found in any introductory book on robotics or mechanics, *e.g.,* [80, 81, 82, 83, 84, 7]. In this section, we review the equations of motion for a manipulator by using the Euler-Lagrange formulation and introduce necessary notations for deriving the equations of motion of mobile manipulators. The manipulator is assumed to be comprised of a serial chain of $n+1$ rigid links including the base. As shown in Figure 2.1, we attach an inertial frame to the base and call it frame 0. Then we choose frames 1 through n such that frame i is rigidly attached to link i. Note that the frame 0 is chosen differently when the dynamic interaction between a mobile platform and a manipulator mounted on the platform is taken into account, which will be discussed in Section 2.3.

In order to represent a relative, kinematic relationship precisely between two adjacent links, we follow the Denavit-Hartenberg convention which is commonly used as a kinematic representation method in robotics community [85]. For the sake of completeness, we briefly explain the Denavit-Hartenberg notation. We follow the convention given in [82] in terms of frame numbering scheme while some of the robotic literature use a different manner [80, 86]. Figure 2.2 shows a pair of adjacent links, link $i-1$ and link i, and their associated joints, joint $i-1$, i, and $i+1$. The relationship between the two links is described by the

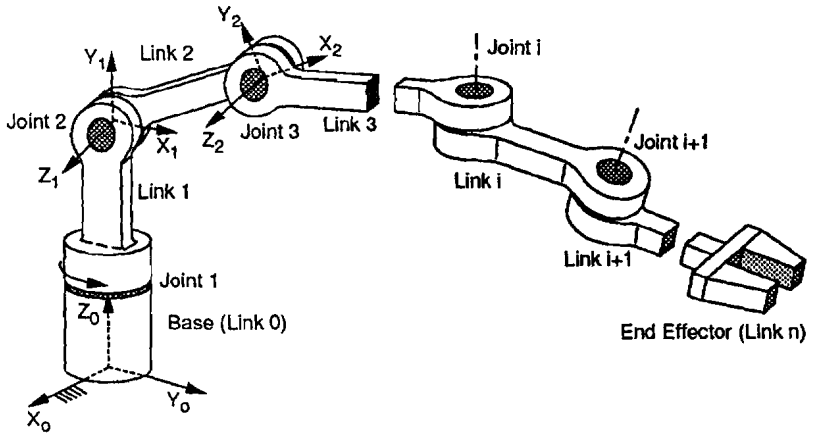

Figure 2.1: Serial manipulator with N degrees-of-freedom.

relative position and orientation of the two coordinate frames attached to the two links. The relative location of the two frames can be completely determined by the following four parameter (see Figure 2.2.)

- a_i the **length** of the common normal, equal to the shortest distance between the z_{i-1} axis and the z_i axis.
- d_i the **offset**, the distance from the origin of the $i-1$ coordinate frame to the intersection point of the z_{i-1} axis and the x_i axis measured along the z_{i-1} axis.
- α_i the **twist**, the angle between the z_{i-1} axis and the z_i axis about the x_i axis in the right-hand sense.
- θ_i the **angle** between the x_{i-1} axis and the x_i about the z_{i-1} axis in the right-hand sense.

By using the above four parameters, the following 4×4 homogeneous matrix represents the transformation from frame i to frame $i-1$.

$$A_i^{i-1} = \begin{bmatrix} \cos\theta_i & -\cos\alpha_i \sin\theta_i & \sin\alpha_i \sin\theta_i & a_i \cos\theta_i \\ \sin\theta_i & \cos\alpha_i \cos\theta_i & -\sin\alpha_i \cos\theta_i & a_i \sin\theta_i \\ 0 & \sin\alpha_i & \cos\alpha_i & d_i \\ 0 & 0 & 0 & 1 \end{bmatrix} \tag{2.1}$$

Then the transformation matrix relating frame i to the base frame (frame 0) is given by

$$T_i = A_1^0 A_2^1 \dots A_i^{i-1} \qquad i = 1, \dots, n \tag{2.2}$$

Let $q = (q_1, \dots, q_n)$ be generalized coordinates for which joint variables, $(\theta_1, \dots, \theta_n)$, are commonly chosen. Let $\mathcal{K}$ and $\mathcal{V}$ be the total kinetic energy and potential energy stored in the dynamic system. The Lagrangian is then defined by

$$\mathcal{L}(q, \dot{q}) = \mathcal{K}(q, \dot{q}) - \mathcal{V}(q) \tag{2.3}$$

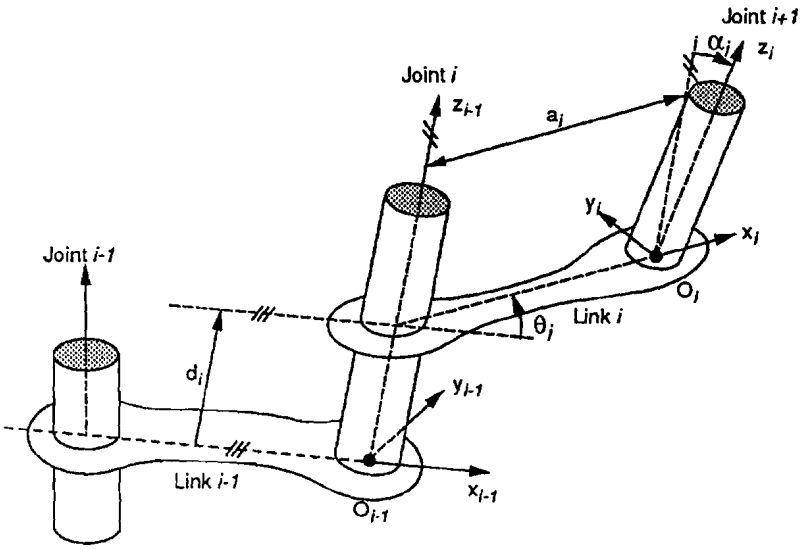

Figure 2.2: Link parameters and coordinate frames.

Using the Lagrangian, equations of motion are obtained by

$$\frac{d}{dt}\frac{\partial \mathcal{L}}{\partial \dot{q}_i} - \frac{\partial \mathcal{L}}{\partial q_i} = Q_i \qquad i = 1, \ldots, n \tag{2.4}$$

where Q_i is the generalized force corresponding to the generalized coordinate q_i.

The kinetic energy and potential energy for the link i are given by

$$\mathcal{K}_i = \frac{1}{2} trace[\sum_{j=1}^{i}\sum_{k=1}^{i} \frac{\partial T_i}{\partial q_j} J_i \frac{\partial T_i^T}{\partial q_k} \dot{q}_j \dot{q}_k] \tag{2.5}$$

$$\mathcal{V}_i = -m_i g^T T_i \bar{r}^{(i)} \tag{2.6}$$

where T_i is defined in Equation (2.2), J_i is the pseudo-inertia matrix of the link i, m_i is the mass of the link i, $g^T = [g_{ox}, g_{oy}, g_{oz}, 0]$ describes the gravitational acceleration with components in terms of the base coordinate frame, and $\bar{r}^{(i)}$ is the vector pointing from the origin of frame i to the centroid of the link with respect to frame i.

The Lagrangian motion equations for the n-link manipulator can then be represented as a second-order nonlinear differential equation:

$$\sum_{j=1}^{n} M_{ij}\ddot{q}_j + \sum_{j=1}^{n}\sum_{k=1}^{n} C_{ijk}\dot{q}_j\dot{q}_k + G_i = Q_i \qquad i = 1, \ldots, n \tag{2.7}$$

where

$$M_{ij} = \sum_{k=max(i,j)}^{n} trace[\frac{\partial T_k}{\partial q_i} J_k \frac{\partial T_k^T}{\partial q_j}] \tag{2.8}$$

$$C_{ijk} = \sum_{h=max(i,j,k)}^{n} trace[\frac{\partial T_h}{\partial q_i} J_h \frac{\partial^2 T_h^T}{\partial q_j \partial q_k}] \tag{2.9}$$

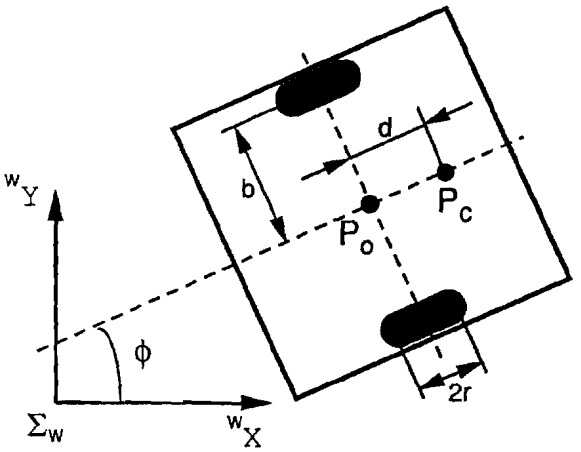

Figure 2.3: Schematic of the wheeled mobile platform.

$$G_i = \sum_{k=i}^{n} m_k g^T \frac{\partial T_k}{\partial q_i} \tilde{r}^{(i)} \tag{2.10}$$

Equation (2.7) can be rewritten as a set of second-order vector differential equations

$$M(q)\ddot{q} + C(q,\dot{q}) + G(q) = Q \tag{2.11}$$

where $M(q)$ is the symmetric inertia matrix, $C(q,\dot{q})$ is the matrix of Coriolis and centrifugal effects, the vector $G(q)$ denotes the gravity terms, and Q is the generalized force vector.

2.2 Equations of Motion of Wheeled Mobile Platforms

In this section, we describe the equations of motion of a wheeled mobile platform. Such a mobile platform is subject to both holonomic and nonholonomic constraints. Therefore, we first discuss constraint equations, followed by derivation of the motion equations. Finally, we present a state space realization of the motion equations and the constraint equations.

2.2.1 Constraint Equations

We consider a wheeled mobile platform whose schematic top view is shown in Figure 2.3. We assume that the mobile platform has two co-axis wheels driven by two independent DC motors, and has four passive supporting wheels at the corners (not shown in the figure). The following notations will be used in the derivation of the constraint equations and dynamic equations.

- P_o: the intersection of the axis of symmetry with the driving wheel axis;
- P_c: the center of mass of the platform;
- d: the distance from P_o to P_c;
- b: the distance between the driving wheels and the axis of symmetry;

r: the radius of each driving wheel;
m_c: the mass of the platform without the driving wheels and the rotors of the DC motors;
m_w: the mass of each driving wheel plus the rotor of its motor;
I_c: the moment of inertia of the platform without the driving wheels and the rotors of the motors about a vertical axis through P_o;
I_w: the moment of inertia of each wheel and the motor rotor about the wheel axis;
I_m: the moment of inertia of each wheel and the motor rotor about the wheel diameter.

The mobile platform is subject to three constraints. The first one is that the mobile robot can not move in the lateral direction, *i.e.*,

$$\dot{y}_o \cos\phi - \dot{x}_o \sin\phi = 0 \tag{2.12}$$

where (x_o, y_o) is the coordinates of point P_o in the inertia frame Σ_w, and ϕ is the heading angle of the mobile robot measured from ${}^wX$-axis. The other two constraints are that the two driving wheels roll and do not slip:

$$\dot{x}_o \cos\phi + \dot{y}_o \sin\phi + b\dot{\phi} = r\dot{\theta}_r \tag{2.13}$$

$$\dot{x}_o \cos\phi + \dot{y}_o \sin\phi - b\dot{\phi} = r\dot{\theta}_l \tag{2.14}$$

where θ_r and θ_l are the angular positions of the two driving wheels, respectively.

Let the generalized coordinates of the mobile robot be $q = (x_o, y_o, \phi, \theta_r, \theta_l)$. The three constraints can be written as follows

$$A(q)\dot{q} = 0 \tag{2.15}$$

where

$$A(q) = \begin{bmatrix} -\sin\phi & \cos\phi & 0 & 0 & 0 \\ -\cos\phi & -\sin\phi & -b & r & 0 \\ -\cos\phi & -\sin\phi & b & 0 & r \end{bmatrix} \tag{2.16}$$

We define a 5×2 dimensional matrix as follows

$$S(q) = [s_1(q)\ s_2(q)] = \begin{bmatrix} cb\cos\phi & cb\cos\phi \\ cb\sin\phi & cb\sin\phi \\ c & -c \\ 1 & 0 \\ 0 & 1 \end{bmatrix} \tag{2.17}$$

where $c = r/2b$. The two independent columns of matrix $S(q)$ are in the null space of matrix $A(q)$, that is, $A(q)S(q) = 0$. We define a distribution spanned by the columns of $S(q)$

$$\Delta = span\{s_1(q),\ \ s_2(q)\}$$

The involutivity of the distribution Δ determines the number of holonomic or nonholonomic constraints [34]. If Δ is involutive, from the Frobenius theorem [87], all the constraints are integrable (thus holonomic). If the smallest involutive distribution containing

Δ (denoted by Δ^*) spans the entire 5-dimensional space, all the constraints are nonholonomic. If $dim(\Delta^*) = 5 - k$, then k constraints are holonomic and the others are nonholonomic.

To verify the involutivity of Δ, we compute the Lie bracket of $s_1(q)$ and $s_2(q)$.

$$s_3(q) = [s_1(q),\ s_2(q)] = \frac{\partial s_2}{\partial q}s_1 - \frac{\partial s_1}{\partial q}s_2 = \begin{bmatrix} -rc\sin\phi \\ rc\cos\phi \\ 0 \\ 0 \\ 0 \end{bmatrix}$$

which is not in the distribution Δ spanned by $s_1(q)$ and $s_2(q)$. Therefore, at least one of the constraints is nonholonomic. We continue to compute the Lie bracket of $s_1(q)$ and $s_3(q)$

$$s_4(q) = [s_1(q),\ s_3(q)] = \frac{\partial s_3}{\partial q}s_1 - \frac{\partial s_1}{\partial q}s_3 = \begin{bmatrix} -rc^2\cos\phi \\ -rc^2\sin\phi \\ 0 \\ 0 \\ 0 \end{bmatrix}$$

which is linearly independent of $s_1(q)$, $s_2(q)$, and $s_3(q)$. However, the distribution spanned by $s_1(q)$,$s_2(q)$,$s_3(q)$ and $s_4(q)$ is involutive. Therefore, we have

$$\Delta^* = span\{s_1(q),\ s_2(q),\ s_3(q),\ s_4(q)\} \tag{2.18}$$

It follows that, among the three constraints, two of them are nonholonomic and the third one is holonomic. To obtain the holonomic constraint, we subtract Equation (2.13) from Equation (2.14).

$$2b\dot{\phi} = r(\dot{\theta}_r - \dot{\theta}_l) \tag{2.19}$$

Integrating the above equation and properly choosing the initial condition of ϕ, θ_r, and θ_l, we have

$$\phi = c(\theta_r - \theta_l) \tag{2.20}$$

which is clearly a holonomic constraint equation. Thus ϕ may be eliminated from the generalized coordinates.

The two nonholonomic constraints are

$$\dot{x}_o\sin\phi - \dot{y}_o\cos\phi = 0 \tag{2.21}$$

$$\dot{x}_o\cos\phi + \dot{y}_o\sin\phi = cb(\dot{\theta}_r + \dot{\theta}_l) \tag{2.22}$$

where $cb = \frac{r}{2}$ as defined early. The second nonholonomic constraint equation in the above is obtained by adding Equations (2.13) and (2.14). It is understood that ϕ is now a shorthand notation for $c(\theta_r - \theta_l)$ rather than an independent variable. We may write these two constraint equations in the matrix form

$$A(q)\dot{q} = 0 \tag{2.23}$$

where the generalized coordinate vector q is now defined as

$$q = \begin{bmatrix} q_1 \\ q_2 \\ q_3 \\ q_4 \end{bmatrix} = \begin{bmatrix} x_o \\ y_o \\ \theta_r \\ \theta_l \end{bmatrix} \tag{2.24}$$

and $A(q)$ is given by

$$A(q) = \begin{bmatrix} a_{11} & a_{12} & a_{13} & a_{14} \\ a_{21} & a_{22} & a_{23} & a_{24} \end{bmatrix} = \begin{bmatrix} -\sin\phi & \cos\phi & 0 & 0 \\ -\cos\phi & -\sin\phi & cb & cb \end{bmatrix} \tag{2.25}$$

2.2.2 Dynamic Equations

We use the Lagrange formulation to establish equations of motion for the mobile robot. The total kinetic energy of the mobile base and the two wheels is

$$K = \frac{1}{2}m(\dot{x}_o^2 + \dot{y}_o^2) + m_c cd(\dot{\theta}_r - \dot{\theta}_l)(\dot{y}_o\cos\phi - \dot{x}_o\sin\phi)$$
$$+ \frac{1}{2}I_w(\dot{\theta}_r^2 + \dot{\theta}_l^2) + \frac{1}{2}Ic^2(\dot{\theta}_r - \dot{\theta}_l)^2 \tag{2.26}$$

where

$$\begin{aligned} m &= m_c + 2m_w \\ I &= I_c + 2m_w b^2 + 2I_m \end{aligned}$$

Lagrange equations of motion for the nonholonomic mobile robot system are governed by [88]

$$\frac{d}{dt}(\frac{\partial K}{\partial \dot{q}_i}) - \frac{\partial K}{\partial q_i} = Q_i - a_{1i}\lambda_1 - a_{2i}\lambda_2, \quad i = 1, \ldots 4 \tag{2.27}$$

where q_i is the generalized coordinate defined in Equation (2.24), Q_i is the generalized force, a_{ij} is from Equation (2.25), and λ_1 and λ_2 are the Lagrange multipliers. Substituting the total kinetic energy (Equation (2.26)) into Equation (2.27), we obtain

$$m\ddot{x}_1 - m_c d(\ddot{\phi}\sin\phi + \dot{\phi}^2\cos\phi) = \lambda_1\sin\phi + \lambda_2\cos\phi \tag{2.28}$$
$$m\ddot{x}_2 + m_c d(\ddot{\phi}\cos\phi - \dot{\phi}^2\sin\phi) = -\lambda_1\cos\phi + \lambda_2\sin\phi \tag{2.29}$$
$$m_c cd(\ddot{x}_2\cos\phi - \ddot{x}_1\sin\phi) + (Ic^2 + I_w)\ddot{\theta}_1 - Ic^2\ddot{\theta}_2 = \tau_1 - cb\lambda_2 \tag{2.30}$$
$$-m_c cd(\ddot{x}_2\cos\phi - \ddot{x}_1\sin\phi) - Ic^2\ddot{\theta}_1 + (Ic^2 + I_w)\ddot{\theta}_2 = \tau_2 - cb\lambda_2 \tag{2.31}$$

where τ_1 and τ_2 are the torques acting on the two wheels. These equations can be written in the matrix form

$$M(q)\ddot{q} + C(q,\dot{q}) = E(q)\tau - A^T(q)\lambda \tag{2.32}$$

where $A(q)$ is defined in Equation (2.25) and

$$M(q) = \begin{bmatrix} m & 0 & -m_c cd\sin\phi & m_c cd\sin\phi \\ 0 & m & m_c cd\cos\phi & -m_c cd\cos\phi \\ -m_c cd\sin\phi & m_c cd\cos\phi & Ic^2 + I_w & -Ic^2 \\ m_c cd\sin\phi & -m_c cd\cos\phi & -Ic^2 & Ic^2 + I_w \end{bmatrix} \tag{2.33}$$

$$C(q,\dot{q}) = \begin{bmatrix} -m_c d\dot{\phi}^2\cos\phi \\ -m_c d\dot{\phi}^2\sin\phi \\ 0 \\ 0 \end{bmatrix} \tag{2.34}$$

$$E(q) = \begin{bmatrix} 0 & 0 \\ 0 & 0 \\ 1 & 0 \\ 0 & 1 \end{bmatrix}$$

$$\tau = \begin{bmatrix} \tau_1 \\ \tau_2 \end{bmatrix}, \qquad \lambda = \begin{bmatrix} \lambda_1 \\ \lambda_2 \end{bmatrix}$$

2.2.3 State Space Realization

In this subsection, we establish a state space realization of the motion equation (2.32) and the constraint equation (2.23). Let $S(q)$ be a 4×2 matrix

$$S(q) = [s_1(q) \quad s_2(q)] = \begin{bmatrix} cb\cos\phi & cb\cos\phi \\ cb\sin\phi & cb\sin\phi \\ 1 & 0 \\ 0 & 1 \end{bmatrix} \tag{2.35}$$

whose columns are in the null space of $A(q)$ matrix in the constraint equation (2.23), *i.e.*, $A(q)S(q) = 0$. From the constraint equation (2.23), the velocity $\dot{q}$ must be in the null space of $A(q)$. It follows that $\dot{q} \in span\{s_1(q), \ s_2(q)\}$, and that there exists a smooth vector $\eta = [\eta_1 \quad \eta_2]^T$ such that

$$\dot{q} = S(q)\eta \tag{2.36}$$

and

$$\ddot{q} = S(q)\dot{\eta} + \dot{S}(q)\eta \tag{2.37}$$

For the specific choice of $S(q)$ matrix in Equation (2.35), we have $\eta = \dot{\theta}$, where $\dot{\theta} = [\dot{\theta}_r \quad \dot{\theta}_l]^T$.

Now multiplying the both sides of Equation (2.32) by $S^T(q)$ and noticing that $S^T(q)A^T(q) = 0$ and $S^T(q)E(q) = I_{2\times 2}$ (the 2×2 identity matrix), we obtain

$$S^T(q)M(q)\ddot{q} + S^T(q)C(q,\dot{q}) = \tau \tag{2.38}$$

Substituting Equation (2.37) into the above equation, we have

$$S^T(q)M(q)(S(q)\dot{\eta} + \dot{S}(q)\eta) + S^T(q)C(q,\dot{q}) = \tau \tag{2.39}$$

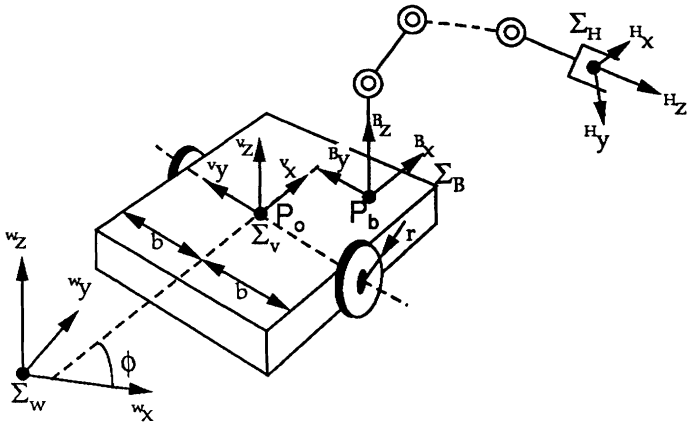

Figure 2.4: Schematic of the mobile manipulator.

By choosing the following state variable

$$x = \begin{bmatrix} x_1 \\ x_2 \\ x_3 \\ x_4 \\ x_5 \\ x_6 \end{bmatrix} = \begin{bmatrix} x_o \\ y_o \\ \theta_r \\ \theta_l \\ \eta_1 \\ \eta_2 \end{bmatrix} = \begin{bmatrix} q \\ \eta \end{bmatrix} \tag{2.40}$$

we may represent the motion equation (2.39) in the state space form

$$\dot{x} = f(x) + g(x)\tau \tag{2.41}$$

where

$$f(x) = \begin{bmatrix} S\eta \\ -(S^T M S)^{-1}(S^T M \dot{S}\eta + S^T V) \end{bmatrix}$$

$$g(x) = \begin{bmatrix} 0 \\ (S^T M S)^{-1} \end{bmatrix}$$

It is noted that the dependent variables for each term have been omitted in the above representation for clarity. All the terms are functions of the state variable x only. Since $\dot{q}$ is not part of the state variable, it is replaced by $S(q)\eta$.

2.3 Equations of Motion of Mobile Manipulators

In this section, we present the equations of motion for a mobile manipulator in such a way that the dynamic interaction between the mobile platform and the manipulator appears explicitly in the equations, which will be utilized in Chapter 6. Figure 2.4 shows the schematic of the mobile manipulator considered here.

The motion equation of the manipulator subject to the vehicle motion is given by the following form[1] [60].

$$M_r(q_r)\,\ddot{q}_r + C_{r1}(q_r, \dot{q}_r) + C_{r2}(q_r, \dot{q}_r, \dot{q}_v) = \tau_r - R_r(q_r, q_v)\,\ddot{q}_v \tag{2.42}$$

where q_r denotes the n-dimensional Lagrangian coordinates of the manipulator, M_r is the inertia matrix[2] whose elements have been defined by Equation (2.8), C_{r1} represents Coriolis and centrifugal terms given by the Equation (2.9), C_{r2} denotes Coriolis and centrifugal terms caused by the angular motion of the platform, τ_r is the input torque/force for the manipulator, and R_r is the inertia matrix which represents the effect of the vehicle dynamics on the manipulator. Comparing Equation (2.42) with Equation (2.7), we note that $C_{r2}(q_r, \dot{q}_r, \dot{q}_v)$ and $R_r(q_r, q_v)\,\ddot{q}_v$ are the terms added to the equation of motion of the manipulator. They represent the dynamic interaction caused by the motion of the mobile platform. The expressions for C_{r2} and R_r are given below.

Suppose that the configuration of a platform is uniquely determined by m independent variables[3], $q_v = [q_{v1}, q_{v2}, \ldots, q_{vm}]^T$. Letting the homogeneous transformation matrix from the base frame (Σ_B) of the manipulator to the inertial frame (Σ_w) denoted by $T_v(q_v)$, the transformation matrix, $\mathcal{T}_i$ from the i-th frame of the manipulator which is now mounted on the platform to the inertial frame is given by

$$\mathcal{T}_i = T_v\, A_1^0\, A_2^1 \ldots A_i^{i-1} \qquad i = 1, \ldots, n \tag{2.43}$$

With the aid of $\mathcal{T}_i$, the elements of C_{r2} and R_v are given by the following formulations.

$$\begin{aligned} C_{r2}^{(i)} &= 2\sum_{j=1}^{m}\sum_{k=1}^{n}\sum_{h=max(i,k)}^{n} trace\left[\frac{\partial \mathcal{T}_h}{\partial q_i}\, J_h\, \frac{\partial \mathcal{T}_h^T}{\partial q_{v,j}\partial q_k}\right]\dot{q}_{v,j}\cdot\dot{q}_k + \\ &\quad \sum_{j=1}^{m}\sum_{k=1}^{m}\sum_{h=i}^{n} trace\left[\frac{\partial \mathcal{T}_h}{\partial q_i}\, J_h\, \frac{\partial \mathcal{T}_h^T}{\partial q_{v,j}\partial q_{v,k}}\right]\dot{q}_{v,j}\cdot\dot{q}_{v,k} \end{aligned} \tag{2.44}$$

$$R_r^{(ij)} = \sum_{k=i}^{n} trace\left[\frac{\partial \mathcal{T}_k}{\partial q_i}\, J_k\, \frac{\partial \mathcal{T}_k^T}{\partial q_{v,j}}\right] \qquad 1 \le i \le n,\ 1 \le j \le m \tag{2.45}$$

The first term in the RHS of Equation (2.44) characterizes Coriolis effect on link i of manipulator due to the coupling of velocities of link k of manipulator and variable $q_{v,j}$ of platform where $1 \le j \le m$ and $1 \le k \le n$. Functional dependence of $C_{r2}^{(i)}$ with respect to q_v is also explained in Appendix B. Similarly, the second term represents the totality of centrifugal forces exerted on link i by $\dot{q}_{v,j}$ of platform if $j = k$, and Coriolis forces exerted on link i due to the velocity coupling of two platform coordinates, *i.e.*, $q_{v,j}$ and $q_{v,k}$ where $j \neq k$.

[1] Note that the gravity term is hereafter dropped from the motion equation of the manipulator unless noted otherwise, since only the planar motion is taken into account for the platform, *i.e.*, no translation along the inertial z-axis or no pitching/rolling motion considered.

[2] The functional dependence of $M_r^{(ij)}$ is described in Appendix A to show that the matrix is independent of the platform variables, q_v, by using a similar method to [89].

[3] This m should not be confused with the number of kinematic constraints in the previous section.

Collecting the velocity terms into C_r, Equation (2.42) then simplifies to

$$M_r(q_r)\,\ddot{q}_r + C_r(q_r, \dot{q}_r, \dot{q}_v) = \tau_r - R_r(q_r, q_v)\,\ddot{q}_v \tag{2.46}$$

Next, the motion equation of the platform has the following form [60, 90]:

$$\begin{aligned} M_{v1}(q_v)\,\ddot{q}_v + C_{v1}(q_v, \dot{q}_v) + C_{v2}(q_r, q_v, \dot{q}_r, \dot{q}_v) \\ = E_v\,\tau_v - A^T\,\lambda - M_{v2}(q_r, q_v)\,\ddot{q}_v - R_v(q_r, q_v)\,\ddot{q}_r \end{aligned} \tag{2.47}$$

where M_{v1} and C_{v1} are the mass inertia matrix and the velocity dependent terms of the platform which are defined in Equations (2.33) and (2.34), respectively, M_{v2} and C_{v2} represent the inertial term and Coriolis and centrifugal terms due to the presence of the manipulator, τ_v is the input torque to the vehicle, E_v is a constant matrix, λ denotes the vector of Lagrange multipliers corresponding to the kinematic constraints, and R_v represents the inertia matrix which reflects the dynamic effect of the arm motion on the vehicle. Note that R_v is obtained by transposing R_r (compare Equations (2.45) and (2.50)). The three terms of Equation (2.47) which are not present in the equation of the platform alone, Equation (2.32), are defined by the following formulations.

$$M_{v2}^{(ij)} = \sum_{k=1}^{n} trace\left[\frac{\partial \mathcal{T}_k}{\partial q_{v,i}}\,J_k\,\frac{\partial \mathcal{T}_k^T}{\partial q_{v,j}}\right] \qquad 1 \le i, j \le m \tag{2.48}$$

$$\begin{aligned} C_{v2}^{(i)} = {} & 2\sum_{j=1}^{n}\sum_{k=1}^{m}\sum_{h=j}^{n} trace\left[\frac{\partial \mathcal{T}_h}{\partial q_{v,i}}\,J_h\,\frac{\partial \mathcal{T}_h^T}{\partial q_j \partial q_{v,k}}\right]\dot{q}_j\,\dot{q}_{v,k} + \\ & \sum_{j=1}^{n}\sum_{k=1}^{n}\sum_{h=max(j,k)}^{n} trace\left[\frac{\partial \mathcal{T}_h}{\partial q_{v,i}}\,J_h\,\frac{\partial \mathcal{T}_h^T}{\partial q_j \partial q_k}\right]\dot{q}_j\,\dot{q}_k \end{aligned} \tag{2.49}$$

$$R_v^{(ij)} = \sum_{k=j}^{n} trace\left[\frac{\partial \mathcal{T}_k}{\partial q_{v,i}}\,J_k\,\frac{\partial \mathcal{T}_k^T}{\partial q_j}\right] \qquad 1 \le i \le m,\ 1 \le j \le n \tag{2.50}$$

The first term in the RHS of Equation (2.49) characterizes Coriolis effect on platform coordinate $q_{v,i}$ due to the coupling of velocities of link j of manipulator and platform coordinate $q_{v,k}$ where $1 \le j \le n$ and $1 \le k \le m$. The second term represents the sum of centrifugal forces exerted on platform coordinate $q_{v,i}$ by link j of manipulator if $j = k$, and Coriolis forces exerted on $q_{v,k}$ due to the velocity coupling of two different links of manipulator.

Collecting the inertial terms and the velocity terms of Equation (2.47) into M_v and C_v, respectively, it simplifies to

$$M_v(q_r, q_v)\,\ddot{q}_v + C_v(q_r, q_v, \dot{q}_r, \dot{q}_v) = E_v\,\tau_v - A^T\,\lambda - R_v(q_r, q_v)\,\ddot{q}_r \tag{2.51}$$

Next, we represent the motion equations of the mobile manipulators in the state space form. Using Equations (2.36) and (2.37), and multiplying Equation (2.51) by S^T, we have

$$S^T(M_v S\dot{\eta} + M_v\dot{S}\eta + C_v) = S^T E_v\tau_v - S^T R_v\ddot{q}_r \tag{2.52}$$

by noting that $S^T A^T = 0$.

Similarly substituting $\ddot{q}_v$ into Equation (2.46), we have

$$M_r\ddot{q}_r + C_r = \tau_r - R_r\dot{S}\eta - R_rS\dot{\eta}. \tag{2.53}$$

Using the state space variable $x = [{q_v}^T\ {q_r}^T\ \eta^T\ {\dot{q}_r}^T]^T$, we obtain

$$\dot{x} = \begin{bmatrix} S\eta \\ \dot{q}_r \\ P^{-1}\xi \end{bmatrix} + \begin{bmatrix} 0 \\ 0 \\ P^{-1}Q \end{bmatrix} \tau \tag{2.54}$$

where

$$P = \begin{bmatrix} S^TM_vS & S^TR_v \\ SR_r & M_r \end{bmatrix} \quad Q = \begin{bmatrix} S^TE_v & 0 \\ 0 & I \end{bmatrix}$$

$$\xi = \begin{bmatrix} -S^TM_v\dot{S}\eta - S^TC_v \\ -C_r - R_r\dot{S}\eta \end{bmatrix} \qquad \tau = \begin{bmatrix} \tau_v \\ \tau_r \end{bmatrix}$$

Applying the following feedback,

$$\tau = Q^{-1}(Pu - \xi) \tag{2.55}$$

we simplify the state equation as:

$$\dot{x} = \begin{bmatrix} S\eta \\ \dot{q}_r \\ 0 \end{bmatrix} + \begin{bmatrix} 0 \\ 0 \\ I \end{bmatrix} u \tag{2.56}$$

Chapter 3

Feedback Control of Wheeled Mobile Platforms

In this chapter, we discuss feedback control of wheeled mobile platforms whose dynamic model has been established in Section 2.2. The discussion is focused on feedback linearization of the dynamic system characterizing wheeled mobile platforms. We first show that the system of wheeled mobile platform (in fact, any dynamic system subject to nonholonomic constraints) is not input-state linearizable by using any smooth static state feedback. We then investigate the input-output linearization and decoupling of the system. Two types of outputs have been addressed. In the first type of output, the center point of the mobile robot on the wheel axis is intended to be controlled. It is known that the point on the wheel axis cannot be controlled using a *static* feedback [91, 92]. We show that the center point can be controlled to track a trajectory by using a *dynamic* nonlinear feedback. The dynamic feedback for achieving the input-output linearization and decoupling has been developed through a three-step algorithm. The second output takes the coordinates of a reference point in front of the mobile robot. The input-output linearization of the system under this output is possible by simply using a static nonlinear feedback.

We also investigate the internal dynamics of the mobile platform system in this chapter. Of particular interest is that the system has unstable internal dynamics under the look-ahead control. The unstable behavior is confirmed by numerical simulations and physical experiments.

3.1 Input-State Linearization

In this section, we study the input-state linearization of the control system (2.41) described in Section 2.2 using static state feedback. To simplify the discussion, we first apply the following state feedback

$$\begin{aligned} \tau &= \alpha^1(x) + \beta^1(x)\mu \\ &= (S^T M \dot{S}\eta + S^T V) + (S^T M S) S^T E \mu \end{aligned} \tag{3.1}$$

where μ is the new input variable. The closed-loop system becomes

$$\dot{x} = f^1(x) + g^1(x)\mu \tag{3.2}$$

where

$$f^1(x) = \begin{bmatrix} S\eta \\ 0 \end{bmatrix}, \qquad g^1(x) = \begin{bmatrix} 0 \\ I_{2\times 2} \end{bmatrix}$$

Theorem 1 *System (3.2) is not input-state linearizable by a smooth state feedback.*

Proof: If the system is input-state linearizable, it has to satisfy two conditions : the strong accessibility condition and the involutivity condition [93, p.179]. We will show that the system does not satisfy the involutivity condition.

Define a sequence of distributions

$$D_j = span\{L^i_{f^1} g^1 \mid i = 0, 1, \ldots, j-1\}, \quad j = 1, 2, \ldots$$

Then the involutivity condition requires that the distributions D_1, D_2, ..., D_6 be all involutive, with 6 being the dimension of the system. $D_1 = span\{g^1\}$ is involutive since g^1 is constant. Next we compute

$$L_{f^1} g^1 = [f^1, g^1] = \frac{\partial g^1}{\partial x} f^1 - \frac{\partial f^1}{\partial x} g^1 = -\begin{bmatrix} S(q) \\ 0 \end{bmatrix}$$

It is easy to verify that the distribution spanned by the columns of $S(q)$ is not involutive. (Actually, if the distribution were involutive, the two constraints (2.21) and (2.22) would be holonomic.) It follows that the distribution $D_2 = span\{g^1, L_{f^1} g^1\}$ is not involutive. Therefore, the system is not input-state linearizable.

Corollary 1 *System (2.41) is not input-state linearizable by a smooth state feedback.*

Proof: A proof similar to that of Theorem 1 can be carried out. Alternatively, system (3.2) can be regarded as a special case of system (2.41).

3.2 Input-Output Linearization and Decoupling

Although the dynamic system of a wheeled mobile robot is not input-state linearizable as shown in the previous section, it may be input-output linearizable. In this section, we study the input-output linearization of two types of outputs. First, the coordinates of the center point P_o are chosen as the output equation. It will be shown that the input-output linearization is not possible by using static state feedback, but is possible by using a dynamic state feedback. Second, the coordinates of a reference point P_r in front of the mobile robot is chosen as the output equation. In this case, the input-output linearization can be achieved by using a static state feedback. Nevertheless, the internal dynamics when the mobile robot moves backwards is unstable.

3.2.1 Controlling the Center Point P_o

Since the mobile robot has two inputs, we may choose an output equation with two independent components. A natural choice for the output equation is the coordinates of the center point P_o, *i.e.*,

$$y = h(x) = \begin{bmatrix} x_1 \\ x_2 \end{bmatrix}. \tag{3.3}$$

Together with this output equation, we will consider the state equation (3.2), assuming that the nonlinear feedback (3.1) is applied to cancel the dynamic nonlinearity. To verify if the system is input-output linearizable, we compute the time derivatives of y.

$$\dot{y} = \frac{\partial h}{\partial x}\dot{x} = \frac{\partial h}{\partial x}\left(f^1(x) + g^1(x)\mu\right) = S_1(x)\eta$$

where

$$S_1(x) = \begin{bmatrix} cb\cos\phi & cb\cos\phi \\ cb\sin\phi & cb\sin\phi \end{bmatrix}$$

Since $\dot{y}$ is not a function of the input μ, we differentiate once more.

$$\ddot{y} = S_1(x)\dot{\eta} + \dot{S}_1(x)\eta = S_1(x)\mu + \dot{S}_1(x)\eta \tag{3.4}$$

where the second term on the right-hand side is evaluated to be

$$\dot{S}_1(x)\eta = c^2 b(\eta_1^2 - \eta_2^2)\begin{bmatrix} -\sin\phi \\ \cos\phi \end{bmatrix}$$

Now that $\ddot{y}$ is a function of the input μ, the decoupling matrix of the system is $S_1(x)$. Since $S_1(x)$ is singular, the system is not input-output linearizable and the output can not be decoupled by using any static state feedback [94, 95, 91].

3.2.2 Dynamic Feedback Control

As shown above, the mobile robot under the output equation (3.3) is not input-output linearizable with any static feedback of the form

$$\mu = \alpha(x) + \beta(x)u \tag{3.5}$$

Nevertheless the input-output linearization may be achieved by using a dynamic feedback of the form [93, 96]

$$\dot{\xi} = f_\xi(x,\xi) + g_\xi(x,\xi)u \tag{3.6}$$

$$\mu = \alpha(x,\xi) + \beta(x,\xi)u \tag{3.7}$$

We follow the dynamic extension algorithm [93, pp.258-269] to derive $f_\xi(\cdot,\cdot)$, $g_\xi(\cdot,\cdot)$, $\alpha(\cdot,\cdot)$, and $\beta(\cdot,\cdot)$ if they exist at all. We divide the algorithm into three steps.

Step 1: Since the rank of the decoupling matrix $S_1(x)$ in Equation (3.4) is *one*, we first apply a static feedback to linearize and decouple *one* output from the others. For the

mobile robot, there are two outputs $y = [y_1 \quad y_2]^T$. We choose to linearize y_1 and decouple it from y_2. Substituting the following static feedback into Equation (3.4)

$$\mu = \alpha^2(x) + \beta^2(x)u = \begin{bmatrix} c(\eta_1^2 - \eta_2^2)\tan\phi \\ 0 \end{bmatrix} + \begin{bmatrix} \frac{1}{cb\cos\phi} & 1 \\ 0 & -1 \end{bmatrix} \begin{bmatrix} u_1 \\ u_2 \end{bmatrix} \tag{3.8}$$

the closed-loop input-output map is then

$$\ddot{y} = \begin{bmatrix} 0 \\ c^2 b(\eta_1^2 - \eta_2^2)\frac{1}{\cos\phi} \end{bmatrix} + \begin{bmatrix} 1 & 0 \\ \tan\phi & 0 \end{bmatrix} \begin{bmatrix} u_1 \\ u_2 \end{bmatrix} \tag{3.9}$$

It is clear that $\ddot{y}_1 = u_1$, that is, the first output y_1 is linearized and controlled only by u_1. Thus u_1 can be designed to achieve the performance requirements for y_1. On the other hand, y_2 is still nonlinear. Further, it is also driven by u_1.

Step 2: We substitute the static feedback (3.8) into Equation (3.2) to obtain the new state equation

$$\begin{aligned} \dot{x} &= f^1(x) + g^1(x)\mu \\ &= f^1(x) + g^1(x)\left(\alpha^2(x) + \beta^2(x)u\right) \\ &= \begin{bmatrix} S\eta \\ c(\eta_1^2 - \eta_2^2)\tan\phi \\ 0 \end{bmatrix} + \begin{bmatrix} 0 & 0 \\ \frac{1}{cb\cos\phi} & 1 \\ 0 & -1 \end{bmatrix} \begin{bmatrix} u_1 \\ u_2 \end{bmatrix} \\ &= f^2(x) + g^2(x)u \end{aligned} \tag{3.10}$$

We now differentiate the second output with respect to the new state equation $\dot{x} = f^2(x) + g^2(x)u$, hoping that u_2 will appear in the derivative of y_2. In the following differentiation, u_1 is treated as a (time-varying) parameter.

$$\begin{aligned} \dot{y}_2 &= cb(\eta_1 + \eta_2)\sin\phi \\ \ddot{y}_2 &= c^2 b(\eta_1^2 - \eta_2^2)\frac{1}{\cos\phi} + \tan\phi\, u_1 \\ y_2^{(3)} &= c^3 b(\eta_1^2 - \eta_2^2)(\eta_1 - \eta_2)\frac{\sin\phi}{\cos^2\phi} + \tan\phi\dot{u}_1 \\ &\quad + \frac{2c^2 b\eta_1}{\cos\phi}\left(c(\eta_1^2 - \eta_2^2)\tan\phi + \frac{u_1}{cb\cos\phi}\right) \\ &\quad + c(\eta_1 - \eta_2)\frac{u_1}{\cos^2\phi} + \frac{2c^2 b(\eta_1 + \eta_2)}{\cos\phi}u_2 \end{aligned}$$

It is seen that u_2 appears in the third-order derivative of y_2. We note that $y_2^{(3)}$ has the following structure

$$y_2^{(3)} = Q_1(x) + Q_2(x)u_1 + Q_3\dot{u}_1 + Q_4 u_2 \tag{3.11}$$

where $Q_i(x)$ can be easily identified.

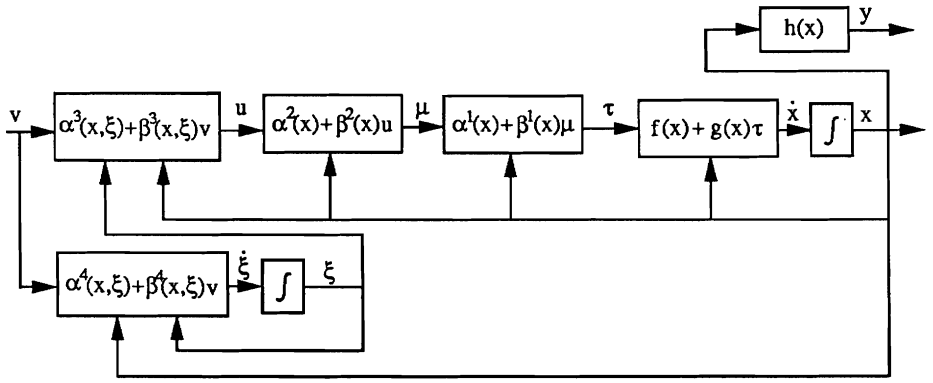

Figure 3.1: Dynamic feedback controller of a mobile robot.

Step 3: Noting Equation (3.11), y_2 will be linearized if we apply the following feedback

$$u_2 = Q_4^{-1}(x)\,(v_2 - Q_1(x) - Q_2(x)u_1 - Q_3(x)\dot{u}_1) \tag{3.12}$$

with $v = [v_1,\ v_2]^T$ being the reference input. However, this feedback depends on $\dot{u}_1$, which can be eliminated by introducing an integrator on the first input channel. Formally, we utilize the following dynamic feedback

$$\dot{\xi} = \alpha^4(x,\xi) + \beta^4(x,\xi)v \tag{3.13}$$
$$u = \alpha^3(x,\xi) + \beta^3(x,\xi)v \tag{3.14}$$

where ξ is one-dimensional and

$$\alpha^4(x,\xi) = 0$$
$$\beta^4(x,\xi) = [1\ \ 0]$$
$$\alpha^3(x,\xi) = \begin{bmatrix} \xi \\ -Q_4^{-1}(x)(Q_1(x) + Q_2\xi) \end{bmatrix}$$
$$\beta^3(x,\xi) = \begin{bmatrix} 0 & 0 \\ -Q_4^{-1}(x)Q_3(x) & Q_4^{-1}(x) \end{bmatrix}$$

After applying the above dynamic feedback, we finally obtain two linearized and decoupled subsystems:

$$y_1^{(3)} = v_1 \tag{3.15}$$
$$y_2^{(3)} = v_2 \tag{3.16}$$

It is noted that the first subsystem is now of third order due to the introduction of the integrator on its input channel. This concludes the dynamic extension algorithm.

The overall dynamic feedback control of the mobile robot is depicted in Figure 3.1. The first feedback (3.1) is to cancel the dynamic nonlinearity in order to simplify the subsequent discussion. The second feedback (3.8) is to linearize y_1 and also decouple it from y_2. The third feedback represented by Equations (3.13) and (3.14) is to linearize y_2.

Finally we comment on the invertibility of the system [97, 98]. Since the differential output rank ρ^* of this particular system is computed by [96]

$$\rho^* = rank\left(\frac{\partial y^{(3)}}{\partial v}\right) = 2$$

which is equal to the number of outputs, the system is right-invertible [97]. This guarantees the success of the above dynamic extension algorithm since a right-invertible system can always be locally decoupled via a dynamic state feedback [97]. Furthermore, since the different output rank is equal to the number of inputs, the system is also left-invertible [98].

3.2.3 Look-Ahead Control

In Section 3.2.1, we showed that the center point P_o of the mobile robot cannot be controlled by using a static feedback. A dynamic feedback is necessary. In this section, we present an alternative control method. The method is motivated from vehicle maneuvering. When operating a vehicle, a driver looks at a point or an area in front of the vehicle. We define a reference point P_r which is L distance (called look-ahead distance) from P_o (see Figure 2.3). We take the coordinates of P_r in the fixed coordinate frame as the output equation, *i.e.*,

$$y = h(x) = \begin{bmatrix} x_1 + L\cos\phi \\ x_2 + L\sin\phi \end{bmatrix} \tag{3.17}$$

To verify if the system is input-output linearizable with this output equation, we compute the derivatives of y.

$$\begin{aligned} \dot{y} = \frac{\partial h}{\partial x}\dot{x} &= \frac{\partial h}{\partial x}\left(f^1(x) + g^1(x)\mu\right) \\ &= \begin{bmatrix} cb\cos\phi - cL\sin\phi & cb\cos\phi + cL\sin\phi \\ cb\sin\phi + cL\cos\phi & cb\sin\phi - cL\cos\phi \end{bmatrix} \begin{bmatrix} \eta_1 \\ \eta_2 \end{bmatrix} = \Phi(x)\eta \end{aligned}$$

Since $\dot{y}$ is not a function of the input μ, we differentiate it once more.

$$\ddot{y} = \Phi(x)\dot{\eta} + \dot{\Phi}(x)\eta = \Phi(x)\mu + \dot{\Phi}(x)\eta$$

The input μ shows up in the second order derivative of y. Clearly, the decoupling matrix in this case is $\Phi(x)$. Since the determinant of $\Phi(x)$ is $(-2c^2bL)$, it is nonsingular as long as the look-ahead distance L is not zero. It follows that the system can be input-output linearized and decoupled [93]. The nonlinear feedback for achieving the input-output linearization and decoupling is

$$\mu = \Phi^{-1}(x)\left(u - \dot{\Phi}(x)\eta\right) \tag{3.18}$$

Applying this nonlinear feedback, we obtain

$$\ddot{y}_1 = u_1 \tag{3.19}$$

$$\ddot{y}_2 = u_2 \tag{3.20}$$

Therefore, the mobile robot can be controlled so that the reference point P_r tracks a desired trajectory. The motion of the mobile robot itself, particularly the motion of the center point P_o, is determined by the internal dynamics of the system which is the topic of the next section. We note that the look-ahead control method degenerates to the control of the center point if $L = 0$.

3.3 Internal Dynamics

3.3.1 Derivation of Internal Dynamics

In this section, we study the behavior of the internal dynamics including the zero dynamics of the mobile platform system under the look-ahead control. For a general discussion of internal dynamics and zero dynamics, see Chapter 6 of [99] or [100].

We first construct a diffeomorphism by which the overall system can be represented in the norm form of nonlinear systems [99]. Since the relative degree of each output is two, we may construct four components of the needed diffeomorphism from the two outputs and its Lie derivative, *i.e.*, $h_1(x)$, $L_f h_1(x)$, $h_2(x)$ and $L_f h_2(x)$. Since the state variable x is six dimensional, we need two more components. We choose the two components to be θ_r and θ_l. Thus the proposed diffeomorphic transformation would be

$$z = T(x) = \begin{bmatrix} z_1 \\ z_2 \\ z_3 \\ z_4 \\ z_5 \\ z_6 \end{bmatrix} = \begin{bmatrix} h_1(x) \\ L_f h_1(x) \\ h_2(x) \\ L_f h_2(x) \\ \theta_r \\ \theta_l \end{bmatrix} \tag{3.21}$$

To verify that $T(x)$ is indeed a diffeomorphism, we compute its Jacobian.

$$\frac{\partial T}{\partial x} = \begin{bmatrix} 1 & 0 & -cL\sin\phi & cL\sin\phi & 0 & 0 \\ 0 & 0 & * & * & cb\cos\phi - cL\sin\phi & cb\cos\phi + cL\sin\phi \\ 0 & 1 & cL\cos\phi & -cL\cos\phi & 0 & 0 \\ 0 & 0 & * & * & cb\sin\phi + cL\cos\phi & cb\sin\phi - cL\cos\phi \\ 0 & 0 & 1 & 0 & 0 & 0 \\ 0 & 0 & 0 & 1 & 0 & 0 \end{bmatrix}$$

It is easy to check that $\frac{\partial T}{\partial x}$ has full rank[1]. Thus $T(x)$ is a valid state space transformation. The inverse transformation $x = T^{-1}(z)$ is given by

$$\begin{aligned} x_1 &= z_1 - L\cos(cz_5 - cz_6) \\ x_2 &= z_3 - L\sin(cz_5 - cz_0) \\ \theta_r &= z_5 \\ \theta_l &= z_6 \end{aligned}$$

[1]The terms denoted by $*$ do not affect the computation of the rank.

$$\begin{bmatrix} \eta_1 \\ \eta_2 \end{bmatrix} = \Phi^{-1} \begin{bmatrix} z_2 \\ z_4 \end{bmatrix}$$

We partition the state variable z into two blocks

$$\begin{aligned} z^1 &= \begin{bmatrix} z_1 & z_2 & z_3 & z_4 \end{bmatrix}^T \\ z^2 &= \begin{bmatrix} z_5 & z_6 \end{bmatrix}^T \end{aligned}$$

After applying the feedback (3.18), the system of the mobile robot is represented in the following normal form.

$$\dot{z}^1 = Az^1 + Bu \tag{3.22}$$

$$\dot{z}^2 = w(z^1,\ z^2) \tag{3.23}$$

$$y = Cz^1 \tag{3.24}$$

where

$$A = \begin{bmatrix} 0 & 1 & 0 & 0 \\ 0 & 0 & 0 & 0 \\ 0 & 0 & 0 & 1 \\ 0 & 0 & 0 & 0 \end{bmatrix}, \qquad B = \begin{bmatrix} 0 & 0 \\ 1 & 0 \\ 0 & 0 \\ 0 & 1 \end{bmatrix}, \qquad C = \begin{bmatrix} 1 & 0 & 0 & 0 \\ 0 & 0 & 1 & 0 \end{bmatrix}$$

$$w(z^1,\ z^2) = \Phi^{-1}(z) \begin{bmatrix} z_2 \\ z_4 \end{bmatrix} = -\frac{1}{2c^2bL} \begin{bmatrix} cb\sin\phi - cL\cos\phi & -cb\cos\phi - cL\sin\phi \\ -cb\sin\phi - cL\cos\phi & cb\cos\phi - cL\sin\phi \end{bmatrix} \begin{bmatrix} z_2 \\ z_4 \end{bmatrix}$$

It is understood that ϕ in the expression of $w(z^1,\ z^2)$ is a short-hand notation for $c(z_5 - z_6)$. Together, the linear state equation (3.22) and the linear output equation (3.24) are an equivalent representation of the input-output map (Equations (3.19) and (3.20)). Equation (3.23) represents the unobservable internal dynamics of the mobile robot under the look-ahead control.

The zero dynamics of a control system is defined as the dynamics of the system when the outputs are identically zero (*i.e.*, $y = 0$, $\dot{y} = 0$, $\ddot{y} = 0$, ...). If the outputs are identically zero, it implies that $z^1 = 0$, and the zero dynamics is

$$\dot{z}^2 = w(0,\ z^2) = 0 \tag{3.25}$$

Thus, z^2 remains constant while the outputs are identically zero. The zero dynamics is stable but not asymptotically stable. In other words, if the reference point P_r remains still, so does the mobile robot (or more specifically, the wheels do not move).

We now look at the internal dynamics while the reference point is in motion. More specifically, we are interested in the internal motion of the mobile robot when it moves straight forward or backward. Let the mobile robot be initially headed in the positive $\mathbf{X}_1$ direction. We assume that the reference point is controlled to move in the negative $\mathbf{X}_1$ direction. The velocity of the reference point is then

$$\begin{bmatrix} \dot{y}_1 \\ \dot{y}_2 \end{bmatrix} = \begin{bmatrix} z_2 \\ z_4 \end{bmatrix} = \begin{bmatrix} -\epsilon(t) \\ 0 \end{bmatrix}$$

where $\epsilon(t) > 0$. Substituting this into the internal dynamics (3.23), we obtain

$$\begin{bmatrix} \dot{z}_5 \\ \dot{z}_6 \end{bmatrix} = \frac{\epsilon(t)}{2c^2bL} \begin{bmatrix} cb\sin\phi - cL\cos\phi \\ -cb\sin\phi - cL\cos\phi \end{bmatrix}$$

A solution of this internal dynamics is

$$z_5^* = -\frac{1}{r}t + c_1 \tag{3.26}$$

$$z_6^* = -\frac{1}{r}t + c_1 \tag{3.27}$$

where c_1 is a constant. That is, the two wheels rotate at exactly the same angular velocity and the mobile platform moves straight in the negative $\mathbf{X}_1$ direction.

We now study the stability of the internal motion described by Equations (3.26) and (3.27). We first change the state variable so that the stability of the internal motion in z^2 can be formulated as the stability of equilibrium points in ζ.

$$\zeta_1 = z_5 - z_5^*$$

$$\zeta_2 = z_6 - z_6^*$$

We may express the internal dynamics in terms of $\zeta = \begin{bmatrix} \zeta_1 & \zeta_2 \end{bmatrix}^T$.

$$\dot{\zeta} = \begin{bmatrix} \dot{\zeta}_1 \\ \dot{\zeta}_2 \end{bmatrix} = \frac{\epsilon(t)}{2c^2bL} \begin{bmatrix} cb\sin(c\zeta_1 - c\zeta_2) - cL\cos(c\zeta_1 - c\zeta_2) \\ -cb\sin(c\zeta_1 - c\zeta_2) - cL\cos(c\zeta_1 - c\zeta_2) \end{bmatrix} + \begin{bmatrix} \frac{1}{r} \\ \frac{1}{r} \end{bmatrix}$$

This system has an equilibrium subspace characterized by

$$E_\zeta = \{\zeta \mid \zeta_1 = \zeta_2\}$$

We may not draw any conclusion based on the linear approximation of the internal dynamics which has an eigenvalue at the origin. We will utilize the Lyapunov method to establish the stability condition. Consider the following candidate for a Lyapunov function

$$V(\zeta) = 1 - \cos(c\zeta_1 - c\zeta_2)$$

In a neighborhood of E_ζ, $V(\zeta) = 0$ if $\zeta \in E_\zeta$, and $V(\zeta) > 0$ if $\zeta \notin E_\zeta$. Thus $V(\zeta)$ is positive definite with respect to E_ζ, and may serve as a Lyapunov function for testing the stability of E_ζ. We compute the derivative of $V(\zeta)$ with respect to the time

$$\dot{V}(\zeta) = \frac{\partial V}{\partial \zeta}\dot{\zeta} = \frac{\epsilon(t)}{L}\sin^2(c\zeta_1 - c\zeta_2)$$

Since $\epsilon(t) > 0$, $\dot{V}(\zeta)$ is also positive definite with respect to E_ζ. Therefore the equilibrium subspace E_ζ is not stable.

On the other hand, if the reference point is controlled to move in the positive $\mathbf{X}_1$ direction, the velocity of the reference point is

$$\begin{bmatrix} \dot{y}_1 \\ \dot{y}_2 \end{bmatrix} = \begin{bmatrix} \dot{z}_2 \\ \dot{z}_4 \end{bmatrix} = \begin{bmatrix} \epsilon(t) \\ 0 \end{bmatrix}$$

where $\epsilon(t) > 0$. Using the same Lyapunov function, we can similarly show that

$$\dot{V}(\zeta) = -\frac{\epsilon(t)}{L} \sin^2(c\zeta_1 - c\zeta_2)$$

along the forward internal motion. Therefore, the forward internal motion is stable. Intuitively, if the mobile platform is "pushed" at the reference point, the internal motion is not stable. If it is "pulled" or "dragged" at the reference point, the internal motion is stable.

3.3.2 Simulation

Simulations and experiments have been conducted to verify the theoretical analysis presented in the preceding section. In particular, simulations and experiments are focused on the verification of unstable behaviors when the mobile robot is commanded to move backward. The desired trajectory is

$$y_1^d(t) = -V_x t \tag{3.28}$$
$$y_2^d(t) = 0 \tag{3.29}$$

where $V_x > 0$ is the desired velocity. The following parameters are used in both simulations and experiments: $L = 0.487m$ and $b = 0.171m$.

Depending on the initial conditions of the state variable x, the following three cases are examined in simulations and experiments:

1. The initial value of x_1 and x_2 are chosen such that the actual reference point coincides with the desired trajectory at $t = 0$, i.e.,

$$y_1(0) = y_1^d(0) = 0$$
$$y_2(0) = y_2^d(0) = 0$$

   The initial values of θ_r, θ_l, η_1, and η_2 are all set to zero. Consequently, the initial heading angle is zero.

2. The initial values of θ_r and θ_l are chosen such that the initial heading angle $\phi(t = 0) = c(\theta_r(0) - \theta_l(0)) = 0.1$ degrees. All other initial conditions are the same as in case 1.

3. The initial conditions are the same as in case 1. However, a disturbance in the heading angle is introduced in the middle of the trajectory. In the simulation, the disturbance is introduced by adding $\Delta\phi = 0.1$ degrees to the actual heading angle for two sampling intervals 3.0 seconds later. In the experiment, the disturbance is introduced by placing a copy of magazine on the floor. When one of the driving wheels runs over the magazine, the heading angle is altered slightly due to different floor conditions at the two wheels.

The sampling rate of the simulations is 100 Hz. The trajectories of the point P_o (see Figure 1) is shown in Figure 3.3. Note that P_o is positioned at the origin at time zero

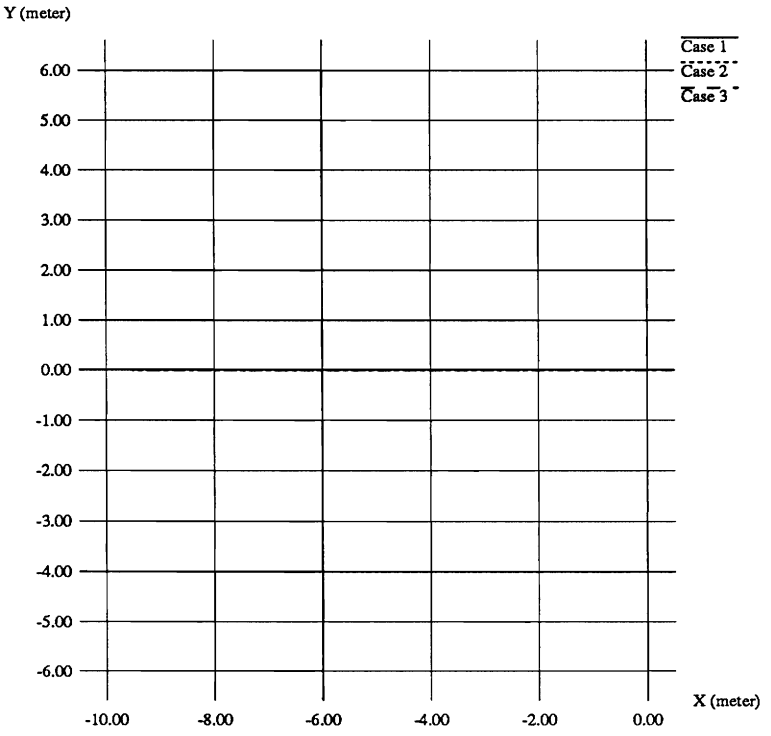

Figure 3.2: The trajectories of the reference point (simulation).

for both figures. Also note that the trajectories for the Case 1 coincide with the X-axis at $Y = 0$ of both figures. For the matter of convenience, the trajectories of P_o for the Case 3 is repeated in Figure 3.4 in which a box and the tip of the line extended from the corner of the box represent the platform and the reference point, respectively. The presence of turnaround is evident in Figure 3.4. In Figures 3.2 and 3.3, it is seen that the platform starts to swivel as soon as a disturbance occurs while, with no disturbance (Case 1), the platform keeps moving backward with the constant heading angle, $\Phi = 0$. These figures shows that a small disturbance can easily cause the trajectory to depart from the equilibrium motion of moving backward to the other equilibrium motion of moving forward.

3.3.3 Experiments

Experiments are conducted using a LABMATE[2] mobile platform which is controlled with the sampling rate of 9 Hz. The trajectories of the reference point and P_o on the wheel axis for the three cases are shown in Figure 3.5 and 3.6, respectively. Also the heading angles are shown in Figure 3.7. Note again that the trajectory for the Case 1 coincides with the X-axis in each figure. Figure 3.7 clearly shows the turnaround of the platform under the influence of the disturbances. The discrepancy in terms of the shape of the trajectories between the simulations and the experiments is due to the fact that, in the simulation the

[2]LABMATE is a trademark of Transitions Research Corporation.

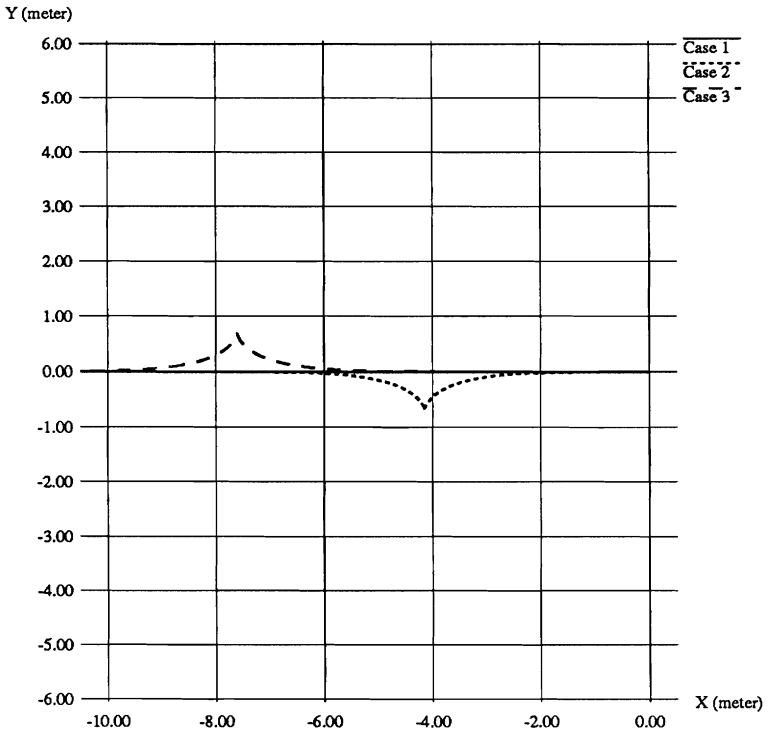

Figure 3.3: The trajectories of the point P_o on the wheel axis (simulation).

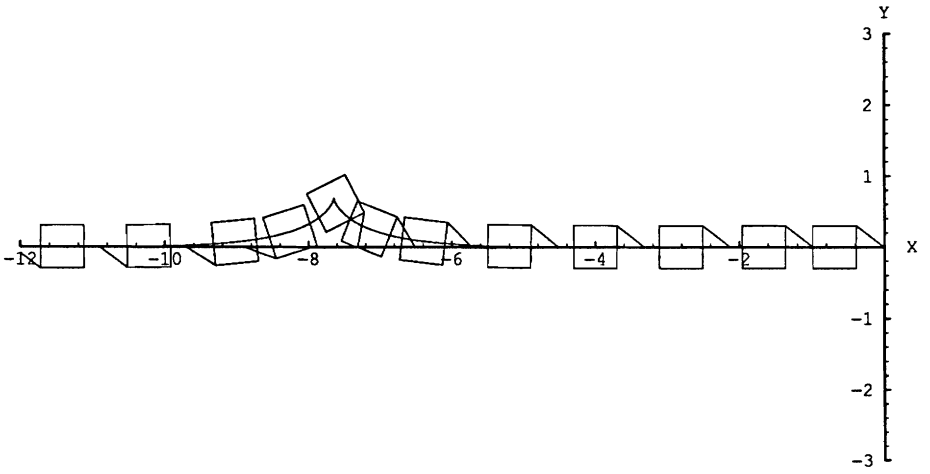

Figure 3.4: The trajectory of the mobile platform in Case 3.

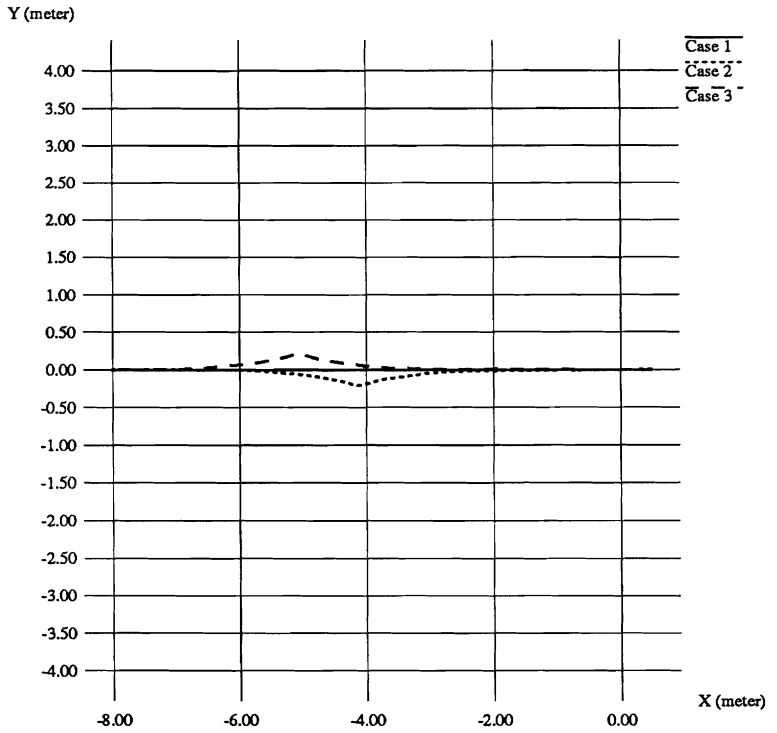

Figure 3.5: The trajectories of the reference point (experiment).

wheels of the platform were controlled at acceleration level, while in the experiments they were controlled at velocity level because of practical limitations.

A positional offset is tested as a different type of disturbance. As shown in Figure 3.8, the desired trajectory (dashed line) has a small offset in the Y direction ($\Delta Y = 7mm$) from the initial position of the LABMATE. The figure shows that the platform converges on the desired trajectory while it turns around on the way. Therefore it has been proved that both positional and rotational displacement can cause a departure from the equilibrium.

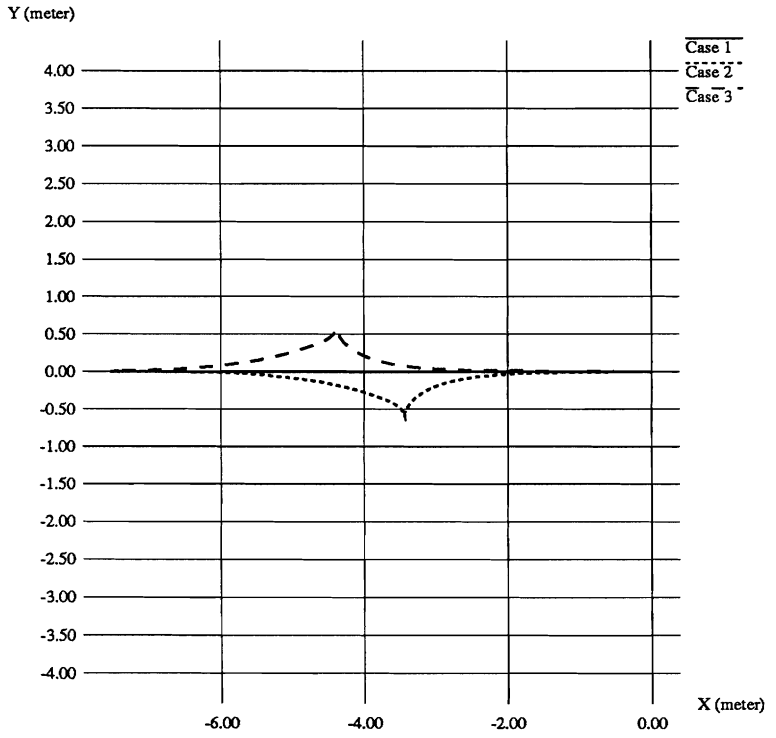

Figure 3.6: The trajectories of P_o on the wheel axis (experiment).

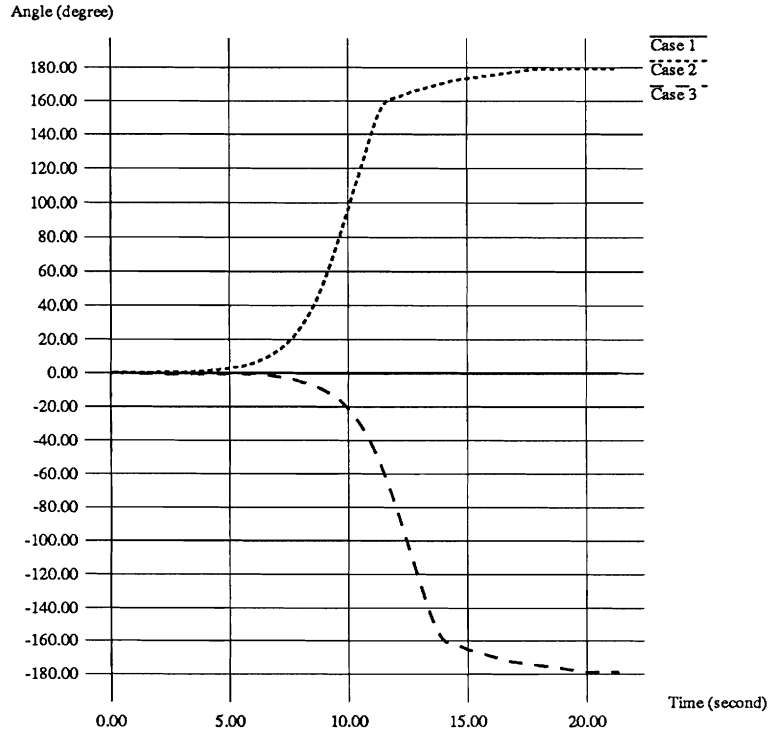

Figure 3.7: The heading angles of the mobile platform (experiment).

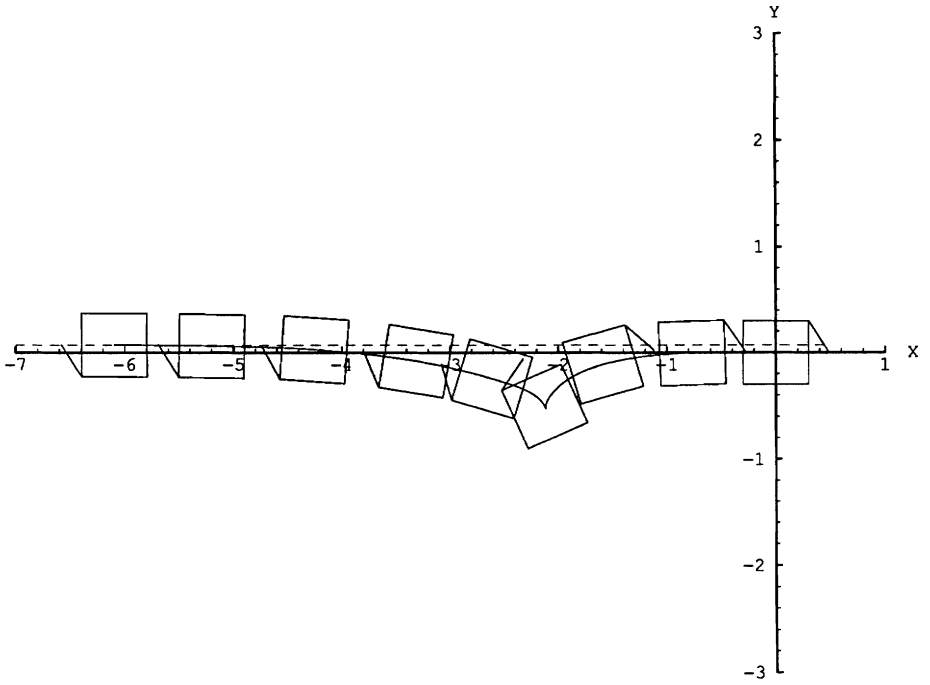

Figure 3.8: The trajectory of the mobile platform with an offset (experiment).

Chapter 4

Coordinated Control of Mobile Manipulators: Dragging Task

4.1 Motivation

When a human writes across a board, he positions his arm in a comfortable writing configuration by moving his body rather than reaching out his arm. Also when humans transport a large and/or heavy object cooperatively, they tend to prefer certain configurations depending on various factors, *e.g.*, the shape and the weight of the object, the transportation velocity, the number of people involved in the task, and so on. A mobile manipulator consists of a mobile platform and a robot manipulator. When a mobile manipulator performs a manipulation task, it is desirable to bring the manipulator into certain preferred configurations by appropriately planning the motion of the mobile platform. If the trajectory of the manipulator end point in a fixed coordinate system (the world coordinate system) is known *a priori*, then the motion of the mobile platform can be planned accordingly. However, if the motion of the manipulator end point is unknown *a priori*, *e.g.*, driven by a visual sensor or guided by a human operator, the path planning has to be made locally and in real time rather than globally and off-line. This chapter presents a planning and control algorithm for the platform in the latter case, which takes the measured joint displacement of the manipulator as the input for motion planning, and controls the platform in order to bring the manipulator into a preferred operating region. While this region can be selected based on any meaningful criterion, the manipulability measure [80] is utilized in this study. By using this algorithm, the mobile platform will be able to "understand the intention of its manipulator and respond accordingly." Since the mobile platform is subject to nonholonomic constraints, the control algorithm is developed using nonholonomic system theory.

This control algorithm has a number of immediate applications. First, a human operator can easily move around the mobile manipulator by "dragging" the end point of the manipulator while the manipulator is in the free mode (compensating the gravity only) [90]. Second, if the manipulator is force-controlled, the mobile manipulator will be able to push against and follow an external moving surface [101]. Third, when two mobile manipulators transport a large object with one being the master and the other being slave,

this algorithm can be used to control the slave mobile manipulator to support the object and follow the motion of the master, resulting in a cooperative control algorithm for two mobile manipulators.

What makes the coordination problem of locomotion and manipulation a difficult one is twofold. First, a manipulator and a mobile platform, in general, have different dynamic characteristics, namely, a mobile platform has slower dynamic response than a manipulator. Second, a wheeled mobile platform is subject to nonholonomic constraints while a manipulator is usually unconstrained. These two issues must be taken into consideration in developing a planning and control algorithm.

4.2 Preferred Operating Regions

There are a few ways to define a preferred operating region. The simplest case is a single point which can be determined by a specific criterion based on the nature of tasks or constraints to which the mobile manipulator is subject. The other choice will be a spatial operating region whose shape should be a function of maneuverbility of a manipulator and a platform and/or *a priori* knowledge of the moving surface which the mobile manipulator must follow. One such example is an ellipse or ellipsoid if the heterogeneity of constraints is taken into account, *e.g.*, the lateral motion of a platform is constrained.

It is natural to define the center of the operating region to be the most preferred point. It is then desirable that the mobile manipulator stays near the center of the region when the system stops moving. It is obvious that this is not a problem with a single point case since it guarantees the reference point to keep track of the optimal point all the time. One major drawback of the preferred operating region of a single point is that even a slight departure from such a point triggers the motion of the system.

The difference in terms of dynamic responses between a manipulator and a platform should also be taken into consideration, since the bandwidth of a platform is generally lower than that of a manipulator. If the task does not require a large motion or if it contains a high bandwidth motion, then it is preferred that the mobile platform does not respond until the deviation reaches a predetermined threshold value. This is especially true if such a deviation is aligned with the direction to which the mobile platform is constrained, because compensating in such a direction requires a large maneuvering from the platform. On the other hand, if the preferred operating region is chosen to be too large, a workspace limit may be encountered or it may cause a large interaction force.

In order to specify a preferred operating region, we will use the concept of manipulability measure introduced by Yoshikawa [80]. The location of the preferred operating region will be determined by maximizing the manipulability measure. The size of the region will be determined by the dynamic characteristics of the mobile platform. For instance, if the region is a single point, the mobile platform must respond to the motion of the moving surface in such a way that the configuration of the manipulator is kept fixed in the optimal configuration in terms of the manipulability measure. A illustrative example for the PUMA type manipulator mounted on a platform is given in Figure 4.1 in which only the first three joints are considered to compute the manipulability measure. In the figure, the manipulator configuration shown in the bold line yields the globally maximal

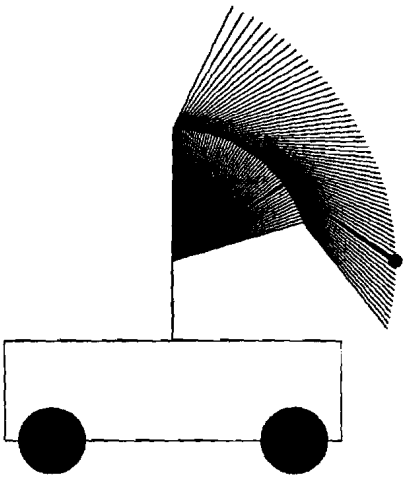

Figure 4.1: Example of preferred configuration of mobile manipulator.

manipulability and others depict optimal configurations with varying end effector height.

4.3 Control Scheme

Two separate controllers are used for the two subsystems, *i.e.*, mobile platform and manipulator. Under the scenario of interest, the manipulator is only compensated for its own gravitational and frictional forces in a feed-forward manner, regardless of the status of the mobile platform. A human operator then drags the end-effector of the manipulator, and the coordination strategy to be described in the next section will issue control commands to the platform. The platform is therefore controlled based on the current status of the manipulator as well as the platform itself. In this section, we present the control algorithm of the mobile platform which is a generalization of Look-Ahead Control described in Section 3.2.3.

The location of the reference point is not restricted except on the wheel axis which requires the dynamic feedback control (see the previous chapter 3.2.1 and 3.2.2). The reference point was chosen on the symmetry axis of the platform in Section 3.2.3. Suppose that the reference point P_r is given by $({}^v x_r, {}^v y_r)$ with respect to the platform coordinate frame, a moving frame whose origin is fixed at P_o (Figure 4.2). Note that ${}^v x_r \neq 0$ has to be assured in order to avoid the reference point on the wheel axis. Taking the coordinates of the reference point in the inertial frame as the output equations,

$$y = h(x) = \begin{bmatrix} x_1 + {}^v x_r \cos\phi - {}^v y_r \sin\phi \\ x_2 + {}^v x_r \sin\phi + {}^v y_r \cos\phi \end{bmatrix} \tag{4.1}$$

Input-output linearizability of the system with the above output equations is easily verified by checking the decoupling matrix which is given by

$$\Phi(x) = \begin{bmatrix} \Phi_{11} & \Phi_{12} \\ \Phi_{21} & \Phi_{22} \end{bmatrix} \tag{4.2}$$

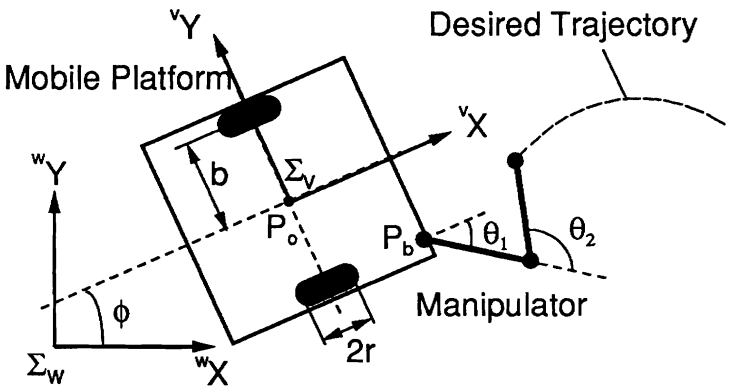

Figure 4.2: Schematic of the mobile platform with 2-DOF manipulator.

where

$$\begin{aligned}
\Phi_{11} &= c((b - {}^{v}y_r)\cos\phi - {}^{v}x_r \sin\phi) \\
\Phi_{12} &= c((b + {}^{v}y_r)\cos\phi + {}^{v}x_r \sin\phi) \\
\Phi_{21} &= c((b - {}^{v}y_r)\sin\phi + {}^{v}x_r \cos\phi) \\
\Phi_{22} &= c((b + {}^{v}y_r)\sin\phi - {}^{v}x_r \cos\phi)
\end{aligned}$$

The determinant of the decoupling matrix is then given by

$$\det(\Phi(x)) = -\frac{{}^{v}x_r\, r^2}{2b} \tag{4.3}$$

From Equation (4.3), ${}^{v}x_r \neq 0$ implies the invertibility of the decoupling matrix which also implies the existence of nonlinear static state feedback achieving the input-output linearization and decoupling.

4.4 Coordination Strategy

For simplicity, a two link planar manipulator attached on the platform (Figure 4.2) is considered in this discussion. Let θ_1 and θ_2 be the joint angles and L_1 and L_2 be the link length of the manipulator. Also let the coordinates of the base of the manipulator with respect to the platform frame ${}^{v}X$-${}^{v}Y$ be denoted by $({}^{v}x_b, {}^{v}y_b)$. We set the reference point to the end point of the manipulator at a preferred configuration. We choose as the preferred configuration the one that maximizes the manipulability measure of the manipulator. If we specify the position of the end point as the desired trajectory for the reference point, the mobile platform will move in such a way that the manipulator is brought into the preferred configuration.

The manipulability measure can be regarded as a distance measure of the manipulator configuration from singular ones at which the manipulability measure becomes zero. At or near a singular configuration, the end point of the manipulator may not easily move in certain directions. The effort of maximizing the manipulability measure leads to keeping the manipulator configuration away from singularity. This notion is very important

especially when a mobile manipulator is required to respond to motions whose range is unknown *a priori*.

The manipulability measure is defined as [80]:

$$w = \sqrt{\det(J(\theta)J^T(\theta))} \tag{4.4}$$

where θ and $J(\theta)$ denote the joint vector and Jacobian matrix of the manipulator. If we consider non-redundant manipulators, Equation (4.4) reduces to

$$w = \mid \det J(\theta) \mid \tag{4.5}$$

For the two-link manipulator shown in Figure 4.2, the manipulability measure w is

$$w = L_1 L_2 \mid \sin\theta_2 \mid \tag{4.6}$$

Note that the manipulability measure is maximized for $\theta_2 = \pm 90°$ and arbitrary θ_1. We choose $\theta_2 = +90°$ and $\theta_1 = -45°$ to be the preferred configuration, denoting them by θ_{1r} and θ_{2r}. Then the coordinates of the reference point with respect to the platform frame ${}^vX$-${}^vY$ is given by

$$\begin{aligned} {}^vx_r &= {}^vx_b + L_1\cos\theta_{1r} + L_2\cos(\theta_{1r}+\theta_{2r}) && (4.7)\\ {}^vy_r &= {}^vy_b + L_1\sin\theta_{1r} + L_2\sin(\theta_{1r}+\theta_{2r}) && (4.8) \end{aligned}$$

We emphasize that ${}^vx_r$ and ${}^vy_r$ are constant and will be used in the representation of the output equation, Equation (4.1). As mentioned in the previous section, the manipulator is regarded as a passive device whose dynamics is neglected. It is assumed that a human operator drags the end effector of the manipulator. The position of the end effector is given as the desired trajectory for the reference point P_r. The manipulator will be kept in the preferred configuration provided that the reference point is able to follow the desired trajectory. Any tracking error of the reference point will leave the manipulator out of the preferred configuration, resulting in a drop of manipulability measure. To count for measurement and communication delay, the current position of the end effector is made available to the mobile platform a fixed number of sampling periods later in the simulation. Five sampling periods of delay are introduced in the simulation described below.

4.5 Simulation Results

We conducted simulations to verify the coordination strategy. In the simulation, the mobile platform is initially directed toward positive ${}^wX$-axis at rest and the initial configuration of the manipulator is $\theta_1 = -45°$ and $\theta_2 = 90°$. Two cases corresponding to two paths shown in Figure 4.3 are simulated:

Case (i): A straight line perpendicular to the ${}^wX$-axis or the initial forward direction of the mobile platform,

Case (ii): A forward slanting line by 45 degree from ${}^wX$-axis.

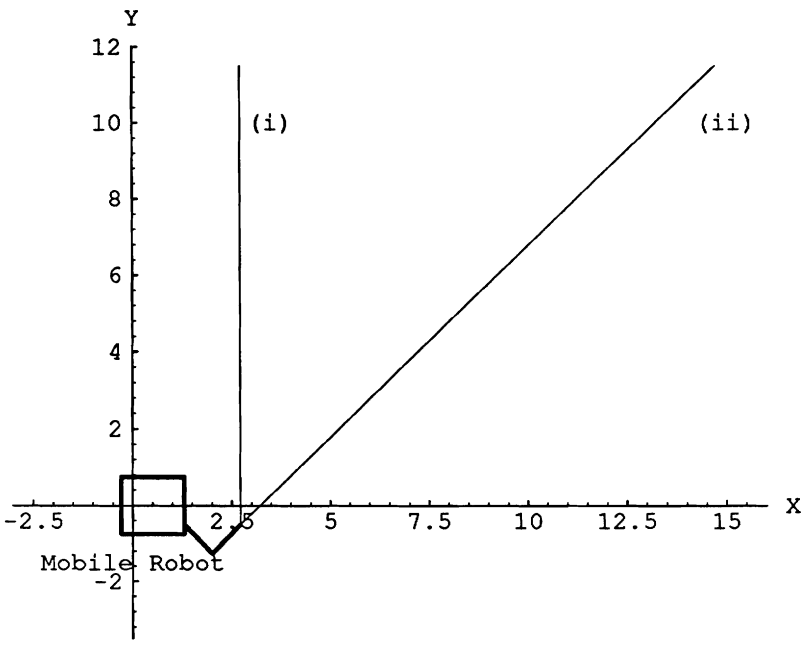

Figure 4.3: Two paths used in the simulation.

The velocity along the paths is constant. The sampling rate is 0.01 sec. The linear state feedback gains for the two subsystems, Equations (3.19) and (3.20), are chosen so that the overall system has a natural frequency $\omega_n = 2.0$ and a damping ratio $\zeta = 1.2$. The higher damping ratio is to simulate the slow response of the mobile platform. For each simulation, we plot the trajectory of P_o, the trajectory of the reference point P_r, the manipulability measure, the joint angles of the manipulator, the heading angle of the platform, and the velocity of the P_o.

1. Figure 4.4 shows the trajectory of point P_o, in which a box[1] represents the mobile platform. Note that the desired trajectory is given for the reference point P_r. P_o has no desired trajectory. Figure 4.5 shows the desired and actual trajectories of the reference point P_r. Note that the two trajectories coincide. The manipulability measure, and the velocity of point P_o are shown in Figure 4.6 and 4.9, respectively. Figure 4.6 shows a little degradation of manipulability measure corresponding to the early maneuver by the mobile platform. The negative value in Figure 4.9 indicates that the mobile platform moved backwards for a short period of time at the very beginning in order to achieve the needed heading angle. Note that the motion of the platform, or more precisely the trajectory of point P_o is not planned. Therefore, the exhibited backward motion is not explicitly planned and is a consequence of the control algorithm. The presence of such backward motion depends on the direction of a desired trajectory, the desired velocity, and the location of the reference point.

[1]These boxes are not equally distributed in time.

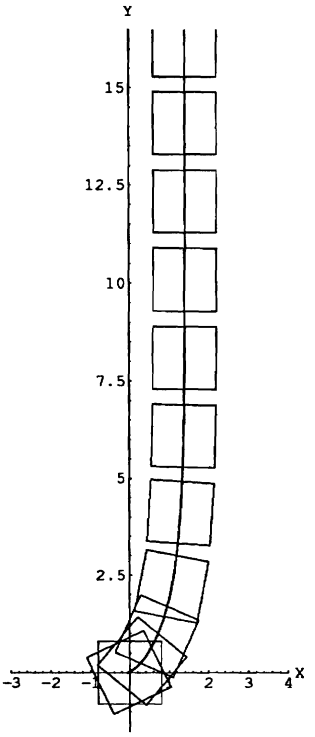

Figure 4.4: Trajectory of the point P_o for Case (i).

2. The results for the slanting trajectory are shown in Figures 4.10 through 4.15. Similarly to Case (i), Figure 4.11 shows that the reference point precisely follows the desired trajectory. From Figure 4.12, the degradation of manipulability measure is somewhat bigger than that of the previous case. Figure 4.15 indicates that no backward motion occurs this time.

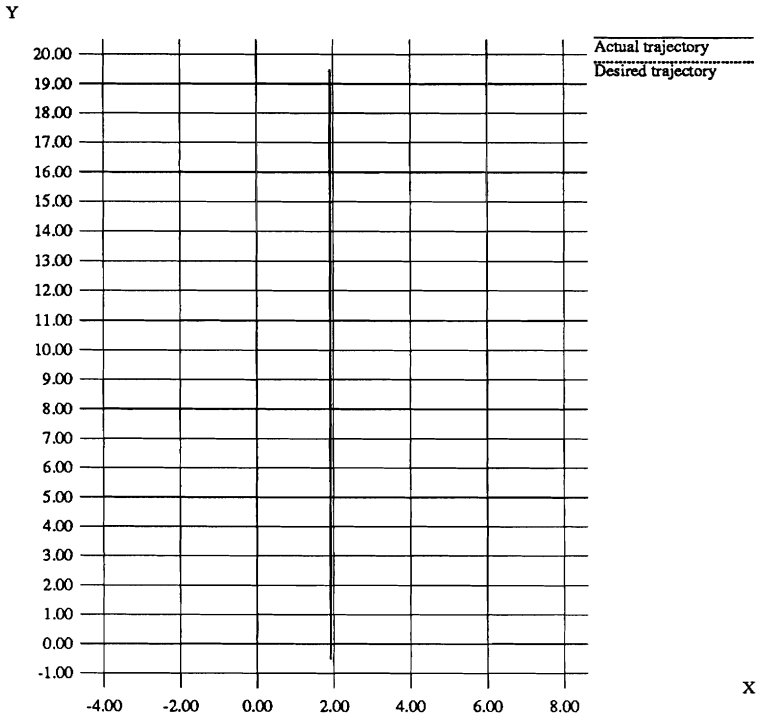

Figure 4.5: Desired and actual trajectories of the reference point for Case (i).

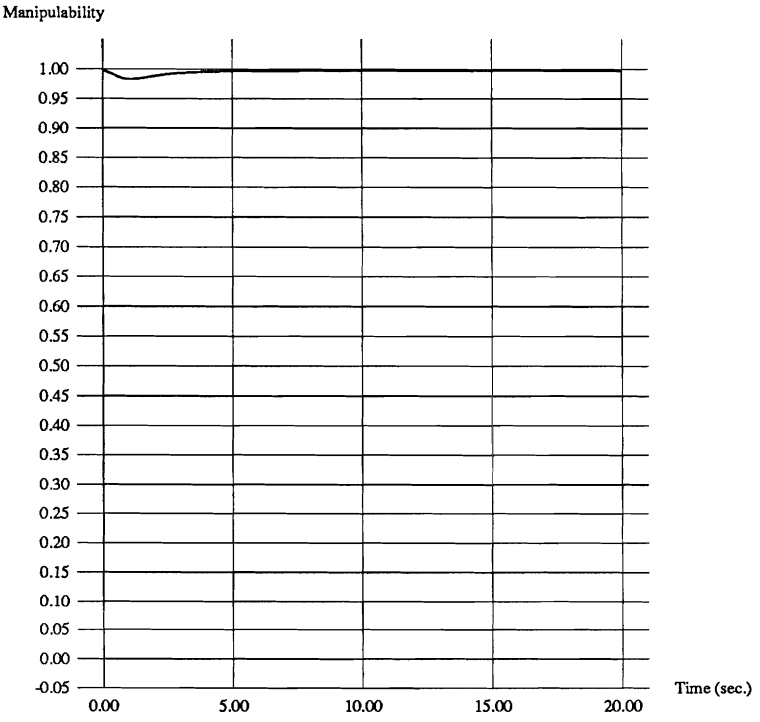

Figure 4.6: Manipulability measure for Case (i).

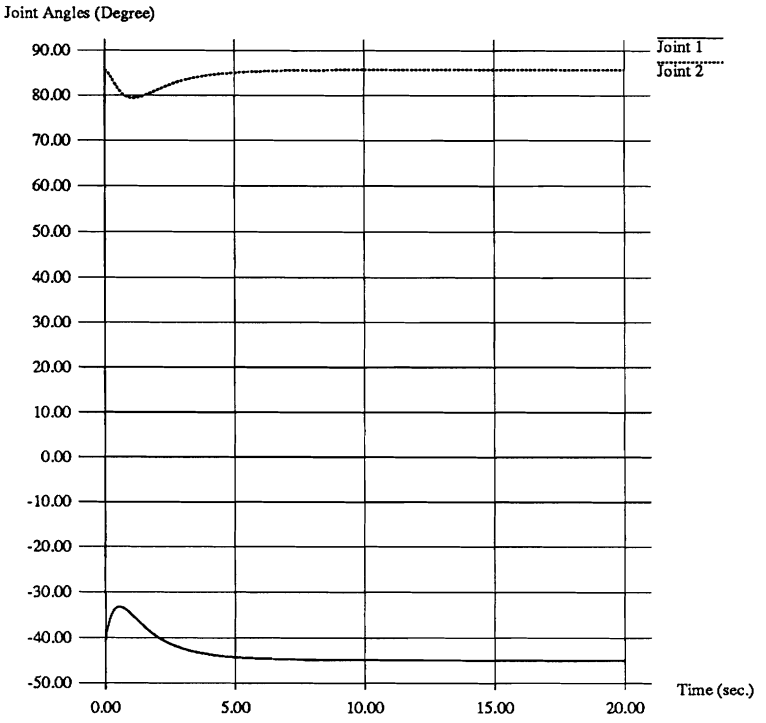

Figure 4.7: Joint angles for Case (i).

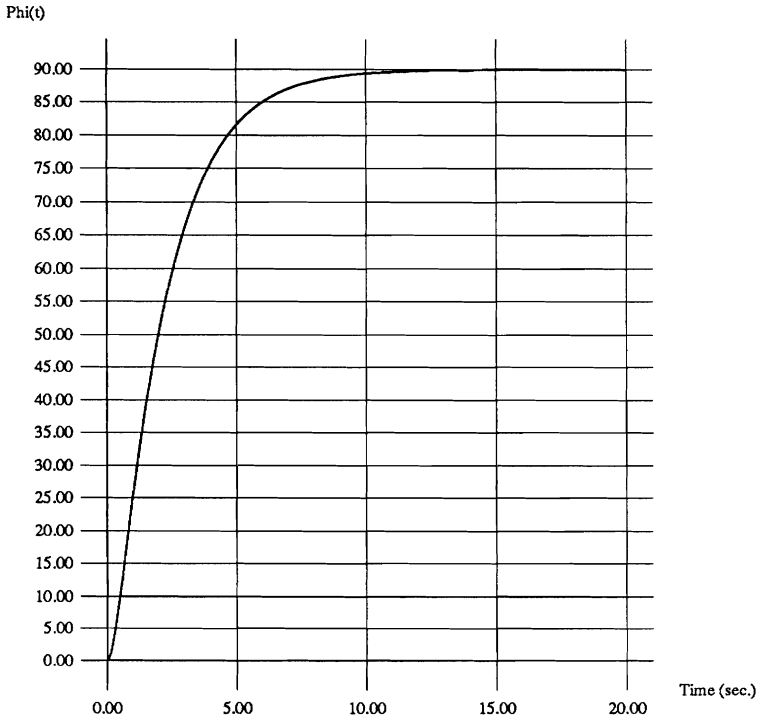

Figure 4.8: Heading angle for Case (i).

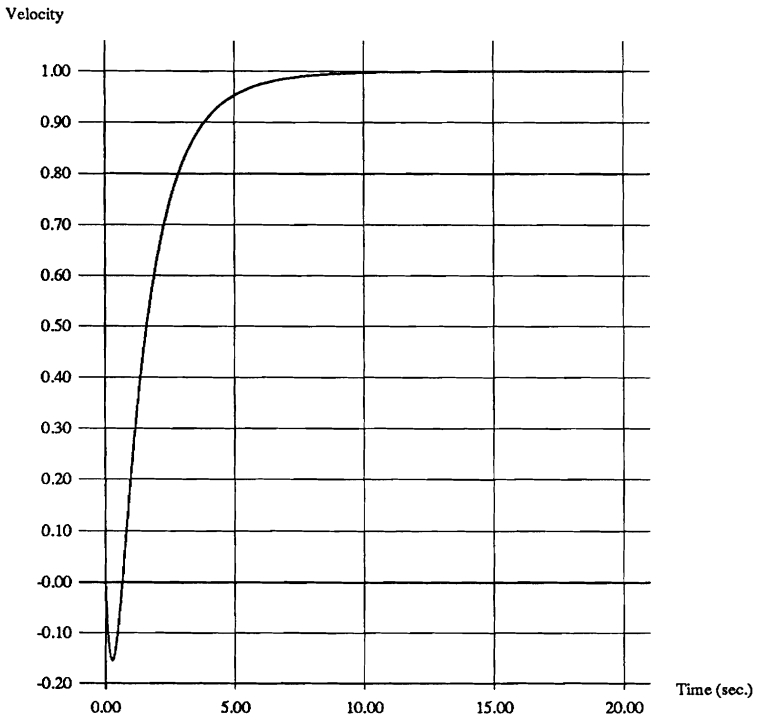

Figure 4.9: Velocity of the point P_o for Case (i).

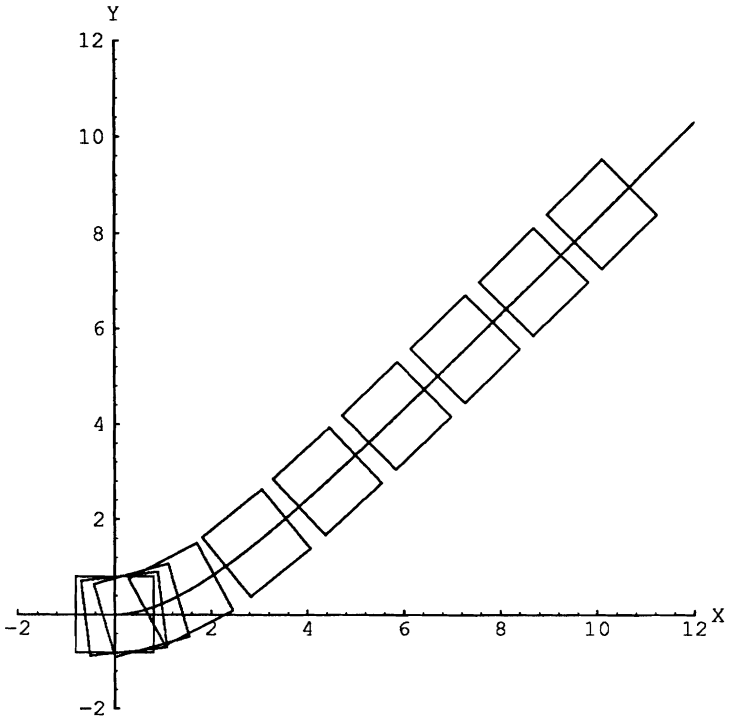

Figure 4.10: Trajectory of the point P_o for Case (ii).

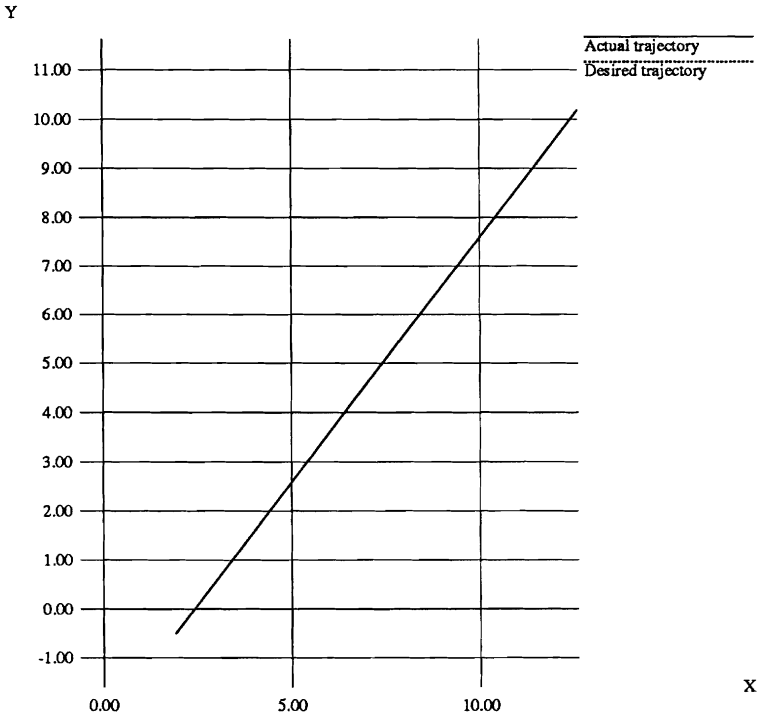

Figure 4.11: Desired and actual trajectories of the reference point for Case (ii).

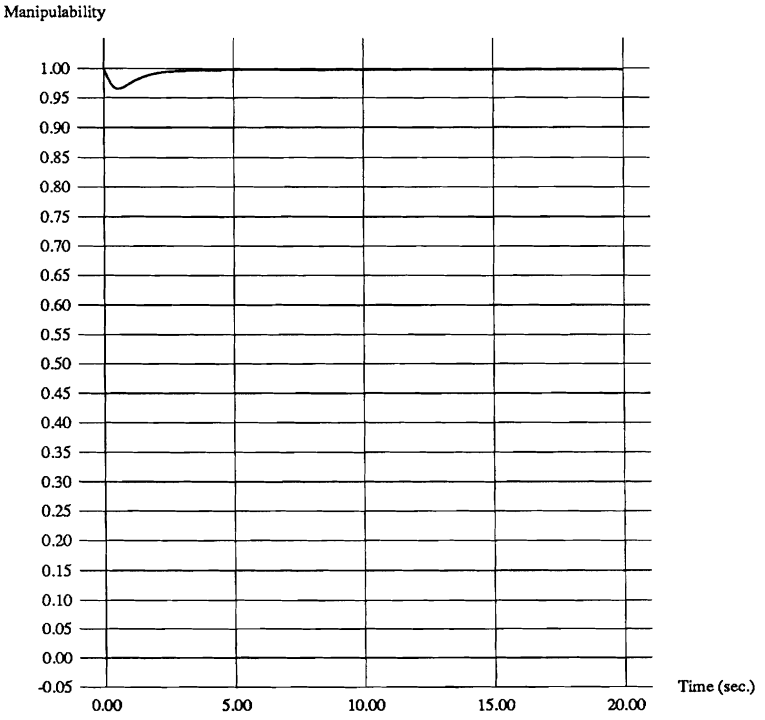

Figure 4.12: Manipulability measure for Case (ii).

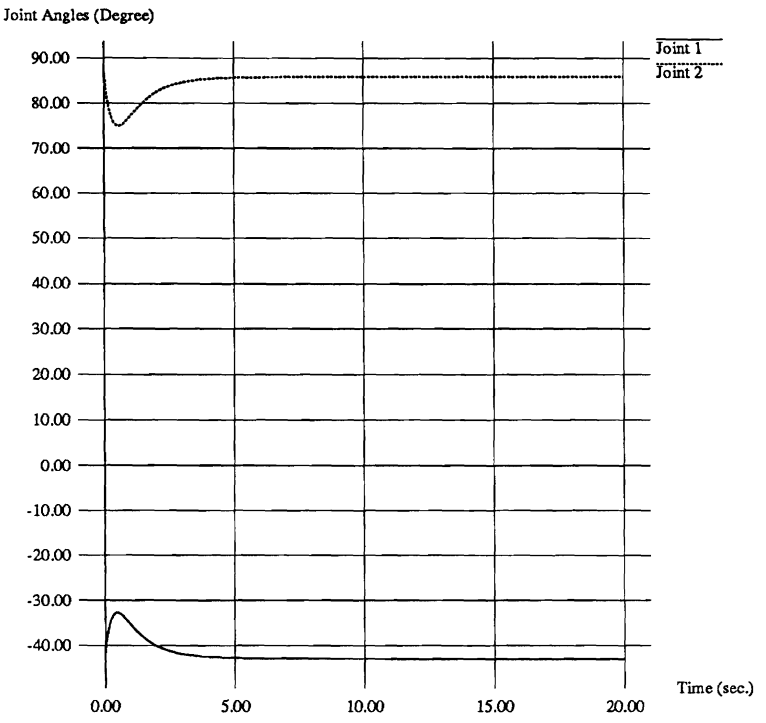

Figure 4.13: Joint angles for Case (ii).

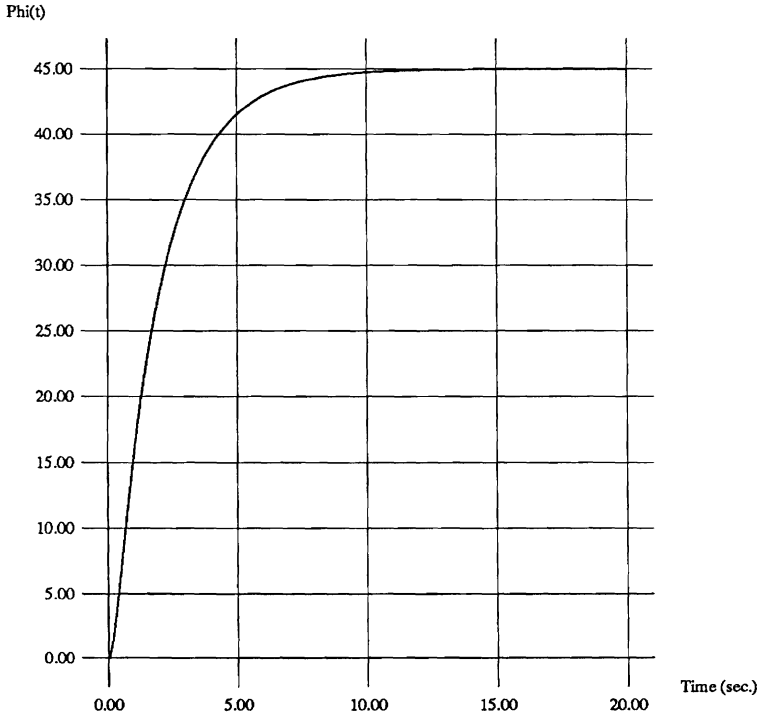

Figure 4.14: Heading angle for Case (ii).

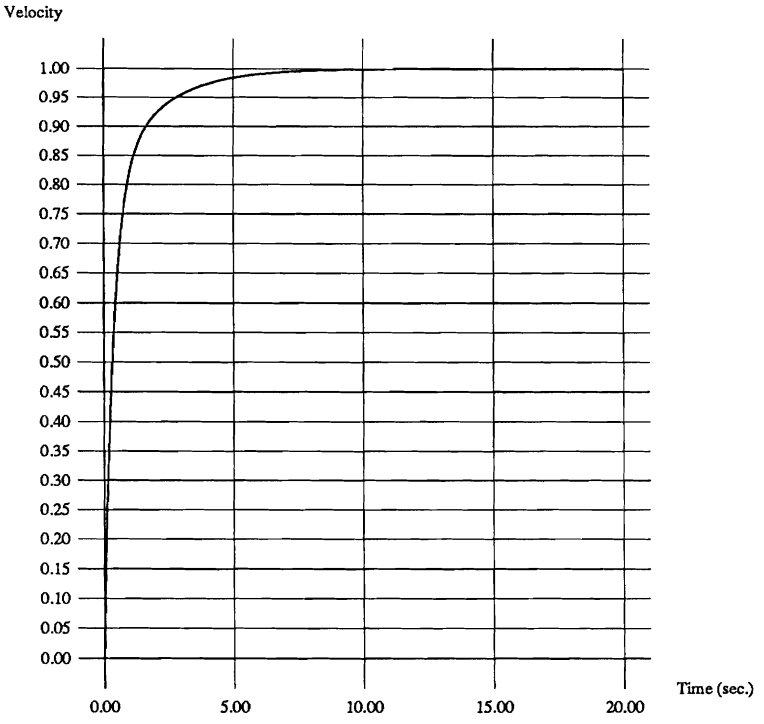

Figure 4.15: Velocity of the point P_o for Case (ii).

Chapter 5

Coordinated Control of Mobile Manipulators: Following Task

5.1 Motivation

The task of the mobile manipulator in this chapter is to push against and to follow a moving surface, as illustrated in Figure 5.1. It is motivated from multiple cooperative mobile manipulators transporting a common object. If one of them is designated to be a leader and the others to be followers, the followers must be able to keep in contact with and follow the object in order to cooperatively transport the object. The moving surface in this case is the object itself.

The focus in this chapter is on control and coordination of the mobile manipulator which is, unlike the previous chapter, under influence of external forces. The objective is then to develop control algorithms for the mobile manipulator so that the end effector of the manipulator maintains contact with the moving surface. The motion of the moving surface is assumed to be unknown. We will not address the issues of navigation and obstacle avoidance, and we will assume that the mobile manipulator operates in an obstacle free environment.

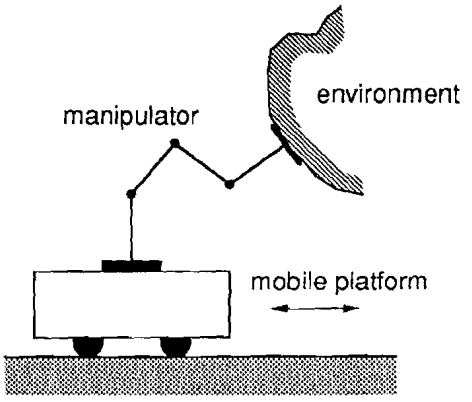

Figure 5.1: A mobile manipulator pushing against a moving surface.

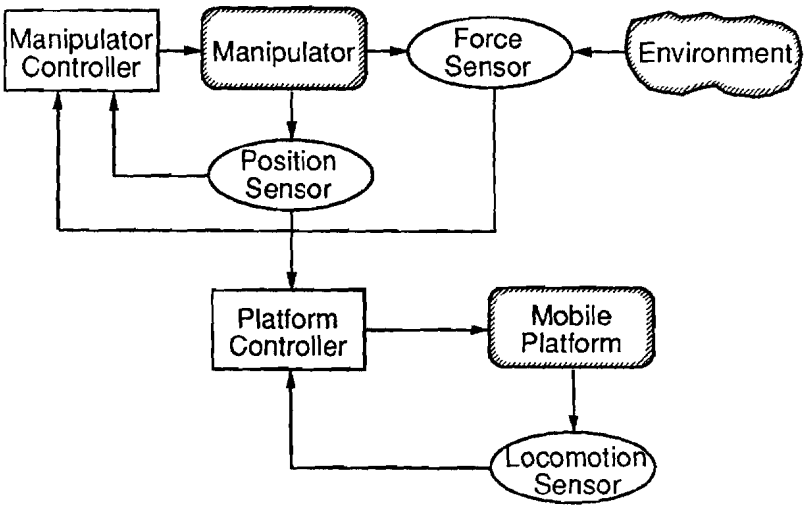

Figure 5.2: Controller architecture of the mobile manipulator.

The manipulator is equipped with a flat-surfaced palm as the end effector which makes contact with the moving surface. A six-dimensional force/torque sensor is installed at the wrist of the manipulator. The approach taken here is to have the manipulator force-controlled in order for the palm to maintain contact with the moving surface. The mobile platform is controlled to configure the manipulator in a preferred operating region in terms of manipulability measure.

5.2 Force Control Algorithm of Manipulator

The objective of the mobile platform is to keep the configuration of the manipulator within the preferred operating region while maintaining contact with a moving object. A schematics of the overall mobile manipulator controller is shown in Figure 5.2. As shown in Figure 5.2, the controller of the manipulator is self-contained in the sense that it is controlled based on its force and position sensing only. The inputs to the mobile platform controller, however, are the measured joint position of the manipulator and its own position reading with respect to the inertial frame. In this section, we present the force control algorithm implemented for PUMA 250 manipulator. The controller for the LABMATE mobile platform which is commonly used in both experiments, the dragging and following tasks, will be described in the next chapter.

It is assumed that the object moves at a reasonably slow speed such that the contact point with the object is always located within the workspace of the manipulator by controlling the motion of the mobile platform.

It can be easily seen that position control is not a suitable choice for the current objective since any position error may result in a separation or cause a large contact force. Here we adopt a variation of the hybrid control scheme proposed by Raibert and Craig [102]. It has a couple of noteworthy differences from conventional hybrid control approaches [102, 103, 104]. First, in our study, the exact geometry of the surface of the

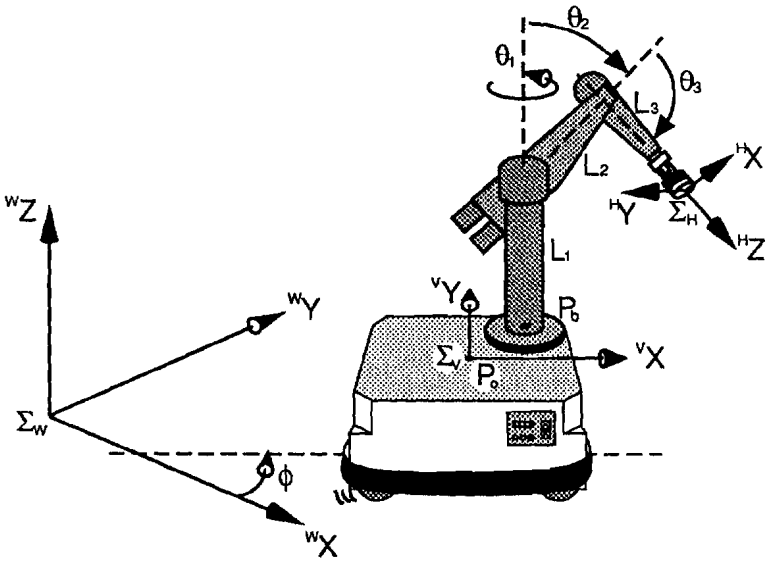

Figure 5.3: Schematic of a PUMA250 mounted on a LABMATE mobile platform.

moving object is not required. The surface is only assumed to be smooth and convex. Second, the use of passive joints plays a key role for the purpose of object following[1]. In our experiments the three joints at wrist serve as passive joints. Making use of the passive joints yields a practical advantage that such passive joints allow the end effector to align itself to the moving surface if a contact is made by a surface rather than by a point. If it is purely a point contact, then it will require either *a priori* knowledge of the trajectory of a moving surface or the exploration process of local geometry at the point of contact. In either case, all six joints have to be actively controlled.

We apply the following explicit force control law[2]. The integral control was chosen due to its characteristics of a zero steady state error and a low-pass filter when a small gain is used [105, 66]. The active damping term is effective to achieve stable contact and avoid bounces and vibrations especially if the contact surface is rigid [71].

$$\begin{aligned} \tau_f &= \tau_{ff} + [K_{fp}]\,\tau_e + [K_{fi}] \int \tau_e dt - [J]^T [K_v]\,\dot{x}_z^H \\ &= [J]^T F_d^H + [K_{fp}][J]^T \Delta F^H + [K_{fi}] \int [J]^T \Delta F^H dt \; - \; [K_v][J]^T [J]\,\dot{q} \end{aligned} \tag{5.1}$$

where:

$\{H\}$ = the hand coordinate system (see Figure 5.3)
$[K_{fp}]$ and $[K_{fi}]$ = force servo gains
$[K_v]$ = active damping gain
$[J]$ and $[J]^T$ = the hand coordinate Jacobian matrix and its transpose

[1] A passive joint is defined as a joint for which only gravity and friction are compensated.

[2] All three degrees-of-freedom are used for controlling forces. Hence there is no position control used though it can be easily combined with force control.

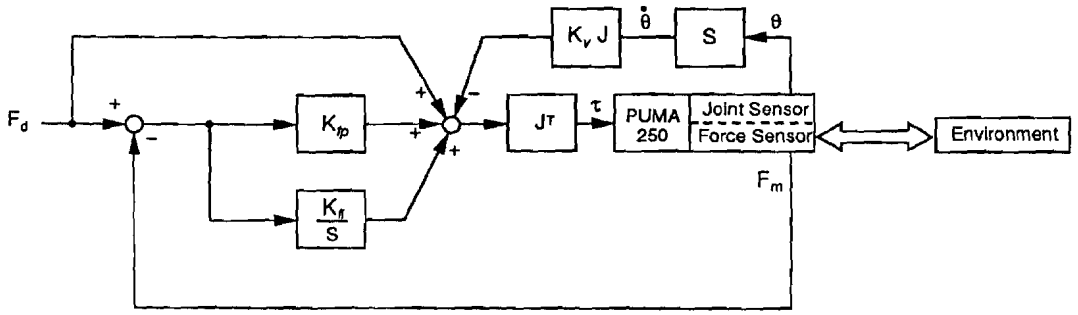

Figure 5.4: Diagram of the explicit force control scheme.

F_d^H = the desired force exerted on the hand
ΔF^H= the force error with respect to $\{H\}$
$\dot{x}_z^H$ = the z-directional velocity with respect to $\{H\}$
$\dot{q}$ = the joint velocities
τ_f = the contribution to actuator torques from the force control subsystem
τ_{ff} = the force feed-forward term
τ_e = the force feedback term

The actuator torque τ is given by

$$\tau = \tau_f + \tau_g \tag{5.2}$$

where τ_g represents the gravity and friction compensations. Note that the gravity and friction compensations are active for all six joints while τ_f is generated only for the first three joints. The diagram of the force control law, Equation 5.1 is depicted in Figure 5.4[3]
.

5.3 Coordination Strategy

Similarly to Section 4.4, the preferred operating region for this task is determined by maximizing the manipulability measure. On computing the manipulability for PUMA 250, we consider the first three joints only, neglecting the degrees of freedom placed at the wrist and neglecting the displacements in the direction of the joint axes.

Let θ_i and L_i, $i = 1, 2, 3$, be the joint angles and the link lengths of the manipulator as shown in Figure 5.3. Also let the coordinates of the manipulator base with respect to the platform frame ${}^vX$-${}^vY$ be denoted by $({}^vx_b, {}^vy_b)$. We choose the preferred configuration of the manipulator that maximizes the manipulability measure as stated above. If the manipulator changes its configuration while following the moving object, the mobile platform will move in such a way that the manipulator is brought into the preferred configuration where the manipulability measure is maximized.

The manipulability measure for PUMA250 is given by

$$w = L_2 L_3 \mid (L_2 \sin\theta_2 + L_3 \sin(\theta_2 + \theta_3)) \sin\theta_3 \mid \tag{5.3}$$

[3]The gravity and friction compensations are omitted in this figure.

Note that θ_1 and L_1 do not affect the value of w. Since L_2 is equal to L_3 for PUMA 250, the maximal manipulability measure is then obtained by $\theta_2 = 54.74^o$ and $\theta_3 = 70.53^o$ denoted by θ_{2r} and θ_{3r}, respectively. If the displacement of the end effector along the z axis of the inertial frame is taken into account, then obtaining a set of joint angles which yields maximal manipulability amounts to solving a constrained nonlinear optimization problem which is formulated as follows.

$$\max_{\theta} \mid \det J(\theta) \mid \tag{5.4}$$

$$\text{subject to: } \tilde{z}_e = z_e(\theta) \tag{5.5}$$

where $J(\theta)$ is the manipulator Jacobian which is a function of θ_1, θ_2 and θ_3, $\tilde{z}_e$ is z coordinate of the end effector with respect to the inertial frame, and $z_e(\theta)$ is a function of θ_2 and θ_3 since θ_1 does not affect $\tilde{z}_e$. The optimal posture of the manipulator with varying $\tilde{z}_e$ is illustrated in Figure 4.1.

Choosing θ_1 so that both the link 2 and the link 3 are placed in parallel to the symmetry axis of the platform, the coordinates of the reference point with respect to the platform frame ${}^vX$-${}^vY$ is given by

$$\begin{aligned} {}^vx_r &= {}^vx_b + L_2 \sin\theta_{2r} + L_3 \sin(\theta_{2r} + \theta_{3r}) && (5.6) \\ {}^vy_r &= {}^vy_b && (5.7) \end{aligned}$$

Note that ${}^vx_r$ and ${}^vy_r$ are constant, and they will be used in the representation of the output equations which will be introduced in the next chapter.

Chapter 6

Dynamic Interaction

6.1 Introduction

In order to fully utilize the advantages offered by a mobile manipulator, it is necessary to understand how to properly and effectively coordinate the motions of the mobile platform and the manipulator. We have approached the coordination problem by looking at the new issues introduced by the combined system that are not present in the individual component. First, combining a mobile platform and a multi-link manipulator creates redundancy. A particular point in the workspace may be reached by moving the manipulator, by moving the mobile platform, or by a combined motion of both. Second, the mobile platform and manipulator dynamically interact with each other. Third, there are two modes of dynamic responses. The dynamic response of a manipulator is, in general, faster than that of a mobile platform. The first issue was addressed in Chapter 4 in which a local coordination of the mobile manipulator was successfully demonstrated. However, the dynamic interaction between the manipulator and the mobile platform were not considered in the development.

The focus of this chapter is on the second issue, that is, the dynamic interaction between the manipulator and the mobile platform. The third issue also shall be addressed indirectly. Based on the motion equations for the mobile manipulator derived in Section 2.3, a nonlinear feedback that completely compensates the dynamic interaction is developed. Then, the effect of the dynamic interaction on the tracking performance is examined by comparing four different cases: (1) without any compensation of the dynamic interaction at all; (2) the mobile platform compensates the dynamic interaction caused by the manipulator; (3) the manipulator compensates the dynamic interaction caused by the mobile platform; and (4) with full compensation of the dynamic interaction with each other.

6.2 Feedback Control

It this section, we will design a nonlinear feedback controller for the mobile manipulator using the feedback linearization method. We first present our choice of output equations for the trajectory tracking purpose. Since a nonholonomic system such as this one is

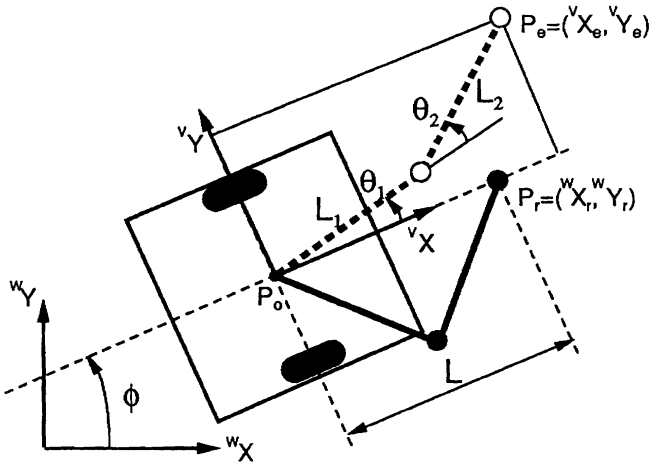

Figure 6.1: 2-DOF arm mounted on the mobile platform.

not input-state linearizable [90], we will instead achieve input-output linearization by the designed nonlinear feedback. For the sake of simplicity, we consider a two link planar manipulator mounted on a mobile platform as shown in Figure 6.1.

6.2.1 Output Equations

Since the mobile platform has two inputs and the two link manipulator also has two inputs (the two joint torques), we may have up to four independent outputs. The task for the mobile manipulator is for the end point of the manipulator to follow a desired trajectory specified in the inertial frame ${}^wX$-${}^wY$. We stress that the desired trajectory in general cannot be followed by the manipulator alone, without the aid from the mobile platform. We will choose output equations based on the following considerations. Since the manipulator is faster in dynamic response, it should be controlled to track the desired trajectory as much as possible. While doing so, the manipulator may overly stretch out and nearly reach the boundary of its workspace. The mobile platform should be controlled in such a way that it brings the manipulator into a preferred configuration as we discussed in Chapter 4.

In Figure 6.1, P_e is the actual location of the end point of the manipulator. The coordinates of P_e in the platform coordinate frame ${}^vX$-${}^vY$ are given by

$$
\begin{aligned}
{}^vx_e &= L_1 \cos\theta_1 + L_2 \cos(\theta_1 + \theta_2) && (6.1)\\
{}^vy_e &= L_1 \sin\theta_1 + L_2 \sin(\theta_1 + \theta_2) && (6.2)
\end{aligned}
$$

In order for the end point to track the desired trajectory, we choose the two coordinates of P_e as part of the output equation. Because the desired trajectory for the entire mobile manipulator is specified in the inertial frame and the coordinates are expressed in the platform coordinate frame, the desired values for these two components of the output equation will be computed based on the desired trajectory and the actual location of the platform in the inertial frame. Since we assume that the wheels of the platform do not

slip, the actual location of the platform will be integrated from the angular position of the wheels measured by the encoders.

Having chosen the two components of the output equation as above, the manipulator will try to track the desired trajectory, with the platform being stationary or in motion. We now choose the other part of the output equation, aiming at making use of the motion of the platform. The idea is to control the platform in such a way that it always bring the manipulator into a preferred configuration. Again we define the preferred configuration in the same way as we did in Chapter 4, *i.e.,* the configuration of the manipulator in which the manipulability measure is maximized. The manipulability measure w is given by Equation 4.6 which is repeated here

$$w = \mid \det J_m \mid = L_1 L_2 \mid \sin\theta_2 \mid$$

Therefore, the manipulability measure is maximized for $\theta_2 = \pm 90°$ and arbitrary θ_1. We choose $\theta_2 = +90°$ and $\theta_1 = -45°$, denoting them by θ_{1r} and θ_{2r}. The manipulator in this configuration is shown in Figure 6.1 by the thick solid lines. The actual configuration of the manipulator is shown by the thick dashed lines. The end point of the manipulator in the preferred configuration is denoted by P_r, called the reference point. By choosing $\theta_1 = -45°$ and assuming $L_1 = L_2$, the reference point is located on the symmetry axis. We note that the reference point is always fixed relative to the platform coordinate frame. The coordinates of the reference point with respect to the inertial frame are given by

$$^w x_r = x_o + (L_1 \cos\theta_{1r} + L_2 \cos(\theta_{1r} + \theta_{2r}))\cos\phi \tag{6.3}$$

$$^w y_r = y_o + (L_1 \sin\theta_{1r} + L_2 \sin(\theta_{1r} + \theta_{2r}))\sin\phi \tag{6.4}$$

where (x_o, y_o) is the coordinates of the centroid of the platform in the inertial frame, P_c which is assumed to coincide with the mid point on the wheel axis P_o, *i.e.,* $d = 0$ in Figure 4.2. We will choose these two coordinates of the reference points as the other part of the output equations. The desired values for these two output components will be set as the actual location of the end point of the manipulator. That is, the platform is controlled so that P_r is brought to the location of P_e, which effectively brings the configuration of the manipulator into the preferred one.

Thus the output equation has four components which are given by

$$y = h(x) = \begin{bmatrix} h_1 \\ h_2 \\ h_3 \\ h_4 \end{bmatrix} = \begin{bmatrix} ^w x_r \\ ^w y_r \\ ^v x_e \\ ^v y_e \end{bmatrix} \tag{6.5}$$

Having defined the output equation, we then design a controller that allows the output to track its desired values.

6.2.2 Input-Output Linearization

We now derive a nonlinear feedback to linearize the input-output relationship of the system described by the state equation (2.56) and the output equation (6.5). To do so, we differentiate the output equation twice, resulting in the following:

$$\ddot{y} = \dot{\Phi}(x)\nu_m + \Phi(x)u \tag{6.6}$$

where $\nu_m = [\nu^T \ \dot{q}_r^T]^T$, and

$$\Phi(x) = \begin{bmatrix} c(b\cos\phi - 2L\sin\phi) & c(b\cos\phi + 2L\sin\phi) \\ c(b\sin\phi + 2L\cos\phi) & c(b\sin\phi - 2L\cos\phi) \\ 0 & 0 \\ 0 & 0 \\ 0 & 0 \\ 0 & 0 \\ -L_1\sin\theta_1 - L_2\sin(\theta_1+\theta_2) & -L_2\sin(\theta_1+\theta_2) \\ L_1\cos\theta_1 + L_2\cos(\theta_1+\theta_2) & L_2\cos(\theta_1+\theta_2) \end{bmatrix}$$

In the expression of $\Phi(x)$ above, c is a constant equal to $r/2b$. Note that there are certain cases under which the above decoupling matrix becomes singular.

(1) $L = 0$: This singularity occurs if the reference point is chosen on the wheel axis as pointed out in [35].
(2) $\theta_2 = 0$: This corresponds to the case in which the arm is fully stretched.
(3) $\theta_2 = 180°$ and $L_1 = L_2$: The second link is retracted and the end effector point coincides with the base point of the manipulator.
(4) $\phi = 0$ and $b = 2L$: This does not occur for our choice of L.
(5) $\phi = \tan^{-1}(\frac{b-2L}{b+2L})$ or $\tan^{-1}(\frac{b+2L}{b-2L})$: ϕ is unlikely to hit these exact values in practice.

Applying the nonlinear state feedback given by

$$u = \Phi^{-1}(x)(v - \dot{\Phi}(x)\nu_m) \tag{6.7}$$

we obtain the following linear and decoupled input-output relationship:

$$\ddot{y}_1 = v_1 \tag{6.8}$$
$$\ddot{y}_2 = v_2 \tag{6.9}$$
$$\ddot{y}_3 = v_3 \tag{6.10}$$
$$\ddot{y}_4 = v_4 \tag{6.11}$$

To complete the controller design, it is necessary to stabilize each of the above four subsystem with another constant state feedback. Therefore, the entire controller for the mobile manipulator consists of nonlinear feedbacks (2.55) and (6.7), followed by a linear feedback.

6.3 Simulation Results

We conduct simulations to evaluate the effect of the dynamic interaction by using a mobile manipulator model. In the simulations, the following three different trajectories are examined. For each trajectory, the mobile platform is initially placed at the origin facing toward the positive X-axis of the inertial frame, implying the heading angle to be zero. The initial joint angles of the manipulator are $\theta_1 = -45°$ and $\theta_2 = +90°$. The whole system is assumed to be stationary at $t = 0$.

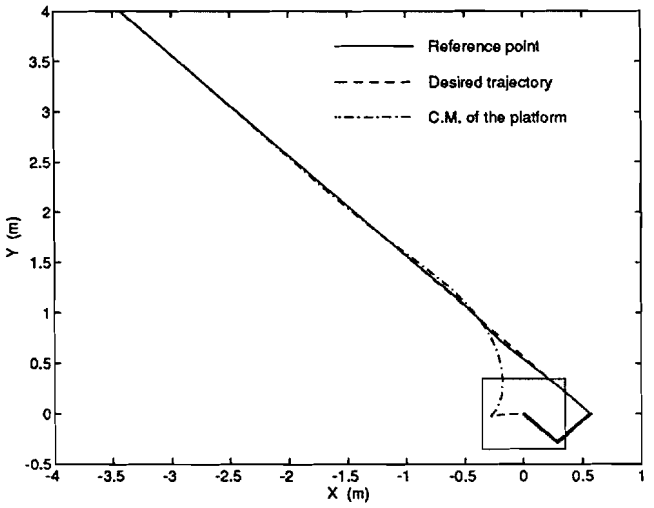

Figure 6.2: Example of the Case (i).

(i) Straight line with a constant velocity along 145° direction with respect to the initial heading angle (Figure 6.2).
(ii) Circular trajectory with $\omega = \pi/3$ and the radius of 0.25 m (Figure 6.4).
(iii) The platform follows a straight line at a constant velocity to 90° direction, and the arm follows an oscillatory motion along ${}^{v}X$-axis. (Figure 6.6).

The following four different cases are compared for each trajectory in terms of the compensation of the dynamic interaction:

- Both the platform and the arm compensated,
- Only the arm compensated,
- Only the platform compensated, and
- No compensation of the dynamic interaction used.

The controller for each of the four cases above is obtained by either considering or dropping the terms representing the dynamic interactions in Equations (2.52) and (2.53). Major parameters of the model used in the simulations are as follows:

The parameters for the platform are based on those of LABMATE platform of Transition Research Corporation. For the manipulator, M_1=M_2=4.0kg, L_1=L_2=0.4m, and I_1=I_2=0.0533kgm^2, where M_i, L_i, and I_i are the mass, the length of link, and the moment of inertia about the center of mass for i-th link. The center of mass is assumed to be at the mid point of the link.

Case (i): Figure 6.3 presents the tracking errors of the reference point. The two cases *without* the dynamic compensation for the platform show larger tracking errors than the other two cases *with* compensation while the platform is making a large maneuver at the early stage.

Case (ii): The tracking errors of the reference point from the circular trajectory are plotted in Figure 6.5. Significance of having the compensation on the manipulator is

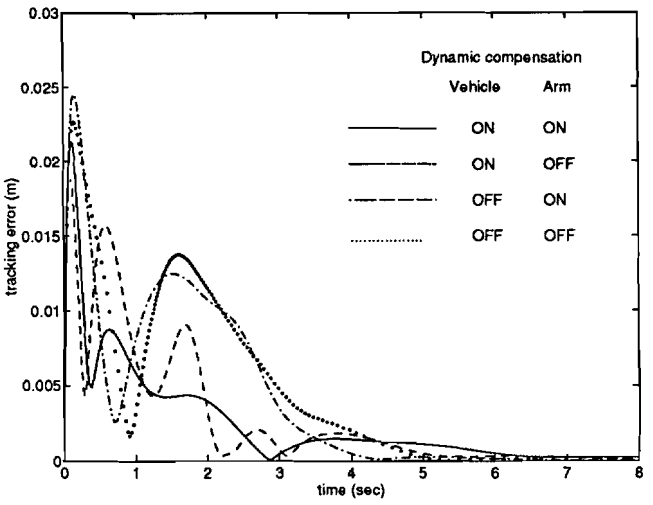

Figure 6.3: Tracking errors for the Case (i).

more evident than in the previous result. It is also observed that the absence of the compensation on the platform does not degrade the performance in terms of the tracking error.

Case (iii): The previous two cases clearly demonstrates the importance of the compensation of the dynamic interaction given by the platform to the manipulator. In those cases, however, the motion of the platform is controlled locally in the sense that it solely depends on the kinematics of the manipulator rather than a preplanned trajectory. Therefore it is difficult to observe the interaction from the manipulator to the platform. For the current case, the platform is to follow an independent trajectory while a manipulator is doing a different task. Figure 6.6 shows an example in which no compensation is employed on any of the system. The oscillatory motion of the manipulator causes a waving motion of the platform (see the right lower figure of Figure 6.6 which is the heading angle of the platform). The tracking errors of the reference point of the platform are shown in Figure 6.7. Clearly the two cases with the compensation on the platform show superior results to the other two without the compensation. In the first two cases, the motion of the manipulator is dynamically compensated by the platform, hence the tracking error converging to zero.

Figure 6.8 shows how the manipulator is affected at the end effector point by the accelerative motion of the platform[1]. In the figure, there are two lines emanated from each point within the workspace of the manipulator. A solid line represents the linear acceleration observed at the end effector which is caused by the unit magnitude of linear acceleration of the platform in positive ${}^{v}X$ direction, A gray line represents the linear acceleration at the end effector which is caused by the unit magnitude of angular acceleration of the platform. The effect of linear acceleration (solid line) displays the non-symmetric distribution due to the right-elbow configuration of the manipulator.

[1]Note that velocity terms are neglected.

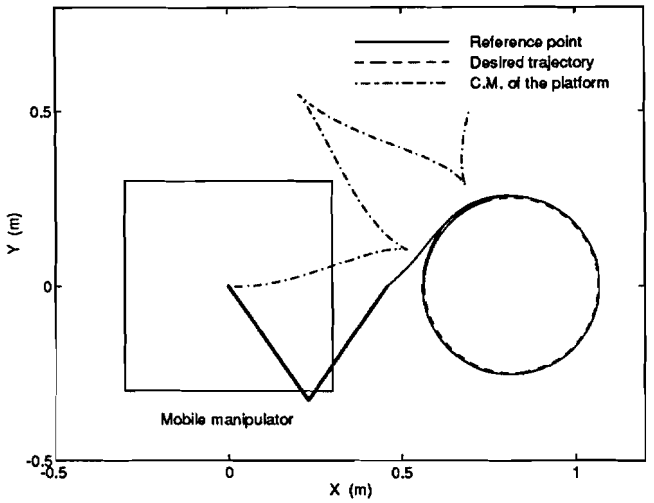

Figure 6.4: Example of the Case (ii).

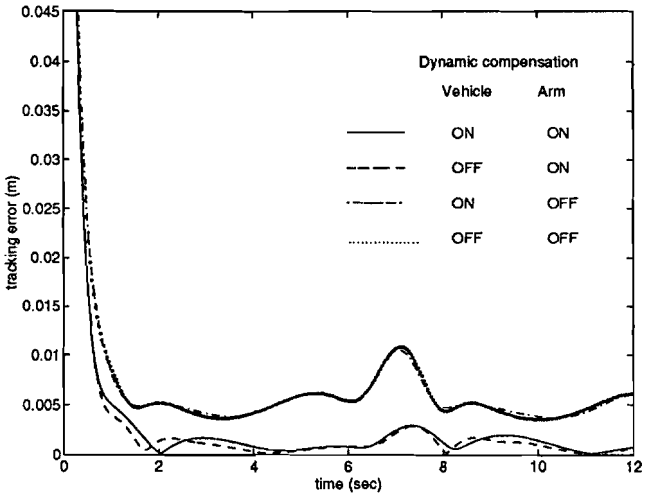

Figure 6.5: Tracking errors for the Case (ii).

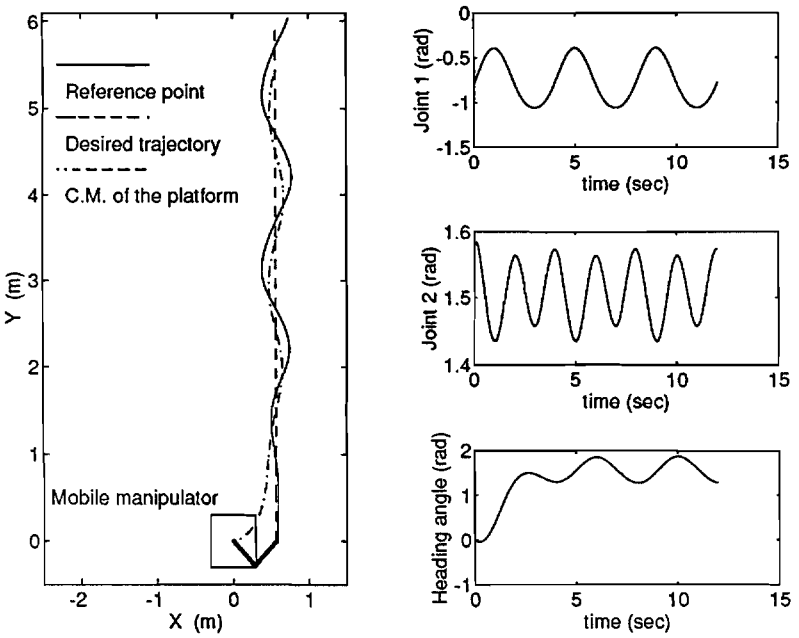

Figure 6.6: Example of the Case (iii).

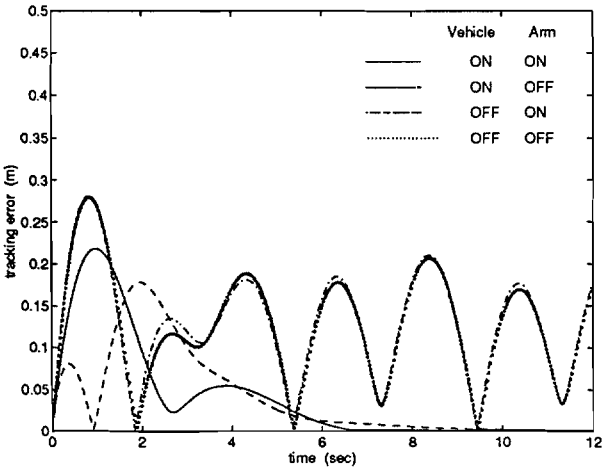

Figure 6.7: Tracking errors for the Case (iii).

Figure 6.9 illustrates how the motion of the platform is affected when the manipulator is accelerated at the end effector point in the positive ${}^{v}X$ direction[2]. Each solid line emanated from a black dot in Figure 6.9 signifies two components; x component represents the linear acceleration and y component the angular acceleration of the platform. It is observed that there is a certain region where the platform is hardly affected by the end-effector motion along ${}^{v}X$ direction. A similar observation can be made for Figure 6.10. There exists a region where the platform is insensitive to the end-effector motion along ${}^{v}Y$ direction. This analysis can be useful for the cases in which the direction of a manipulatory task frequently used is known *a priori*.

[2]In Figures 6.8 through 6.10, ${}^{v}X$ coincides with ${}^{w}X$.

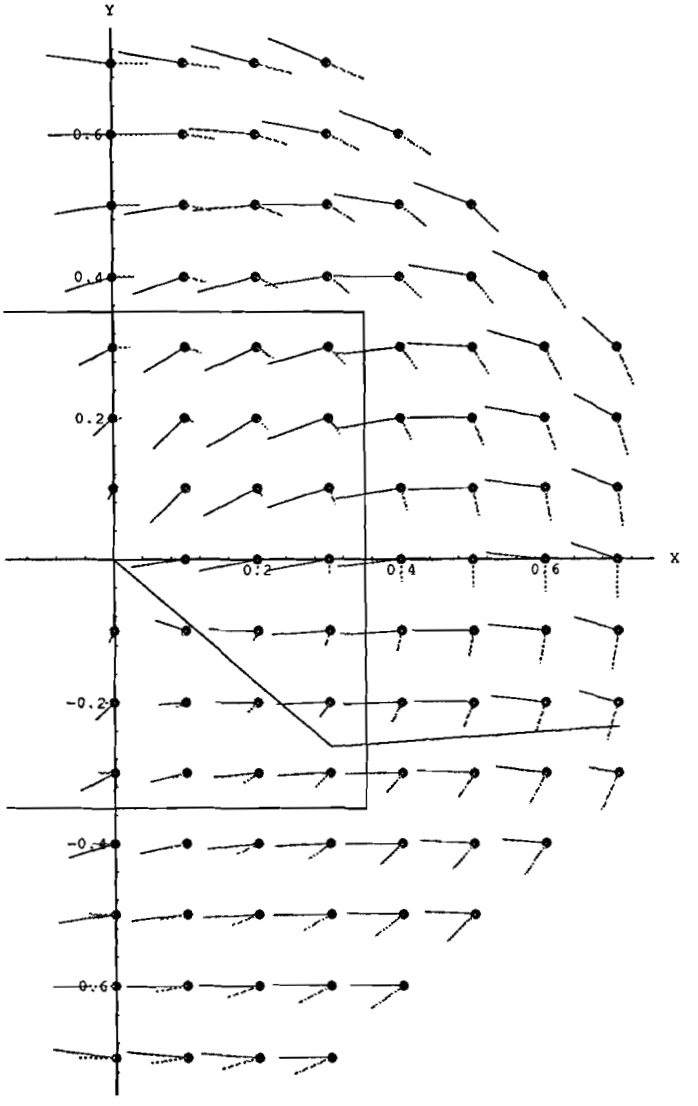

Figure 6.8: Effect of the motion of the platform on the manipulator.

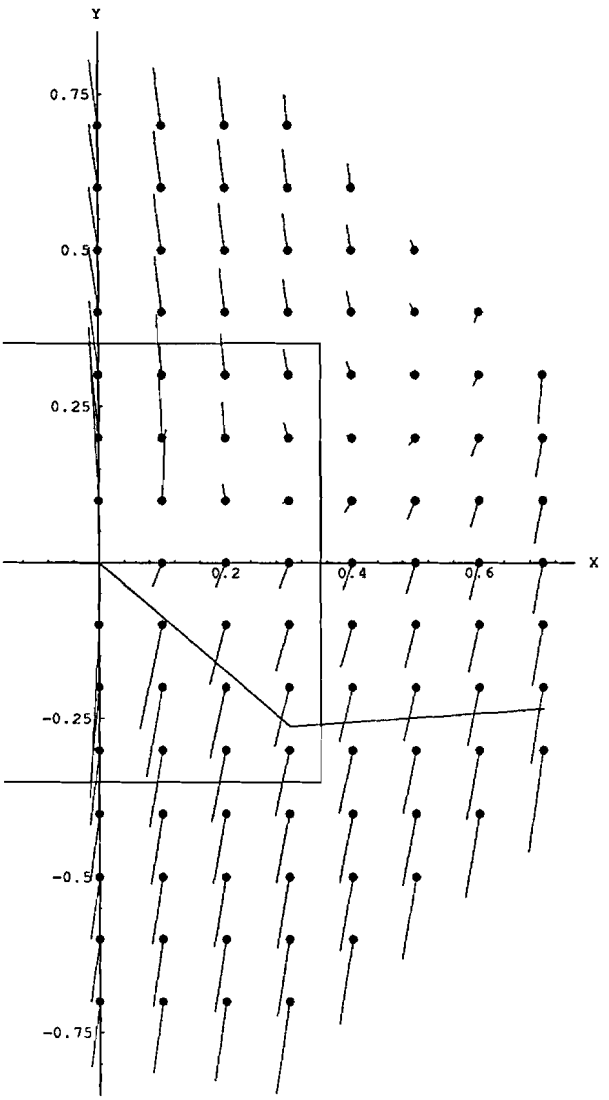

Figure 6.9: Effect of the motion of the manipulator on the platform (${}^{v}X$-direction).

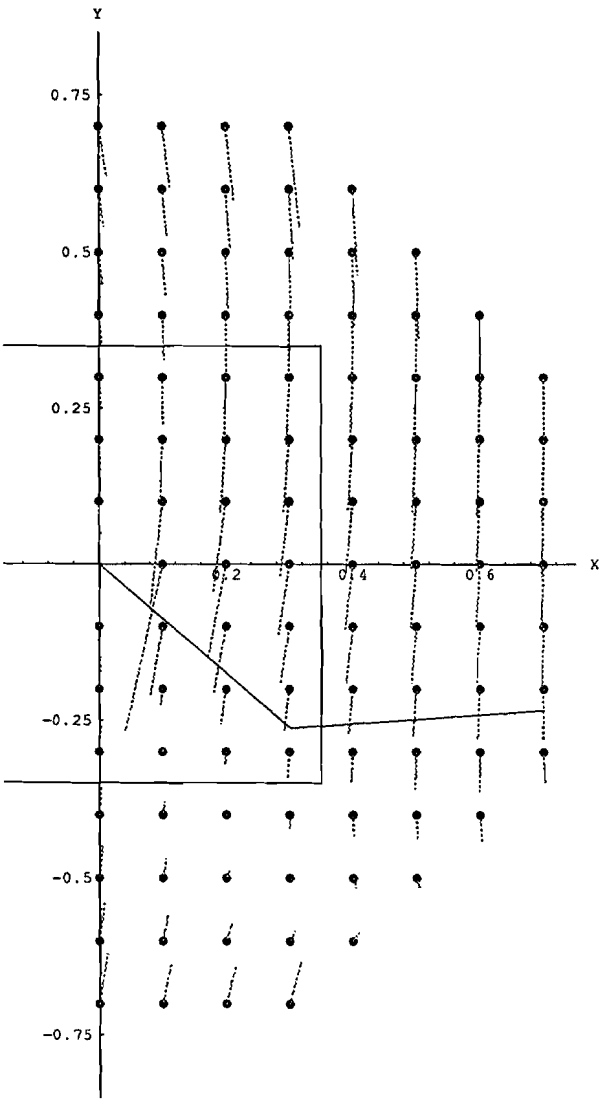

Figure 6.10: Effect of the motion of the manipulator on the platform (${}^{v}Y$-direction).

Chapter 7

Experiments

In this chapter, the experimental results for two different scenarios are presented: the dragging task and the following task which are described in Chapters 4 and 5, respectively. First, the description of the experimental setup is given. Secondly, the control scheme specific for the experimental mobile platform is presented, Next the experimental results for the dragging case are provided, followed by the results for the following case.

7.1 Experimental Setup

The experimental mobile manipulator consists of a PUMA 250 6-DOF manipulator and a LABMATE platform whose picture is shown in Figure 7.1. The manipulator has a flat-surface palm which is equipped with a Zebra six-dimensional force/torque sensor. Next, the hardware architecture of the experimental setup is depicted in Figure 7.2. The system uses two 80286-based IBM PC/AT; one for the PUMA 250 and the other for the LABMATE platform. The former computer is equipped by an AMD29000 high speed floating point coprocessor and is used as the host computer. It is configured in such a way that the 280286 processor performs all the I/O interface operations (user interface and sensor/manipulator interface) while the AMD29000 carries out the real-time computations of the control algorithm. The PC/AT has a parallel interface to the PUMA Unimation controller, through which the desired joint torque values are directly written to the DACs (Digital-Analog Converters) and the encoder counts are read back to the PC/AT. The second PC/AT which is connected with the host PC/AT via a parallel interface merely serves as a data transmitter between the host PC/AT and the LABMATE platform due to the low bandwidth of the platform.

The kinematic and dynamic parameters for the PUMA 250 are presented in Table 7.1 where $C.O.M.$ represents the distance from the i-th joint axis to the center of mass of link i. Note that the joints 4 and 6 are locked, and that the joint 5 is position-controlled so that the palm surface becomes vertical with respect to the inertial frame. The parameters for the LABMATE are listed in Table 7.2. The notations in Table 7.2 have been defined in Section 2.2. The Zebra force/torque sensor uses a set of semiconductor strain gauges and has the capability of measuring $10g$ of minimum force, $20kg$ of maximum force, and $1000kg\text{-}mm$ of maximum moment.

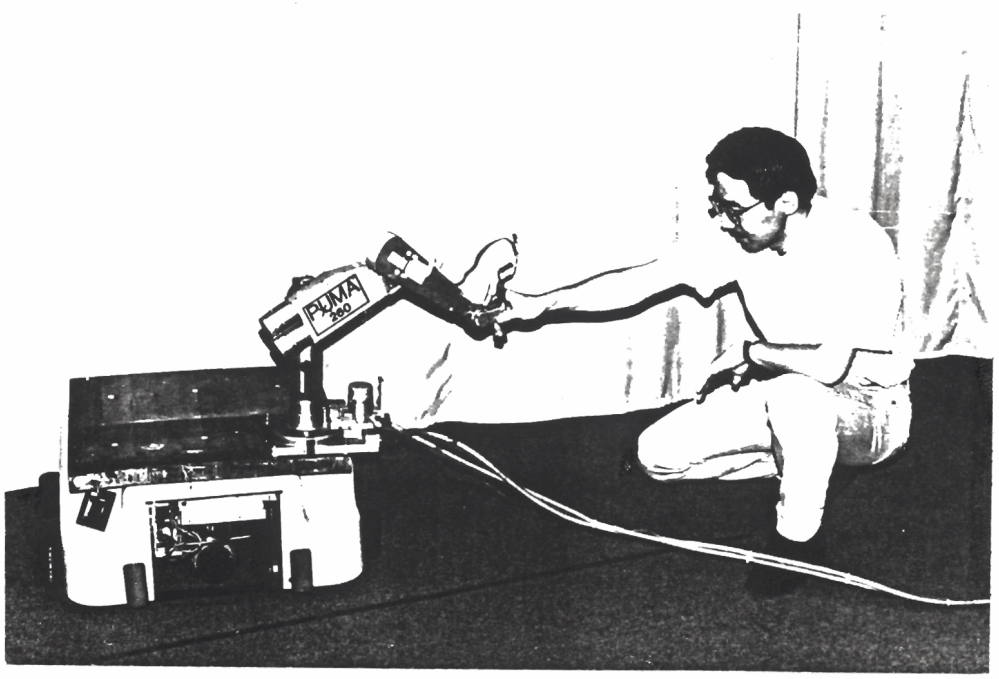

Figure 7.1: Mobile manipulator used in the experiments.

Parameters / *Link Number*	*Link Length* $[m]$	*Link Mass* $[kg]$	*C.O.M.* $[m]$	*Link Inertia* $[kgm^2]$	*Torque Const.* $[DAC/Nm]$
1	0.318	1.5	0	0.00045	174
2	0.203	2.4	0	0.145	154
3	0.203	1.1	0.06	0.052	250
5	0.093	0.54	0.054	0.00727	-890

Table 7.1: Parameters of the PUMA 250.

Parameters	*Values*	*Units*
d	0	m
b	0.171	m
r	0.075	m
m_c	94.0	kg
m_w	5.0	kg
I_c	6.609	kgm^2
I_w	0.010	kgm^2
I_m	0.135	kgm^2

Table 7.2: Parameters of the LABMATE platform.

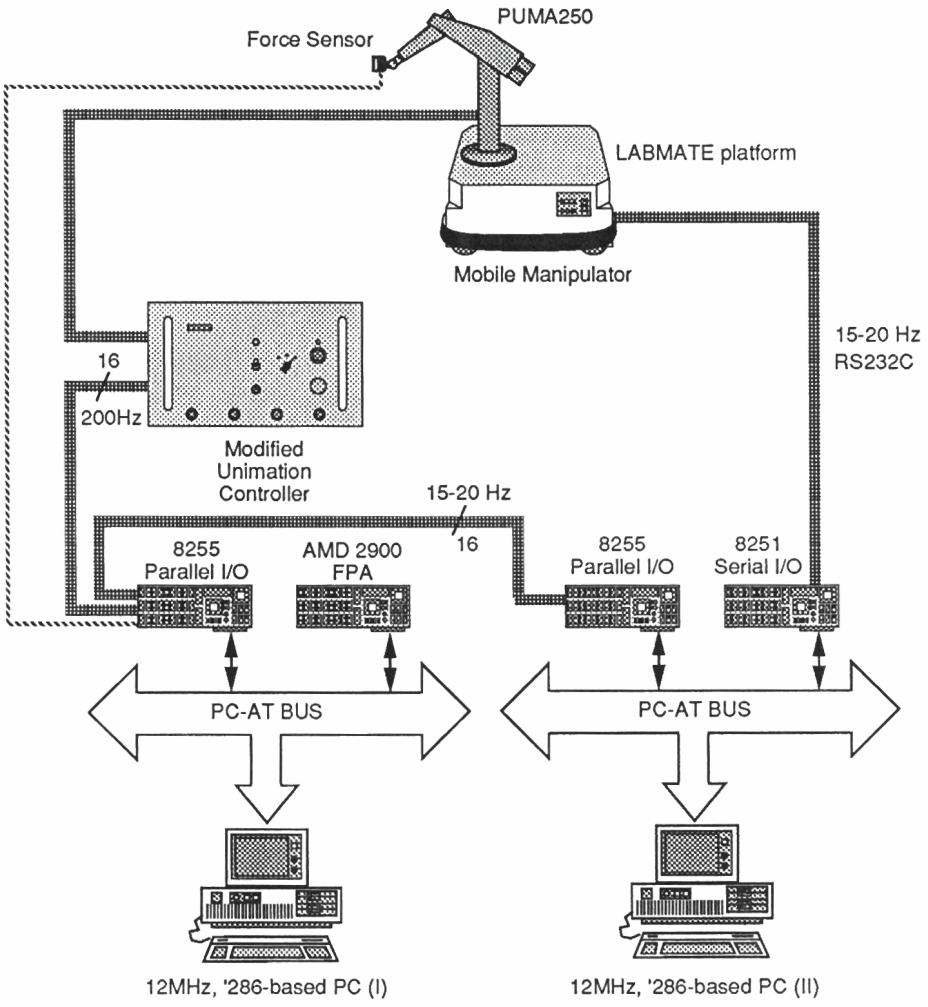

Figure 7.2: Hardware architecture for the experimental setup.

7.2 Control Scheme of LABMATE Mobile Platform

In this section, we present the controller for LABMATE platform which is a little different and simplified from the one described in Chapter 3 and Section 4.3 due to the physical limitation of the mobile platform[1].

Here we consider only one nonholonomic constraint, which reflects the fact that the platform must move in the direction of the axis of symmetry, *i.e.*,

$$\dot{y}_o \cos\phi - \dot{x}_o \sin\phi = 0 \tag{7.1}$$

where (x_o, y_o) is the coordinates of the origin of the platform frame, P_o, in the inertial frame (see Figure 5.3). Again the reference point for the platform is selected such that it corresponds to the end point of the manipulator at a preferred configuration at which the manipulability measure is maximized. As mentioned in Section 5.3, the coordinates of the reference point with respect to the platform frame are defined by Equations (5.6) and (5.7). Denoting the reference point with respect to the inertial frame by $({}^w x_r, {}^w y_r)$, the coordinates are given by

$$\begin{aligned} {}^w x_r &= x_o + {}^v x_r \cos\phi - {}^v y_r \sin\phi & (7.2)\\ {}^w y_r &= y_o + {}^v x_r \sin\phi + {}^v y_r \cos\phi & (7.3) \end{aligned}$$

By taking the coordinates of the reference point to be the output equation

$$y = [{}^w x_r \quad {}^w y_r]^T \tag{7.4}$$

the necessary and sufficient condition for input-output linearization is that the decoupling matrix has full rank [93]. With the output equation (7.4), the decoupling matrix Φ for the system is

$$\Phi = \begin{bmatrix} \Phi_{11} & \Phi_{12} \\ \Phi_{21} & \Phi_{22} \end{bmatrix} \tag{7.5}$$

where

$$\begin{aligned} \Phi_{11} &= \cos\phi & (7.6)\\ \Phi_{12} &= -{}^v y_r \cos\phi - {}^v x_r \sin\phi & (7.7)\\ \Phi_{21} &= \sin\phi & (7.8)\\ \Phi_{22} &= -{}^v y_r \sin\phi + {}^v x_r \cos\phi & (7.9) \end{aligned}$$

The nonlinear feedback for achieving input-output linearlization as well as input-output decoupling is then given by [90]:

$$u = \Phi^{-1} v \tag{7.10}$$

The linearized and decoupled subsystems are described by:

$$\begin{aligned} \dot{y}_1 &= v_1 & (7.11)\\ \dot{y}_2 &= v_2 & (7.12) \end{aligned}$$

[1] We can not directly command the motor torques.

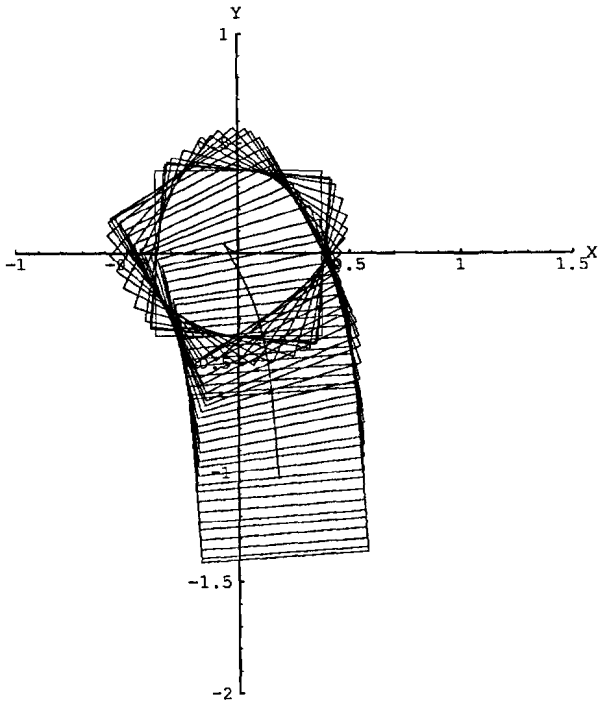

Figure 7.3: Trajectory of the P_o and the motion of platform.

7.3 Experimental Results of Dragging Task

The control algorithm stated in Section 4.3 and 4.4 and modified as above is implemented with the experimental mobile manipulator. Under this scenario, only the first three joints of the manipulator are taken into account, *i.e.*, no wrist joints are considered. The sampling rates of PUMA 250 and LABMATE are 250 and 16 Hz, respectively. In the experiment the end effector of the mobile manipulator which is at rest and in an optimal configuration at the beginning is dragged by a human operator. For comparison purpose it is dragged along the direction normal to the initial heading direction of LABMATE, which corresponds to the first trajectory in the simulations. Figure 7.3 shows the trajectories of the origin of the platform frame (P_o) and the reference point. The former trajectory indicates the platform initially goes backward and then starts moving forward. This observation agrees with the simulation result in the previous section though their transient behaviors are somewhat different. Figure 7.5 depicts the velocity of the point P_o of LABMATE, which also exhibits the presense of the initial backup. Note that dragging ceases at about 14 seconds. Manipulability measure is shown in Figure 7.7. The manipulability slightly drops at the beginning and is maintained at the same level while the platform is in motion. It then comes back to a nearly optimal configuration after dragging stops. The slight degradation during motion is mainly due to the communication delay.

7.4 Experimental Results of Following Task

In the following scenario, the manipulator is initialized in the optimal configuration in terms of manipulability measure, hence the platform remains still at the beginning. The manipulator is force-controlled according to the method described in Section 5.2 such that

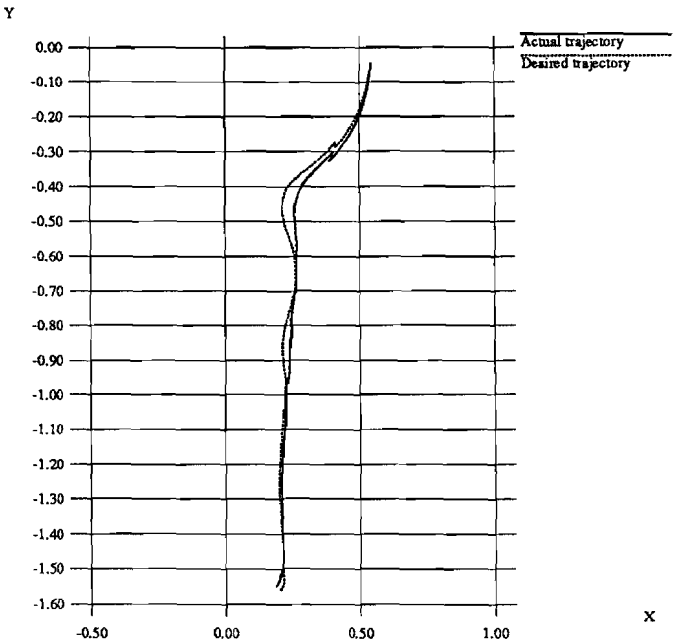

Figure 7.4: Trajectories of the reference point.

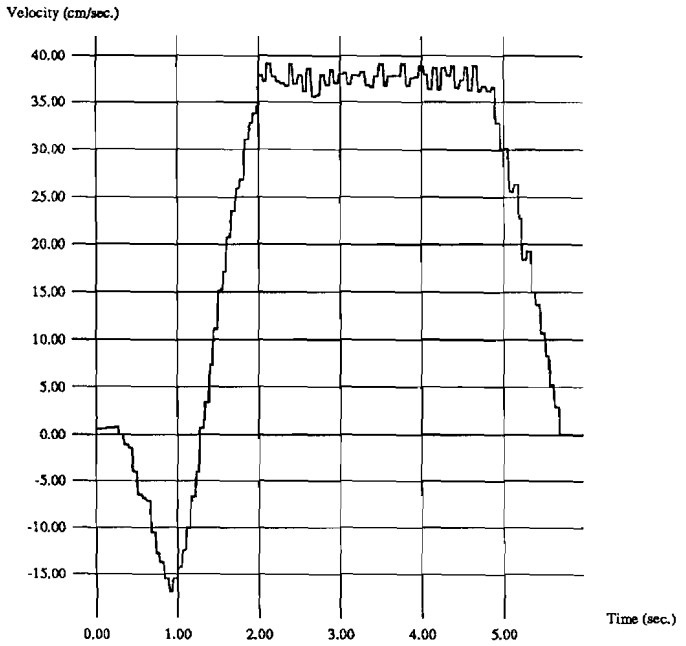

Figure 7.5: Velocity of the point P_o of LABMATE.

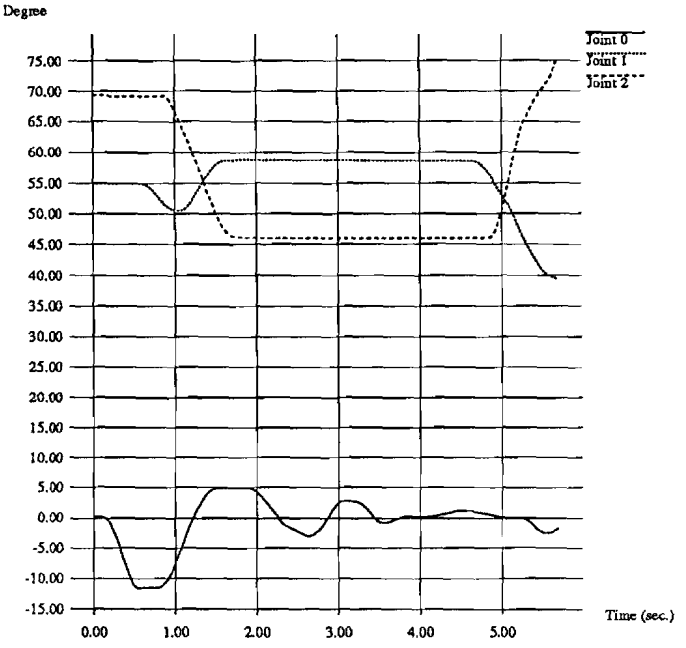

Figure 7.6: Joint angles of PUMA 250.

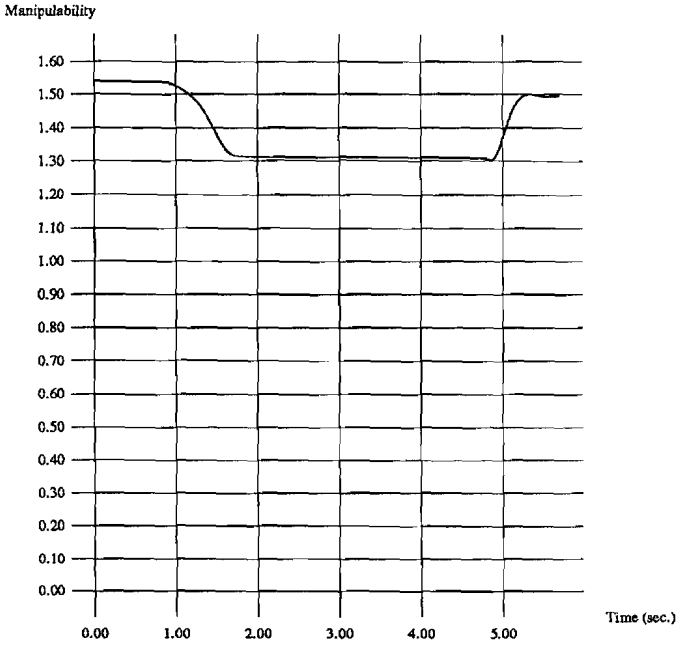

Figure 7.7: Manipulability measure.

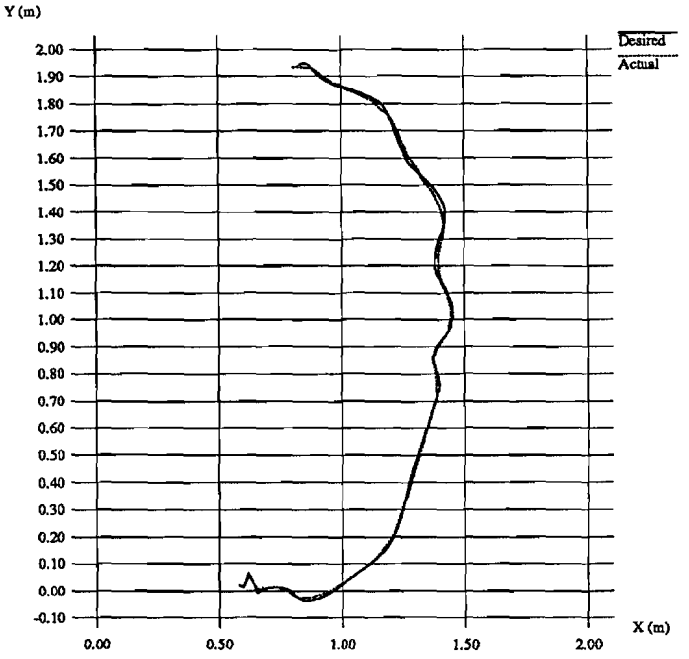

Figure 7.8: Trajectory of the reference point.

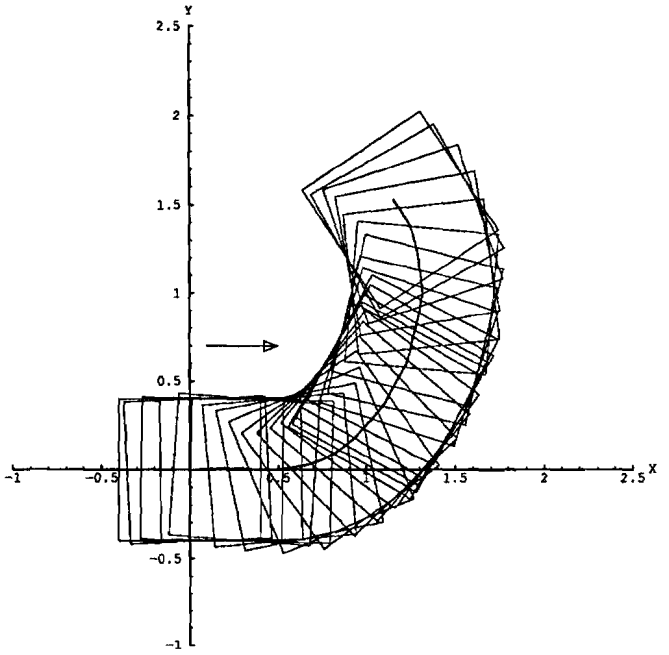

Figure 7.9: Experimental trajectory of the mobile platform.

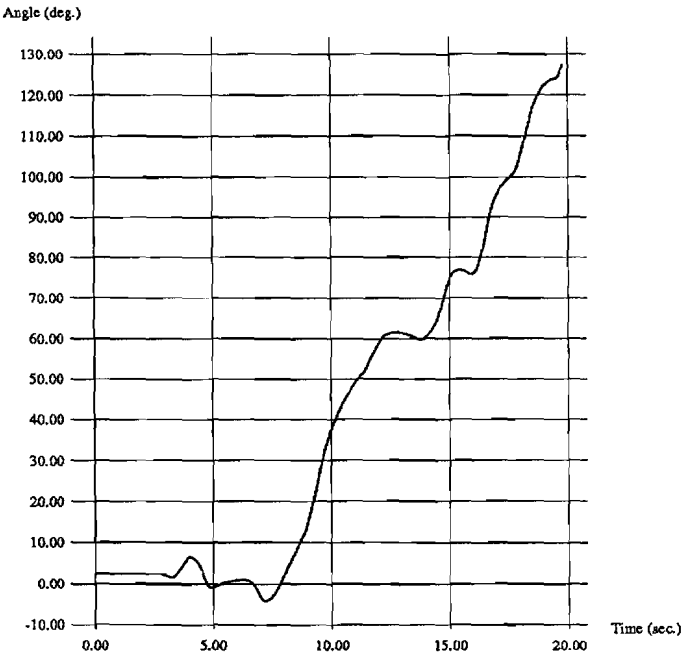

Figure 7.10: Heading angle.

a normal force exerted on the palm is regulated at a prescribed value. The motion of the platform is planned and controlled according to Section 5.3 and 7.2.

In the experiment a human operator guides the end effector of the manipulator. The control rates for the manipulator and the platform are 200 Hz and 16 Hz, respectively. Note that the sampling rate of the manipulator is slower than the one used in the dragging experiment. This is due to the presence of a force sensor. The trajectory of the reference point which is roughly a circular arc is depicted in Figure 7.8. It can be seen from the figure that the reference point is able to track the desired trajectory very well. The motion of the mobile platform is shown in Figure 7.9, accompanied by the trajectory of the point on the wheel axis.

The heading angle of the platform following the object motion is shown in Figure 7.10 in which the transition of the heading angle is more clearly seen.

The manipulability measure is shown in Figure 7.11. Since the maximal possible value of the manipulability measure is 1.6 for the manipulator, it is clear from Figure 7.11 that the manipulator is being kept in a good configuration in terms of manipulability while the entire system is in motion. The measured forces are shown in Figure 7.12. The desired normal force exerted at the palm is linearly increased until it reaches 15 Newtons (the dotted line in the upper half of Figure 7.12). The normal force is maintained near the desired value although some fluctuation is observed. The two curves in the lower half of Figure 7.12 are the measured tangential forces in the x- and y-axis of the hand coordinates.

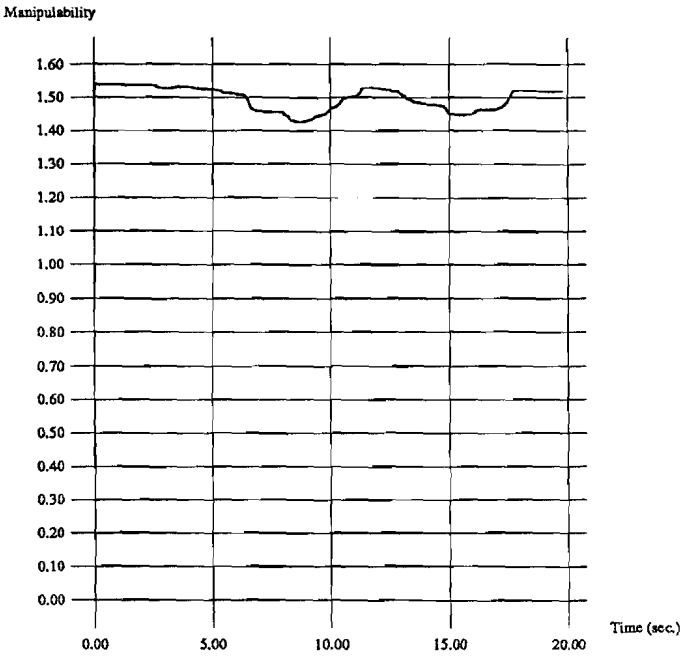

Figure 7.11: Manipulability measure.

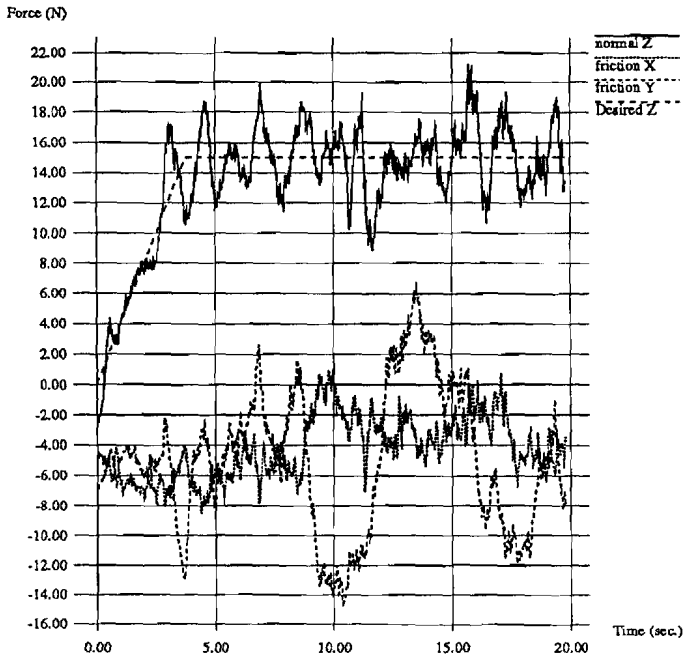

Figure 7.12: Measured forces.

Chapter 8

Summary

8.1 Contributions

In this thesis proposal, we have investigated modeling and feedback control of mobile manipulators. A mobile manipulator under consideration in this study is made of a robotic manipulator and a mobile platform. It combines the manipulation capability of the manipulator and the mobility of the mobile platform. The study is focused on finding control algorithms that effectively coordinate manipulation and mobility. The main contributions of the study are summerized below.

- **Modeling of mobile manipulators.** We developed an approach for deriving motion equations of the mobile manipulator. In this approach, motion equations of the mobile manipulator are derived based on the already available motion equations of the manipulator and the mobile platform, rather than from scratch. The additional velocity and inertial coupling effects between the manipulator and the mobile platform are properly taken into consideration. In addition to being simple, this approach allows us to conveniently investigate the dynamic interaction between the manipulator and mobile platform.

- **Feedback control of wheeled mobile platforms.** We studied control properties of the dynamic system that describes the motion of a wheeled mobile platform. Such a system is subject to nonholonomic constraints and has a number of unique properties. In particular, we showed that a nonholonomic system is not input-state linearizable, but possibly input-output linearizable with a proper choice of the output equation. For the wheeled mobile platform, if the output equation is chosen to be the coordinates of a point on the wheel axis, the system is not input-output linearizable by using any static state feedback. In this case, we showed that a dynamic state feedback makes the input-output linearization possible. For other choice of the output equation, we showed that a static state feedback is sufficient for input-output linearization purpose. In particular, the look-ahead control method is introduced, in which the output equation is chosen as the coordinates of a reference point in front of the platform.

- **The internal dynamics and zero dynamics.** We investigated the internal dynamics of the wheeled mobile platform under the look-ahead control method. We showed that the zero dynamics of the system is stable, but the internal dynamics is not always stable. In particular, we proved, by means of Lyapunov's second method, that the internal dynamics when the platform is controlled to move backwards is unstable. The existence of such unstable internal motions has been verified by both simulation and experiment.

- **Coordination of manipulation and mobility.** We developed a coordination algorithm for the mobile manipulator based on the concept of preferred operating region. With the coordination algorithm, the mobile platform moves in response to the motion of the manipulator in such a way that the manipulator is always maintained in the optimal configuration in terms of the manipulability measure. The algorithm has been utilized to perform two types of tasks: dragging motion and following motion.

- **Dynamic interaction.** Based on the motion equations of the mobile manipulator, the dynamic interaction between the manipulator and the mobile platform has been investigated through simulations on selected trajectories. The simulation results indicated that, depending on the type of the trajectory chosen, the compensation of the dynamic interaction of the platform affected by the manipulator is more effective than that of the manipulator caused by the motion of the platform, or vice versa.

- **Experiments.** The dragging motion and the following motion with explicit force control scheme have been implemented on the experimental mobile manipulator which consists of a PUMA 250 and a LABMATE platform. In the dragging motion, similar results have been obtained to those in the simulation. In the following motion where the mobile manipulator follows a moving object while the manipulator exerts a force to the object to support it, it has been shown that the mobile manipulator successfully follows the trajectory of a human operator while maintaining the contact force pushing against the palm of the operator.

8.2 Works to be done

- The dynamic interaction described in Chapter 6 will be tested on the experimental mobile manipulator. This is aimed at investigating the significance of the dynamic interaction under practical circumstances.

- Alternative approaches which provide a mobile manipulator with more flexibility will be investigated. The current coordination strategy chooses the preferred operating region to be a single point where the manipulability measure is maximized. This implies that even a slight departure from the point of the manipulator results in the motion of the mobile platform to compensate it. This may not be desirable in certain situations. For instance, if the motion of the manipulator is contained in the neighborhood of the optimal posture, the mobile platform then should not respond

even if the manipulator is deviated from the best posture.

- Effects of an external force will be taken into account under certain circumstances. This consideration renders more applicability of the proposed coordination algorithm since, in many cases, the interaction with an environment is ubiquitous.

Appendix A

Functional Dependence of Inertial Matrix, $M_r^{(ij)}$

The objective of this appendix is to prove that $M_r^{(ij)}$ is independent of platform coordinates, q_v. The proof is a little different from [89] in the sense that we do not assume any specific structure for the platform, *e.g.*, serial link chain, while [89] was based on the manipulator consisting of N serial links. Therefore some of the matrix simplification techniques used in [89] do not apply to our case.

$$M_r^{(ij)} = \sum_{k=\max(i,j)}^{n} trace\left[\frac{\partial \mathcal{T}_{m,k}}{\partial q_i} J_k \frac{\partial \mathcal{T}_{m,k}^T}{\partial q_j}\right] \tag{A.1}$$

Let

$$M_r^{(ij)} \stackrel{\text{def}}{=} \sum_{k=\max(i,j)}^{n} M_r^{(ij)}(k)$$

Then $M_r^{(ij)}(k)$ is defined as

$$M_r^{(ij)}(k) = trace\left[\frac{\partial \mathcal{T}_k}{\partial q_i} J_k \frac{\partial \mathcal{T}_k^T}{\partial q_j}\right] \tag{A.2}$$

Assuming $i \geq j$ without loss of generality,

$$\begin{aligned}
M_r^{(ij)}(k) &= trace\Big[T_v A_1^0 A_2^1 \ldots A_{i-1}^{i-2} \frac{\partial A_i^{i-1}}{\partial q_i} A_{i+1}^i \ldots A_k^{k-1} J_k \\
&\quad A_k^{k-1^T} \ldots A_{j+1}^{j^T} \frac{\partial A_j^{j-1^T}}{\partial q_j} A_{j-1}^{j-2^T} \ldots A_2^{1^T} A_1^{0^T} T_v^T\Big] \\
&= trace\Big[T_v A_1^0 A_2^1 \ldots A_{i-1}^{i-2} Q_i A_i^{i-1} A_{i+1}^i \ldots A_k^{k-1} J_k \\
&\quad A_k^{k-1^T} \ldots A_{j+1}^{j^T} A_j^{j-1^T} Q_j^T A_{j-1}^{j-2^T} \ldots A_2^{1^T} A_1^{0^T} T_v^T\Big] \\
&= trace\Big[\underbrace{Q_j^T A_{j-1}^{j-2^T} \ldots A_2^{1^T} A_1^{0^T} T_v^T T_v A_1^0 A_2^1 \ldots A_{j-1}^{j-2} A_j^{j-1} \ldots A_{i-1}^{i-2} Q_i}
\end{aligned}$$

$$A_i^{i-1}\, A_{i+1}^{i} \ldots A_k^{k-1}\, J_k\, A_k^{k-1^T} \ldots A_j^{j-1^T}\Big] \tag{A.3}$$

where the matrix Q_i is

$$Q_i \stackrel{\text{def}}{=} \begin{bmatrix} 0 & -1 & 0 & 0 \\ 1 & 0 & 0 & 0 \\ 0 & 0 & 0 & 0 \\ 0 & 0 & 0 & 0 \end{bmatrix} \text{ for a rotational joint } i \tag{A.4}$$

and

$$Q_i \stackrel{\text{def}}{=} \begin{bmatrix} 0 & 0 & 0 & 0 \\ 0 & 0 & 0 & 0 \\ 0 & 0 & 0 & 1 \\ 0 & 0 & 0 & 0 \end{bmatrix} \text{ for a prismatic joint } i \tag{A.5}$$

Now we focus on the underbraced portion of Equation (A.3). Denoting the underbraced part by U, it is represented by

$$U = Q_j^T\, \Lambda\, Q_i \tag{A.6}$$

where $\Lambda = T_{j-1}^{0^T}\, T_v^T\, T_v\, T_{j-1}^0\, T_{i-1}^{j-1}$.

Suppose that T_v, T_{j-1}^0, and T_{i-1}^{j-1} are given by the following forms

$$T_v = \begin{bmatrix} R_v & p_v \\ 0 & 1 \end{bmatrix}, \quad T_{j-1}^0 = \begin{bmatrix} R_1 & p_1 \\ 0 & 1 \end{bmatrix}, \quad T_{i-1}^{j-1} = \begin{bmatrix} R_2 & p_2 \\ 0 & 1 \end{bmatrix} \tag{A.7}$$

where R and p represent 3×3 rotational matrix and 3-dimensional translational column vector, respectively, and the functional dependence of each term is given by

$$\begin{array}{ll} R_v = R_v(q_v), & p_v = p_v(q_v) \\ R_1 = R_1(q_1, \ldots, q_{j-1}), & p_1 = p_1(q_1, \ldots, q_{j-1}) \\ R_2 = R_2(q_j, \ldots, q_{i-1}), & p_2 = p_2(q_j, \ldots, q_{i-1}) \end{array}$$

Substituting the above symbols into Equation (A.7), Λ has the following form

$$\Lambda = T_{j-1}^{0^T}\, T_v^T\, T_v\, T_{j-1}^0\, T_{i-1}^{j-1} = \begin{bmatrix} R_2 & p_2 + R_2^T(p_1 + R_v^T p_v) \\ (p_1^T + p_v^T R_v) R_1 R_2 & * \end{bmatrix} \tag{A.8}$$

where $* = (p_1^T + p_v^T R_v)(R_1 p_2 + p_1) + p_1^T R_v^T p_v + p_v^T p_v + 1$.

Now we examine functional dependence of $U = Q_j^T\, \Lambda\, Q_i$ by checking four different cases in terms of the type of the two joints, i and j.

- Both i and j are revolute joints

$$Q_i = Q_j = \begin{bmatrix} 0 & -1 & 0 & 0 \\ 1 & 0 & 0 & 0 \\ 0 & 0 & 0 & 0 \\ 0 & 0 & 0 & 0 \end{bmatrix} = \begin{bmatrix} K & 0 \\ 0 & 0 \end{bmatrix} \quad \text{where} \quad K = \begin{bmatrix} 0 & -1 & 0 \\ 1 & 0 & 0 \\ 0 & 0 & 0 \end{bmatrix}$$

Then

$$U = \begin{bmatrix} K^T R_2 K & 0 \\ 0 & 0 \end{bmatrix} \tag{A.9}$$

$M_r^{ij}(k)$ is therefore independent of q_v, $q_0, \ldots, q_{j-1}$.

- Both i and j are prismatic joints

$$Q_i = Q_j = \begin{bmatrix} 0 & 0 & 0 & 0 \\ 0 & 0 & 0 & 0 \\ 0 & 0 & 0 & 1 \\ 0 & 0 & 0 & 0 \end{bmatrix} = \begin{bmatrix} 0 & l \\ 0 & 0 \end{bmatrix} \quad \text{where} \quad l = \begin{bmatrix} 0 \\ 0 \\ 1 \end{bmatrix}$$

Then

$$U = \begin{bmatrix} 0 & 0 \\ 0 & l^T R_2 l \end{bmatrix} \tag{A.10}$$

$M_r^{ij}(k)$ is therefore independent of q_v, $q_0, \ldots, q_{j-1}$.

- i is revolute and j is prismatic

$$Q_i = \begin{bmatrix} 0 & -1 & 0 & 0 \\ 1 & 0 & 0 & 0 \\ 0 & 0 & 0 & 0 \\ 0 & 0 & 0 & 0 \end{bmatrix}, \quad Q_j = \begin{bmatrix} 0 & 0 & 0 & 0 \\ 0 & 0 & 0 & 0 \\ 0 & 0 & 0 & 1 \\ 0 & 0 & 0 & 0 \end{bmatrix}$$

$$U = \begin{bmatrix} 0 & 0 \\ l^T R_2 K & 0 \end{bmatrix} \tag{A.11}$$

Thus $M_r^{ij}(k)$ is independent of q_v, $q_0, \ldots, q_{j-1}$.

- i is prismatic and j is revolute

$$Q_i = \begin{bmatrix} 0 & 0 & 0 & 0 \\ 0 & 0 & 0 & 0 \\ 0 & 0 & 0 & 1 \\ 0 & 0 & 0 & 0 \end{bmatrix}, \quad Q_j = \begin{bmatrix} 0 & -1 & 0 & 0 \\ 1 & 0 & 0 & 0 \\ 0 & 0 & 0 & 0 \\ 0 & 0 & 0 & 0 \end{bmatrix}$$

$$U = \begin{bmatrix} 0 & K^T R_2 l \\ 0 & 0 \end{bmatrix} \tag{A.12}$$

Thus $M_r^{ij}(k)$ is independent of q_v, $q_0, \ldots, q_{j-1}$.

From Equations (A.9) through (A.12), it is shown that M_r^{ij} is independent of the platform variable, q_v.

Appendix B

Functional Dependence of Velocity Term, $C_{r2}^{(i)}$

In this appendix, we examine functional dependence of the velocity term in terms of platform coordinate, q_v. The velocity term is defined by Equation (2.44) which is restated below for convenience.

$$\begin{aligned} C_{r2}^{(i)} &= 2\sum_{j=1}^{m}\sum_{k=1}^{n}\sum_{h=max(i,k)}^{n} trace\left[\frac{\partial \mathcal{T}_h}{\partial q_i} J_h \frac{\partial \mathcal{T}_h^T}{\partial q_{v,j}\partial q_k}\right]\dot{q}_{v,j}\cdot\dot{q}_k + \\ &\quad \sum_{j=1}^{m}\sum_{k=1}^{m}\sum_{h=i}^{n} trace\left[\frac{\partial \mathcal{T}_h}{\partial q_i} J_h \frac{\partial \mathcal{T}_h^T}{\partial q_{v,j}\partial q_{v,k}}\right]\dot{q}_{v,j}\cdot\dot{q}_{v,k} \end{aligned}$$

Let

$$C_{r2}^{(i)} \stackrel{\text{def}}{=} 2\sum_{j=1}^{m}\sum_{k=1}^{n}\sum_{h=max(i,k)}^{n} C_{r2.1}^{ijk}(h) + \sum_{j=1}^{m}\sum_{k=1}^{m}\sum_{h=i}^{n} C_{r2.2}^{ijk}(h) \tag{B.1}$$

The two terms on the RHS are then defined as

$$\begin{aligned} C_{r2.1}^{ijk}(h) &= trace\left[\frac{\partial \mathcal{T}_h}{\partial q_i} J_h \frac{\partial \mathcal{T}_h^T}{\partial q_{v,j}\partial q_k}\right]\dot{q}_{v,j}\cdot\dot{q}_k \\ C_{r2.2}^{ijk}(h) &= trace\left[\frac{\partial \mathcal{T}_h}{\partial q_i} J_h \frac{\partial \mathcal{T}_h^T}{\partial q_{v,j}\partial q_{v,k}}\right]\dot{q}_{v,j}\cdot\dot{q}_{v,k} \end{aligned}$$

Assuming $i \geq k$ without loss of generality,

$$\begin{aligned} C_{r2.1}^{ijk}(h) &= trace\Big[T_v A_1^0 A_2^1 \ldots A_{i-1}^{i-2} Q_i A_i^{i-1} \ldots A_h^{h-1} J_h \\ &\qquad A_h^{h-1^T} \ldots A_i^{i-1^T} \ldots A_k^{k-1^T} Q_k^T \ldots A_1^{0^T} \frac{\partial T_v}{\partial q_{v,j}}\Big] \\ &= trace\Big[A_i^{i-1} \ldots A_h^{h-1} J_h A_h^{h-1^T} \ldots A_i^{i-1^T} \ldots A_k^{k-1^T} \\ &\qquad \underbrace{Q_k^T A_k^{k-1^T} \ldots A_1^{0^T} \frac{\partial T_v}{\partial q_{v,j}} T_v A_1^0 A_2^1 \ldots A_{i-1}^{i-2} Q_i}\Big] \end{aligned} \tag{B.2}$$

where the matrix Q is defined in Equations (A.4) and (A.5).

Denoting the underbraced portion in Equation (B.2) by V, it is given by

$$V = Q_k^T \, \Gamma \, Q_i \tag{B.3}$$

where $\Gamma = T_{k-1}^{0^T} \dfrac{\partial T_v}{\partial q_{v,j}} T_v \, T_{i-1}^0 \, Q_i$.

Suppose that T_v, T_{k-1}^0, and T_{i-1}^0 are represented by the following forms

$$T_v = \begin{bmatrix} R_v & p_v \\ 0 & 1 \end{bmatrix}, \quad T_{k-1}^0 = \begin{bmatrix} R_{k-1} & p_{k-1} \\ 0 & 1 \end{bmatrix}, \quad T_{i-1}^0 = \begin{bmatrix} R_{i-1} & p_{i-1} \\ 0 & 1 \end{bmatrix} \tag{B.4}$$

The derivative of T_v with respect to $q_{v,j}$ is then given by

$$\frac{\partial T_v}{\partial q_{v,j}} = \begin{bmatrix} \frac{\partial R_v}{\partial q_{v,j}} & \frac{\partial p_v}{\partial q_{v,j}} \\ 0 & 0 \end{bmatrix} \stackrel{\text{def}}{=} \begin{bmatrix} \partial R_{v,j} & \partial p_{v,j} \\ 0 & 0 \end{bmatrix} \tag{B.5}$$

Depending on the type of joints, i and k, V is computed to the four different cases.

- Both i and k are revolute joints

$$V = \begin{bmatrix} K^T \, R_k^T \, \partial R_{v,j}^T \, R_v \, R_{i-1} \, K & 0 \\ 0 & 0 \end{bmatrix} \tag{B.6}$$

- Both i and k are prismatic joints

$$V = \begin{bmatrix} 0 & 0 \\ 0 & l^T \, R_k^T \, \partial R_{v,j}^T \, R_v \, R_{i-1} \, l \end{bmatrix} \tag{B.7}$$

- i is revolute and k is prismatic

$$V = \begin{bmatrix} 0 & K^T \, R_k^T \, \partial R_{v,j}^T \, R_v \, R_{i-1} \, l \\ 0 & 0 \end{bmatrix} \tag{B.8}$$

- i is prismatic and k is revolute

$$V = \begin{bmatrix} 0 & 0 \\ l^T \, R_k^T \, \partial R_{v,j}^T \, R_v \, R_{i-1} \, K & 0 \end{bmatrix} \tag{B.9}$$

From Equations (B.6) through (B.9), V is independent of platform variable q_v if and only if $\partial R_{v,j}^T \, R_v$ is independent of q_v. If the platform involves no rotational motion, then R_v becomes identity matrix, implying $\partial R_{v,j}^T$ vanishes. Therefore $q_{v,j}$ is assumed to be a rotational variable about an arbitrary axis originated at the origin of the inertial frame. Without loss of generality, $q_{v,j}$ may be chosen to be a parameter for one of commonly used representation methods of rotation, *i.e.*, Euler angles, Roll-Pitch-Yaw angles, angle-axis representation [86]. It is then straight forward to show that $\partial R_{v,j}^T \, R_v$ becomes a skew-symmetric matrix which does not include the variable, $q_{v,j}$.

Bibliography

[1] I. J. Cox and G. T. Wilfong. *Autonomous Robot Vehicles.* Springer-Verlag, Berlin, Germany, 1990.

[2] S. S. Iyengar and A. Elfes. *Autonomous Mobile Robots: Perception, Mapping, and Navigation.* Volume 1, IEEE Computer Society Press, Los Alamitos, CA, 1991.

[3] S. S. Iyengar and A. Elfes. *Autonomous Mobile Robots: Control, Planning, and Architecture.* Volume 2, IEEE Computer Society Press, Los Alamitos, CA, 1991.

[4] R. Bajcsy. Cooperative agents: machines and humans. In *Proceedings of 1993 International Conference on Advanced Robotics*, pages 115–119, Tokyo, Japan, November 1993.

[5] R. Carlton and S. Bartholet. The evolution of the application of mobile robotics to nuclear facility operations and maintenance. In *Proceedings of 1987 International Conference on Robotics and Automation*, pages 720–726, Raleigh, NC, April 1987.

[6] M. Jamshidi and P. J. Eicker. *Robotics and Remote Systems for Hazardous Environment.* Prentice-Hall, Englewood Cliffs, NJ, 1993.

[7] H. Goldstein. *Classical Mechanics.* Addison-Wesley Publishers, Reading, MA, 1980.

[8] P. F. Muir and C. P. Neuman. Kinematic modeling for feedback control of an omni-directional mobile robot. In *Proceedings of 1987 International Conference on Robotics and Automation*, pages 1772–1778, Raleigh, NC, April 1987.

[9] G. Campion and G. Bastin. On adaptive linearizing control of omnidirectional mobile robots. In M. A. Kaashoek, J. H. van Schuppen, and A. C. M. Ran, editors, *Robust Control of Linear Systems and Nonlinear Control*, pages 531–538, Birkhauser, Boston, MA, 1990.

[10] D. Feng, M. B. Friedman, and B. H. Krogh. The servo-control system for an omnidirectional mobile robot. In *Proceedings of 1989 International Conference on Robotics and Automation*, pages 1566–1571, Scottsdale, AZ, May 1989.

[11] M. West and H. Asada. Design of a holonomic omnidirectional vehicle. In *Proceedings of 1992 International Conference on Robotics and Automation*, pages 97–103, Nice, France, May 1992.

[12] S. K. Saha, J. Angeles, and J. Darcovich. The kinematic design of a 3-dof isotropic mobile robot. In *Proceedings of 1993 International Conference on Robotics and Automation*, pages 283–288, Vol. 1, Atlanta, GA, May 1993.

[13] Y. Nakamura and S. Savant. Nonlinear tracking control of autonomous underwater vehicles. In *Proceedings of 1992 International Conference on Robotics and Automation*, pages A4–A9, Nice, France, May 1992.

[14] O. J. Sordalen, M. Dalsmo, and O. Egeland. An exponentially convergent control law for an underwater vehicle with nonholonomic constraints. In *Proceedings of 1993 International Conference on Robotics and Automation*, pages 790–795, Vol. 3, Atlanta, GA, May 1993.

[15] J. Kerr and B. Roth. Analysis of multifingered hands. *The International Journal of Robotics Research*, 4(4), 1986.

[16] Z. Li and J. F. Canny. Motion of two rigid bodies with rolling constraint. *IEEE Transactions on Robotics and Automation*, 6(1):62–72, February 1990.

[17] Z. Vafa and S. Dubowsky. On the dynamics of manipulators in space using the virtual manipulator approach. In *Proceedings of 1987 International Conference on Robotics and Automation*, pages 579–585, Raleigh, NC, April 1987.

[18] Y. Nakamura and R. Mukherjee. Nonholonomic path planning of space robots. In *Proceedings of 1989 International Conference on Robotics and Automation*, pages 1050–1055, Scottsdale, AZ, May 1989.

[19] E. Papadopoulos. Nonholonomic behavior in free-floating space manipulators and its utilization. In Z. Li and J. F. Canny, editors, *Nonholonomic Motion Planning*, pages 423–445, Kluwer Academic Publishers, 1993.

[20] T. R. Kane and M. P. Scher. A dynamical explanation of the falling cat phenomenon. *Journal of Solids and Structures*, 5:663–670, 1969.

[21] T. R. Kane. Experimental investigation of an astronaut maneuvering scheme. *Journal of Biomechanics*, 5:313–320, 1972.

[22] C. Fernandes, L. Gurvits, and Z. Li. Optimal nonholonomic motion planning for a falling cat. In Z. Li and J. F. Canny, editors, *Nonholonomic Motion Planning*, pages 379–421, Kluwer Academic Publishers, 1993.

[23] Ju I. Neĭmark and N. A. Fufaev. *Dynamics of Nonholonomic Systems.* American Mathematical Society, Providence, RI, 1972.

[24] Z. Li and J. F. Canny. *Nonholonomic Motion Planning.* Kluwer Academic Publishers, Boston, MA, 1993.

[25] J-P. Laumond. Feasible trajectories for mobile robots with kinematic and environmental constraints. In O. L. Hertzberger and F. C. A. Groen, editors, *Intelligent Autonomous Systems*, pages 346–354, Elsevier Science Publishers, Amsterdam, the Netherlands, 1987.

[26] P. Jacobs and J. Canny. Planning smooth paths for mobile robots. In *Proceedings of 1989 International Conference on Robotics and Automation*, pages 2–7, Scottsdale, Arizona, May 1989.

[27] J. Barraquand and J-C. Latombe. On nonholonomic mobile robots and optimal maneuvering. In *Proceedings of Fourth IEEE International Symposium on Intelligent Control*, pages 340–347, Albany, NY, September 1989.

[28] J-C. Latombe. *Robot Motion Planning.* Kluwer Academic Publishers, Boston, MA, 1991.

[29] G. Lafferriere and H. J. Sussmann. A differential geometric approach to motion planning. In Z. Li and J. F. Canny, editors, *Nonholonomic Motion Planning*, pages 235–270, Kluwer Academic Publishers, 1993.

[30] R. M. Murray and S. S. Sastry. Steering nonholonomic systems in chained form. In *Proceedings of 30th IEEE Conference on Decision and Control*, pages 1121–1126, Brighton, England, December 1991.

[31] R. M. Murray and S. S. Sastry. Steering nonholonomic systems using sinusoids. In *Proceedings of 29th IEEE Conference on Decision and Control*, pages 2097–2101, Honolulu, Hawaii, December 1990.

[32] O. J. Sordalen. Conversion of the kinematics of a car with n trailers into a chained form. In *Proceedings of 1993 International Conference on Robotics and Automation*, pages 382–387, Vol. 1, Atlanta, GA, May 1993.

[33] R. W. Brockett. Asymptotic stability and feedback stabilization. In R. W. Brockett, R. S. Millman, and H. J. Sussmann, editors, *Differential Geometric Control Theory*, pages 181–191, Birkhauser, Boston, MA, 1983.

[34] G. Campion, B. d'Andrea-Novel, and G. Bastin. Controllability and state feedback stabilization of non holonomic mechanical systems. In C. Canudas de Wit, editor, *Lecture Notes in Control and Information Science*, pages 106–124, Springer-Verlag, 1991.

[35] C. Samson and K. Ait-Abderrahim. Feedback control of a nonholonomic wheeled cart in cartesian space. In *Proceedings of 1991 International Conference on Robotics and Automation*, pages 1136–1141, Sacramento, CA, April 1991.

[36] Y. Kanayama, Y. Kimura, F. Miyazaki, and T. Noguchi. A stable tracking control method for an autonomous mobile robot. In *Proceedings of 1990 International Conference on Robotics and Automation*, pages 384–389, Cincinati, OH, May 1990.

[37] C. Samson and K. Ait-Abderrahim. *Mobile robot control Part 1: Feedback control of non holonomic wheeled cart in Cartesian space.* Technical Report No. 1288, INRIA, Sophia-Antipolis, France, 1990.

[38] C. Samson. Velocity and torque feedback control of a nonholonomic cart. In C. Canudas de Wit, editor, *Lecture Notes in Control and Information Science*, pages 125–151, Springer-Verlag, 1991.

[39] C. Samson. Time-varying feedback stabilization of nonholonomic car-like mobile robots. *The International Journal of Robotics Research*, 8(5):3–14, February 1993. missing info.

[40] J-B. Pomet. Explicit design of time-varying stabilizing contol laws for a class of controllable systems without drift. *Systems and Control Letters*, 18:147–158, 1992.

[41] J-B. Pomet, B. Thuilot, G. Bastin, and G. Campion. A hybrid strategy for the feedback stabilization of nonholonomic mobile robots. In *Proceedings of 1992 International Conference on Robotics and Automation*, pages 129–134, Nice, France, May 1992.

[42] L. Gurvits and Z. Li. Smooth time-periodic feedback solution for nonholonomic motion planning. In Z. Li and J. F. Canny, editors, *Nonholonomic Motion Planning*, pages 53–108, Kluwer Academic Publishers, 1993.

[43] A. M. Bloch and N. H. McClamroch. Control of mechanical systems with classical nonholonomic constraints. In *Proceedings of 28th IEEE Conference on Decision and Control*, pages 201–205, Tampa, FL, December 1989.

[44] A. M. Bloch, N. H. McClamroch, and M. Reyhanoglu. Controllability and stabilizability properties of a nonholonomic control system. In *Proceedings of 29th IEEE Conference on Decision and Control*, pages 1312–1314, Honolulu, HW, December 1990.

[45] C. Canudas de Wit and O. J. Sordalen. Exponential stabilization of mobile robots with nonholonomic constraints. *IEEE Transactions on Automatic Control*, 37(11):1791–1797, November 1992.

[46] R. A. Brooks. Visual map making for a mobile robot. In *Proceedings of 1985 International Conference on Robotics and Automation*, pages 824–829, St. Louis, Missouri, March 1985.

[47] R. A. Brooks. A robust layered control system for a mobile robot. *IEEE Transactions on Robotics and Automation*, 2(1):14–23, March 1986.

[48] A.C. Kak, B. A. Roberts, K. M. Andress, and R.L. Cromwell. Experiments in the integration of world knowledge with sensory information for mobile robots. In *Proceedings of 1987 International Conference on Robotics and Automation*, pages 734–740, Raleigh, NC, April 1987.

[49] R. Chatila and J-P. Laumond. Position referencing and consistent world modeling for mobile robots. In *Proceedings of 1985 International Conference on Robotics and Automation*, pages 138–145, St. Louis, Missouri, March 1985.

[50] M. Asada. Map building for a mobile robot from sensory data. *IEEE Transactions on Systems, Man, and Cybernetics*, 37(6):312–322, November/December 1990.

[51] L. Matthies and A. Elfes. Integration of a sonar and stereo range data using a grid-based representation. In *Proceedings of 1988 International Conference on Robotics and Automation*, pages 727–733, Philadelphia, PA, April 1988.

[52] A. M. Waxman, J. J. LeMoigne, L. S. Davis, B. Srinivasan, and T. R. Kushner. A visual navigation system for autonomous land vehicles. *IEEE Transactions on Robotics and Automation*, 3(2):121–141, 1987.

[53] D. J. Kriegman, E. Triendl, and T. O. Binford. A mobile robot: sensing, planning, and locomotion. In *Proceedings of 1987 International Conference on Robotics and Automation*, pages 402–408, Raleigh, NC, April 1987.

[54] D. J. Kriegman, E. Triendl, and T. O. Binford. Stereo vision and navigation in buildings for mobile robots. *IEEE Transactions on Robotics and Automation*, 5(6):792–803, December 1989.

[55] J. Leonard, H. F. Durrant-Whyte, and I. J. Cox. Dynamic map building for an autonomous mobile robot. In *Proceedings of 1990 International Conference on Intelligent Robots and Systems*, pages 89–95, July 1990.

[56] I. J Cox. Blanche – an experiment in guidance and navigation of an autonomous robot vehicle. *IEEE Transactions on Robotics and Automation*, 7(2):193–204, 1991.

[57] H. Seraji. An on-line approach to coordinated mobility and manipulation. In *Proceedings of 1993 International Conference on Robotics and Automation*, pages 28–35, Vol. 1, Atlanta, GA, May 1993.

[58] F. G. Pin and J. C. Culioli. Multi-criteria position and configuration optimization for redundant platform/manipulator systems. In *Proceedings of 1990 International Conference on Intelligent Robots and Systems*, pages 103–107, July 1990.

[59] W. Miksch and D. Schroeder. Performance-functional based controller design for a mobile manipulator. In *Proceedings of 1992 International Conference on Robotics and Automation*, pages 227–232, Nice, France, May 1992.

[60] K. Liu and F. L. Lewis. Decentralized continuous robust controller for mobile robots. In *Proceedings of 1990 International Conference on Robotics and Automation*, pages 1822–1827, Cincinati, OH, May 1990.

[61] K. Liu and F. L. Lewis. Application of robust control techniques to a mobile robot system. *Journal of Robotic Systems*, 9(7):893–913, 1992.

[62] G. J. Wiens. Effects of dynamic coupling in mobile robotic systems. In *Proceedings of SME Robotics Research World Conference*, pages 43–57, Gaithersburg, Maryland, May 1989.

[63] J. Joshi and A. A. Desrochers. Modeling and control of a mobile robot subject to disturbances. In *Proceedings of 1986 International Conference on Robotics and Automation*, pages 1508–1513, San Francisco, CA, April 1986.

[64] N. A. M. Hootsmans. *The Motion Control of Manipulators on Mobile Vehicles.* PhD thesis, Department of Mechanical Engineering, Massachusetts Institute of Technology, Cambridge, MA, January 1992.

[65] D. E. Whitney. Historical perspective and state of the art in robot force control. In *Proceedings of 1985 International Conference on Robotics and Automation*, pages 262–268, St. Louis, Missouri, March 1985.

[66] R. Volpe and P. Khosla. An experimental evaluation and comparison of explicit force control strategies for robotic manipulators. In *Proceedings of 1992 American Control Conference*, pages 758–764, Chicago, IL, June 1992.

[67] H. Inoue. *Force Feedback in Precise Assembly Tasks.* Technical Report AIM-308, MIT Artificial Intelligence Laboratory, Cambridge, MA, 1974.

[68] R. P. Paul and B. Shimano. Compliance and control. In *Proceedings of the Joint Automatic Control Conference*, pages 694–699, Purdue University, West Lafayette, IN, July 1976.

[69] S. D. Eppinger. *Modeling Robot Dynamic Performance of Endpoint Force Control.* PhD thesis, Department of Mechanical Engineering, Massachusetts Institute of Technology, Cambridge, MA, September 1988.

[70] R. A. Volpe. *Real and Artificial Forces in the Contrl of Manipulators: Theory and Experiments.* PhD thesis, Department of Physics, The Robotics Institute, Carnegie Mellon University, Pittsburgh, PA, September 1990.

[71] O. Khatib and J. Burdick. Motion and force control of robot manipulators. In *Proceedings of 1986 International Conference on Robotics and Automation*, pages 1381–1386, San Fransisco, CA, March 1986.

[72] S. Eppinger and W. Seering. Understanding bandwidth limitations in robot force control. In *Proceedings of 1987 International Conference on Robotics and Automation*, pages 904–909, Raleigh, NC, April 1987.

[73] C. H. An and J. M. Hollerbach. Dynamic stability issues in force control of manipulators. In *Proceedings of 1987 International Conference on Robotics and Automation*, pages 890–896, Raleigh, NC, April 1987.

[74] Y. Xu and R. P. Paul. On position compensation and force control stability of a robot with a compliant wrist. In *Proceedings of 1988 International Conference on Robotics and Automation*, pages 1173–1178, Philadelphia, PA, April 1988.

[75] M. H. Raibert and J. J. Craig. Hybrid position/force control of manipulators. *Transactions of ASME, Journal of Dynamic Systems, Measurement, and Control*, 103(2):126–133, June 1981.

[76] C. H. An and J. M. Hollerbach. Kinematic stability issues in force control of manipulators. In *Proceedings of 1987 International Conference on Robotics and Automation*, pages 897–903, Raleigh, NC, April 1987.

[77] J. K. Salisbury. Active stiffness control of a manipulator in cartesian coordinates. In *Proceedings of 19th IEEE Conference on Decision and Control*, pages 95–100, December 1980.

[78] D. E. Whitney. Force feedback control of manipulator fine motions. *Transactions of ASME, Journal of Dynamic Systems, Measurement and Control*, 91–97, June 1977.

[79] N. Hogan. Impedance control: an approach to manipulation – theory, implementation, and applications. *Transactions of ASME, Journal of Dynamic Systems, Measurement and Control*, 107:1–24, March 1985.

[80] T. Yoshikawa. *Foundations of Robotics: Analysis and Control.* The MIT Press, Cambridge, MA, 1990.

[81] A. J. Koivo. *Fundamentals for Control of Robotic Manipulators.* John Wiley & Sons, Inc., 1989.

[82] R. P. Paul. *Robot Manipulators: Mathematics, Programming, and Control.* The MIT Press, Cambridge, MA, 1981.

[83] M. Spong and M. Vidyasagar. *Robot Dynamics and Control.* John Wiley & Sons, Inc., New York, 1989.

[84] H. Asada and J. J. E. Slotine. *Robot Analysis and Control.* John Wiley & Sons, Inc., New York, 1986.

[85] J. Denavit and R. S. Hartenberg. A kinematic notation for lower pair mechanisms. *Journal of Applied Mechanics*, 22:215–221, June 1955.

[86] J. J. Craig. *Introduction to Robotics: Mechanics and Control.* Addison Wesley Publishing Company, 2nd edition, 1989.

[87] W. M. Boothby. *An Introduction to Differentiable Manifolds and Riemannian Geometry.* Academic Press, New York, NY, 1975.

[88] R. M. Rosenberg. *Analytical Dynamics of Discrete Systems.* Plenum Press, New York, NY, 1977.

[89] V. D. Tourassis and C. P. Neuman. Properties and structure of dynamic robot models for control engineering applications. *Mechanism and Machine Theory*, 20(1):27–40, 1985.

[90] Y. Yamamoto and X. Yun. Coordinating locomotion and manipulation of a mobile manipulator. In *Proceedings of 31st IEEE Conference on Decision and Control*, pages 2643–2648, Tucson, AZ, December 1992.

[91] B. d'Andrea-Novel, G. Bastin, and G. Campion. Modelling and control of non holonomic wheeled mobile robots. In *Proceedings of 1991 International Conference on Robotics and Automation*, pages 1130–1135, Sacramento, CA, April 1991.

[92] C. Samson and K. Ait-Abderrahim. Feedback stabilization of a nonholonomic wheeled mobile robot. In *Proceedings of 1991 International Conference on Intelligent Robots and Systems*, Osaka, Japan, July 1991.

[93] H. Nijmeijer and A. J. van der Schaft. *Nonlinear Dynamic Control Systems.* Springer-Verlag, New York, 1990.

[94] C. Samson and K. Ait-Abderrahim. Feedback control of a nonholonomic wheeled cart in cartesian space. In *Proceedings of 1991 International Conference on Robotics and Automation*, pages 1136–1141, Sacramento, CA, April 1991.

[95] A. Isidori. *Nonlinear Control Systems: An Introduction.* Springer-Verlag, Berlin, New York, 1985.

[96] J. W. Grizzle, M. D. Di Benedetto, and C. H. Moog. Computing the differential output rank of a nonlinear system. In *Proceedings of 26th IEEE Conference on Decision and Control*, pages 142–145, Los Angeles, CA, December 1987.

[97] J. Descusse and C. H. Moog. Dynamic decoupling for right-invertible nonlinear systems. *Systems and Control Letters*, 8:345–348, 1987.

[98] M. Fliess. A new approach to the structure at infinity of nonlinear systems. *Systems and Control Letters*, 7:419–421, 1986.

[99] J. J. E. Slotine and W. Li. *Applied Nonlinear Control.* John Wiley & Sons, Inc., Englewood Cliffs, NJ, 1991.

[100] A. De Luca. Zero dynamics in robotic systems. In C. I. Byrnes and A. Kurzhansky, editors, *Nonlinear Synthesis*, pages 68–87, Birkhauser, Boston, MA, 1991.

[101] Y. Yamamoto and X. Yun. Control of mobile manipulators following a moving surface. In *Proceedings of 1993 International Conference on Robotics and Automation*, pages 1–6, Vol. 3, Atlanta, GA, May 1993.

[102] M. H. Raibert and J. J. Craig. Hybrid position/force control of manipulators. *Transactions of ASME, Journal of Dynamic Systems, Measurement, and Control*, 103(2):126–133, June 1981.

[103] T. Yoshikawa. Dynamic hybrid position/force control of robot manipulators — description of hand constraints and calculation of joint driving force. *IEEE Journal of Robotics and Automation*, RA-3(5):386–392, October 1987.

[104] T. Yoshikawa, T. Sugie, and M. Tanaka. Dynamic hybrid position/force control of robot manipulators - controller design and experiment. *IEEE Transactions on Robotics and Automation*, 4(6):699–705, December 1988.

[105] E. Colgate and N. Hogan. An analysis of contact instability in terms of passive physical equivalence. In *Proceedings of 1989 International Conference on Robotics and Automation*, pages 404–409, Scottsdale, Arizona, May 1989.